

High Energy Photoproduction

J.M. Butterworth and M. Wing
Department of Physics and Astronomy
University College London
Gower St. London WC1E 6BT
England.

Abstract

The experimental and phenomenological status of high energy photoproduction is reviewed. Topics covered include the structure of the photon, production of jets, heavy flavours and prompt photons, rapidity gaps, energy flow and underlying events. The results are placed in the context of the current understanding of QCD, with particular application to present and future hadron and lepton colliders.

1 Introduction

The photon is one of the earliest and most influential of the concepts contributing to the so-called “Standard Model” which summarizes the current understanding of particle physics. The debate as to whether light has a wave- or particle-like nature was a key issue in the physics of more than one century, and with both Newton and Einstein numbered amongst the participants. The answer, within quantum mechanics, is “both!”, since quanta of light (as well as all other quanta, including those usually thought of as particles) may exhibit wave- or particle-like properties depending upon the experiments being carried out. These quanta of light are, of course, photons.

In Quantum Electrodynamics (QED), photons arise from the breaking of $U(1)$ gauge symmetry and are responsible for electromagnetic interactions. In the generalisation to the electroweak theory embedded in the Standard Model, they still mediate the electromagnetic interaction, but are now a linear combination of the neutral bosons arising from the breaking of the $U(1)$ hypercharge and $SU(2)$ isospin symmetries, and acquire massive companions in the Z and W bosons.

If wave/particle and electroweak double identities were not enough for a single boson, yet another manifestation of the photon becomes dominant in high energy photoproduction. In many aspects, the photon appears very much like a hadron. That is, its interaction cross-sections behave (apart from a normalisation factor) very much like hadronic cross-sections, and at the highest energies the photon even appears to “contain” quarks and gluons, just as the proton or, more specifically, a vector meson, does. Because of this, photoproduction experiments have played an important role in the development of the strongly interacting sector of the Standard Model, Quantum Chromodynamics (QCD). This review thus contains much about QCD which touches on general hadronic physics.

High energy photon beams are generally generated by high energy electron or positron beams. High energy photoproduction was taken into a new regime by the HERA electron-proton collider, which, as the first lepton-hadron collider, dramatically extended the energy reach for photon-hadron as well as electron-hadron interactions.

Since the photon always carries less energy than the parent lepton beam, photoproduction experiments are rarely, if ever, at the energy frontier in terms of searches for new physics. Nevertheless, the large cross-sections and unique kinematics do mean that in several areas they still set the best limits on physics beyond the standard model. These cases are discussed in Section 5.

Also because of the symbiotic relation with electron beams, photon-photon collisions are an unavoidable feature of electron-positron colliders, both past and future. Providing information on the one hand on the general features of hadronic collisions, and on the

other on the interactions of the photon, photoproduction data are useful, and sometimes critical, for experimenters at the next generation of particle colliders, specifically the Large Hadron Collider at CERN and the International Linear electron-positron Collider currently under development. These connections, as well as those with cosmic-ray physics, are also explored herein.

2 Phenomenology of photoproduction

In this chapter we introduce the language and concepts needed to discuss high-energy photoproduction in term of the Standard Model (SM) of particle physics. Within the SM, the interactions of the photon should be describable using the language of fundamental fermions and gauge bosons. However, as described below, the strong interaction (QCD) plays an important part in photoproduction, and in QCD perturbative calculations are only possible in the region of asymptotic freedom, that is when a “hard” (short distance, high energy) scale is present in the problem. This is not always, or even usually, the case in high energy photoproduction, and thus other phenomenological ideas must also be used.

2.1 Total γp cross-section and “elastic” photoproduction

Photon-proton cross-sections at centre-of-mass energies above a few GeV have for many years been related to hadron-hadron cross-sections using the Vector Dominance model (VDM) [1,2]. The physics behind this is that since the photon couples to charged-fermion pairs, a part of its cross-section may be described by considering the interaction between a hadron and a virtual fermion pair. This part of the cross-section will on the face of it be suppressed by an additional coupling, since if considered perturbatively it is a higher order correction. For fermions which do not interact strongly this suppression is such that they do not greatly affect the total cross-section. However, for a $\gamma \rightarrow q\bar{q}$ splitting, the interactions between the quarks and a hadronic target are strong, the perturbative language does not work, and in fact this configuration in general dominates the total cross-section. A good picture of this is that the virtual $q\bar{q}$ pair radiates gluons and becomes a virtual, quasi-hadronic object with the same quantum numbers as the photon. A vector meson is very close to being such an object.

This picture is borne out in the data, shown in Fig. 1. Hadronic cross-sections may be fitted to a high precision in Regge phenomenology, in which the dominant contributions arise from Reggeon exchange, which falls with increasing centre-of-mass energy, and Pomeron exchange, which rises. Thus in this language, the high energy photoproduction cross-section is dominated by Pomeron exchange. In this model, the intercept of the Pomeron and Reggeon, which determine the energy dependence of the cross-section, are the same as those determined from hadron-hadron interactions. As an example, two such fits from Donnachie and Landshoff are shown in the figure. The 1992 fit predates HERA data and is made over the range $6 < \sqrt{s} < 20$ GeV. It has a single Pomeron term and a single Reggeon term. The 2004 fit includes HERA data (photoproduction, as well as DIS data for $Q^2 < 45$ GeV²) and allows an additional second Pomeron term. The difference

in this figure is small. The other curves in the figure are discussed in Section 2.2 below.

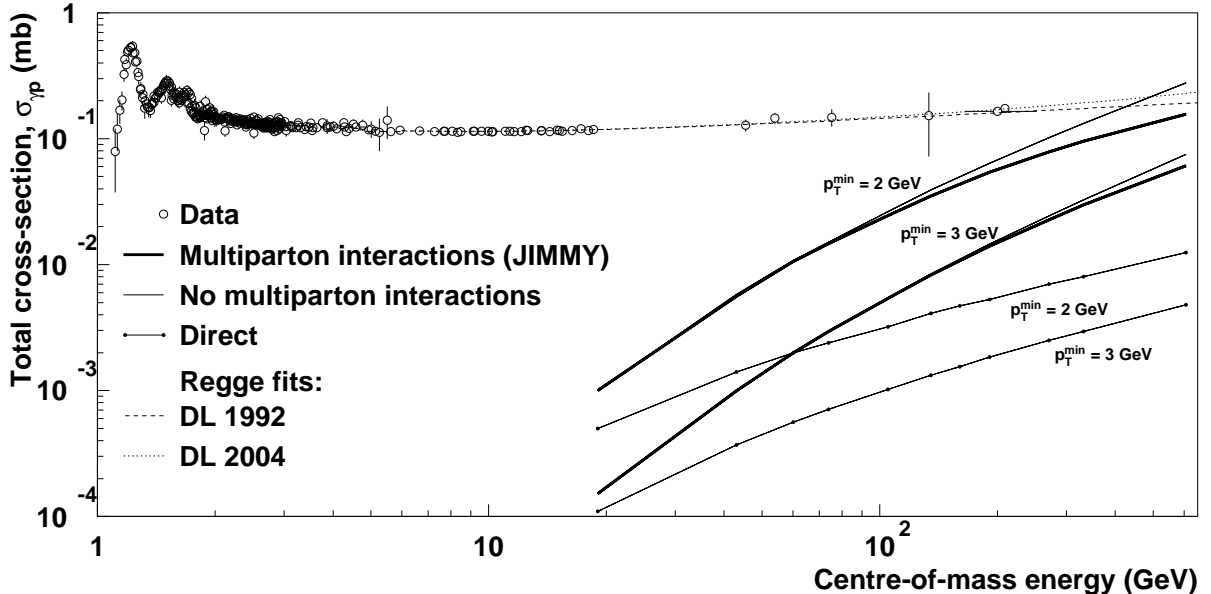


Figure 1: The total γp cross-section [3] compared to the predictions of various models. The Regge fits shown are those of Donnachie-Landshoff (1992 [4] and 2004 [5]).

Another application of the VDM is seen in the exclusive photoproduction of vector mesons, $\gamma p \rightarrow Vp$. In the language of the VDM, this is a quasi-elastic process in which the photon fluctuates into a virtual vector meson state which is then moved on mass-shell by the collision with the proton.

The photoproduction cross-section for several vector meson states is shown as a function of the photon-proton centre-of-mass energy, W , in Fig. 2. The inclusive cross-section is also shown. All the cross-sections rise with W . This is expected from Regge models where the cross-section is driven by Pomeron exchange between the vector meson and the proton. However, for high-mass vector mesons (J/ψ , Υ) where a hard transverse scale is available due to the vector meson mass, the cross-section rises more rapidly with W . This is explained in perturbative models [6] where the cross-section is partonic, and is dominated by gluon exchange. The strong rise is a direct result of the rapid rise in the gluon density in the proton [7].

This process is amenable to analysis and measurement as a function of several different energy scales (the vector meson mass, the photon virtuality Q^2 , W) and is a sensitive probe of the transition between soft and hard QCD. Information on the helicity structure of the interaction may be gained by studying the angular distributions of the decay products. The phenomenology of vector meson production in both DIS and photoproduction has

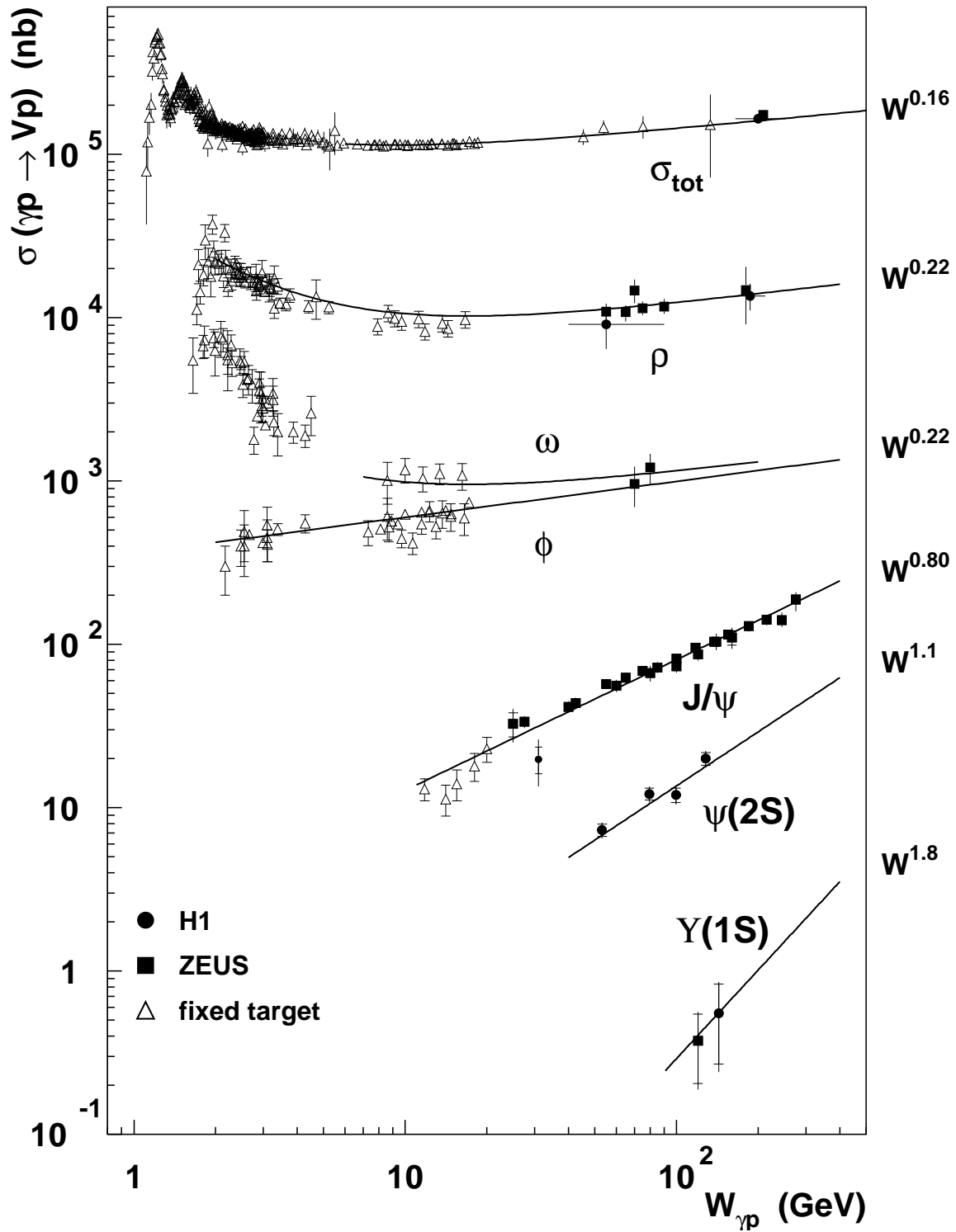


Figure 2: The total γp cross-section compared to the cross-sections [8] for exclusive vector meson production [9].

recently been reviewed elsewhere [10].

Exclusive vector meson production is a particular case of a diffractive process; that is a process where the proton loses a small fraction of its energy and either remains intact, or dissociates into a low-mass, forward-going, hadronic state. More inclusive diffractive cross-sections are discussed in Section 4.7.

2.2 Photoproduction and perturbative QCD

Since there is good agreement between the VDM and the data for total and low-mass-quasi-elastic cross-sections, it is clear that QCD effects, *i.e.* quarks and gluons, dominate the cross-section. Since the initial $\gamma \rightarrow q\bar{q}$ splitting may in general have very low virtuality, the interactions of the quarks will not be entirely perturbative, even if a hard scale is present somewhere in the process. This is a similar situation to that pertaining in hadron-hadron collisions, and the method for dealing with it is the same - the cross-section is factorised into a hard partonic cross-section and a parton distribution function (PDF). The soft (long distance) physics, as well as divergences associated with collinear emission of quarks and gluons, is collected in an effective photon structure, analogous to the parton distributions within the proton¹. A general schematic formula for perturbative QCD calculations of photoproduction processes may therefore be written;

$$d\sigma_{\gamma p \rightarrow X} = \sum_{a,b} \int_0^1 dx_\gamma \int_0^1 dx_p f_{a/\gamma}(x_\gamma, \mu_R, \mu_{F\gamma}) f_{b/p}(x_p, \mu_R, \mu_{Fp}) d\hat{\sigma}_{ab \rightarrow cd}(x_\gamma, x_p, \mu_R), \quad (1)$$

where x_γ and x_p are the longitudinal momentum fractions of the parton a in the photon and the parton b in the proton, respectively. The term $f_{a/\gamma}$ ($f_{b/p}$) represents the PDF of partons with flavour a (b) in the photon (proton). The factorisation scale for the photon (proton) is denoted by $\mu_{F\gamma}$ (μ_{Fp}), and μ_R is the renormalisation scale. The term $d\hat{\sigma}_{ab \rightarrow cd}$ is the hard (partonic) cross-section. This perturbative cross-section diverges at low values of the relative transverse momentum, p_T , of the scattered partons (c and d), and thus the whole expression is only valid for p_T above some minimum value \hat{p}_T^{min} . This means that the cross-section in Eq.1 is really only a part of the photon-proton cross-section; that part in which a hard scale resolves the parton structure of the proton and photon. Such processes are known as *resolved* processes. Soft scatters are not included.

Following on from the VDM, one might expect the parton densities $f_{a/\gamma}(x_\gamma, \mu_R, \mu_{F\gamma})$ to be essentially built out of those of the vector mesons into which the photon may fluctuate.

¹ for a recent review of the theory of hard photoproduction, see [11]

Indeed, this is the starting point for most models of photon structure. However, all such models must also take into account the fact that for any evolution of the structure with $\mu_{F\gamma}$, the $\gamma \rightarrow q\bar{q}$ splitting also plays a role. This term is of course absent in the vector meson case, and so gives rise to an additional contribution to resolved processes. This is referred to as the anomalous (or pointlike) component of the photon structure.

This component arises from the probability that the photon splits into a $q\bar{q}$ pair at a scale too high for the approximation to a bound vector meson state to work. Taking this further, the photon may in fact not split into a $q\bar{q}$ pair at any scale below that of the hard process being considered, and thus may enter directly into the hard matrix element of the calculation. To account for this possibility, terms are included in Eq.1 in which parton a is the photon, and $f_{a/\gamma}(x_\gamma, \mu_R, \mu_{F\gamma})$ is $\delta(1 - x_\gamma)$. Processes involving these terms are known as direct photoproduction.

The separation between *resolved* and *direct* processes, and the subdivision of resolved process into anomalous and VDM components, has more to do with the limitations of our ability to calculate QCD cross-sections than with fundamental physics. The separations are not unique and depend upon the approximations being employed in any given calculation. Nevertheless, as long as this is borne in mind, the labels are useful tools for exploring the complex world of photon physics.

In the above discussion, the transverse momentum of the scattered partons is taken to define the hard scale. In general, this hard scale can be provided by other aspects of the process, such as the mass of a heavy quark. This is discussed further in Section 4.3.

Two predictions using Eq.1 are shown in Fig. 1, for two different values of \hat{p}_T^{\min} and using the GRV LO [12] PDF sets for the photon and the CTEQ5 LO [13] PDFs for the proton. The hard contribution to the total cross-section depends very strongly on \hat{p}_T^{\min} . It is a small fraction of the total for centre-of-mass energies below around 100 GeV, but rises quickly as the energy increases. The contribution from direct processes is also shown separately.

2.3 Eikonal models and the underlying event

The effects of hadronic “remnants”, *i.e.* those parts of the proton or resolved photon which do not participate in the hard scatter, can be significant. Further interactions between the remnant may lead to activity in the final state which can disrupt the measurement of the short distance process of interest. The description of such effects is in general beyond the scope of perturbative QCD. However, perturbative ideas combined with other assumptions can be used to build models of such effects. The basic ideas of the eikonal model derive from the observation that for partonic scatters above some

minimum transverse momentum, \hat{p}_T^{min} , the values of the hadronic momentum fraction x which are probed decrease as the centre-of-mass energy, \sqrt{s} , increases. Since the proton structure function rises rapidly at small x , high parton densities are probed. Thus as discussed above and shown in Fig. 1, the perturbatively-calculated cross-section grows rapidly with \sqrt{s} . However, at such high densities, the probability of more than one partonic scattering in a single hadron-hadron event may become significant. Allowing such multiple scatters reduces the total cross-section, and increases the activity in the final state of the collisions.

An interesting historical aside is that some pQCD-based calculations [14–16] of the total cross-section, which were made before HERA data, showed that the photoproduction cross-section might, at high enough centre-of-mass energies (≈ 1 TeV, equivalent to a 1 PeV photon on a fixed target), be comparable to typical hadronic cross-sections (≈ 1 mb), and even to the cross-section for a photon to initiate an electromagnetic shower in air (≈ 100 mb). This was seen as a possible explanation for an observed excess [17] of muons in ultra-high-energy cosmic ray point sources. However, eikonal corrections were either absent or incorrectly implemented in these calculations, and the highest of them also made use of very singular parton densities in the photon. Most of them are inconsistent with the HERA measurements at 200 GeV (40 TeV equivalent fixed target). With more reasonable photon PDFs [15] and a correct application of eikonalisation [18], the models are consistent with HERA data, but do not allow a fast enough rise to explain the muon excess. In any case, the point source observations were not confirmed by subsequent experiments [19]. If the observed showers were not from point sources, there is no reason why they could not have been initiated by protons rather than hadrons, and so the puzzle goes away. Nevertheless, the photoproduction cross-section should be a significant input to simulations of high-energy cosmic-ray air-shower simulations.

In any case, the widely used models assume some distribution of the matter inside the hadron in impact parameter, b , space which is independent of the momentum fraction, x . The multiparton interaction rate is then calculated either

1. by using the cross-section for the hard subprocess, the conventional parton densities, and the area overlap function, $A(b)$ [20, 21]; or
2. by comparing the perturbative result with the Regge fit to derive a mean number of scatters, and using Poisson statistics to obtain the multiplicity distribution [22].

In the former approach, impact-parameter correlations are built in via the area overlap function. In the latter approach these are absent in the simplest model, but may be introduced by using more complicated matter distributions. More recent developments also fold in the parton showering in a scale-ordered manner [23].

The approach which does not use the Regge fit as an input reduces the hard scattering

contribution to the total cross-section, as shown in Fig.1. Comparisons of both types of model to data are discussed in Sections 3.1 and 4.7.

2.4 Jets and fragmentation

Due to colour confinement, quarks and gluons are never observed as free, final-state particles. When quarks or gluons are scattered with high momentum transfers, the observable results are “jets” of hadrons. Jets are defined and reconstructed by a variety of algorithms, all of which in one way or another identify hadrons which are close to each other in phase space, and whose bulk kinematic properties reflect the kinematics of the short-distance parton scatter.

Thus, jets with a transverse momentum $p_T > \hat{p}_T^{\min}$ should be present in a fraction of the photoproduction cross-section as discussed in the previous section. In addition, in eikonal models some events will have more than one jet pair. Several calculations exist of hard cross-sections in photoproduction, including leading-logarithmic parton-shower Monte Carlo programs [24–28] and next-to-leading order (NLO) partonic calculations of jets [29–33], hadrons [34, 35] and prompt photons [36–38]. The Monte Carlos give in general a more realistic final state, but are very unreliable in normalisation due to the fact that the matrix elements are currently leading order (LO). The NLO calculations are more accurate in normalisation but in general need to have corrections applied for hadronisation effects, and are less reliable in some event properties due to the fact that they only allow at most one parton radiation in addition to the primary jet pair.

Many measurements of photoproduction jet cross-sections have been made. These have led to many extensions in the understanding of QCD, the photon and the proton. These measurements and their consequences are discussed in detail in the subsequent sections.

2.5 Virtual photons

As mentioned previously, the highest energy photoproduction studies are all carried out with quasi-real, rather than real, photon beams. In this case the photoproduction regime is defined by some more-or-less arbitrary requirement on the maximum virtuality of the photon. Somewhere on the other side of this cut is the deep inelastic scattering regime. There is a lot to be learned by studying the transition between these two regimes.

In the hard photoproduction regime, the photon is probed at some scale μ by a hard process, for example jet production. As the photon virtuality approaches μ , it cannot develop structure on a scale large enough to be resolved by the hard process, and the photon structure therefore reduces to a perturbative splitting into a collinear $q\bar{q}$ pair (see

for example [11]). The development of photon structure between these extremes, and what it might tell us, is discussed in Section 3.4.

In the proton rest frame, the $q\bar{q}$ system is developed from the photon a long time before the interaction with the proton and may be considered as a dipole (see [39] and references therein). As photon virtuality increases, the average size of the interacting dipole decreases [40]. Therefore the probability of reabsorption, or rescattering, of any forward going particle (generally a proton or a neutron) is expected to decrease as Q^2 increases. This is discussed in Section 4.7.

3 The dual nature of the photon

3.1 Resolved and direct

Photoproduction occurs in a lepton-proton collider such as HERA when a quasi-real photon, emitted from the incoming positron, collides with a parton from the incoming proton. At HERA, the majority of photoproduction processes are peripheral collisions at low transverse momentum where the products of the collision continue in the general direction of travel of the incoming particles. However, as discussed in the previous chapter, in a subset of events short distance processes occur which involve a *hard* scatter and the production of jets. In *direct* photoproduction, the simplest such process, the photon acts as a pointlike object and couples to the quarks in the proton. As discussed in Section 2.2, the photon can also act as a source of partons, one or more of which interacts with a parton in the proton; this is called the *resolved* process.

Examples of hard scattering processes are shown in Fig. 3. High transverse momentum photoproduction processes are calculated to next-to-leading order in QCD. The photon structure describes the probability of finding a parton in the photon with a momentum fraction, x_γ , at a scale E_T . Parametrisations of the photon structure incorporate both the VDM and anomalous components. At high enough scales, the VDM component is negligible and the photon structure function can be fully calculated in QCD [41].

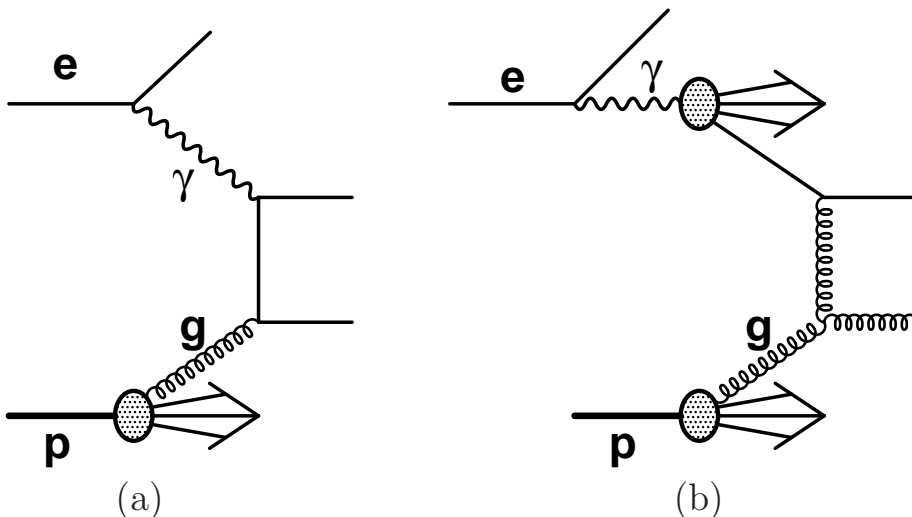


Figure 3: Examples of direct and resolved dijet photoproduction diagrams in LO QCD. (a) shows a boson-gluon fusion (BGF) process. The other direct process is QCD Compton scattering. (b) shows one of many possible resolved photon diagrams, which may involve quarks and gluons from the photon and the proton.

To test this perturbative picture, the direct component was searched for in photon-hadron

collisions by comparing the data with those from hadron-hadron collisions. The WA69 collaboration at CERN performed measurements of the charged particle distribution in photon-proton, pion-proton and kaon-proton collisions [42]. Fixed-target collisions for the different types of incident beam used the same experimental apparatus to measure the final state. The energy of the photon beam was varied between 110 and 170 GeV corresponding closely to the incident pion and kaon beam energy of 140 GeV. To compare the photon-beam data with that of hadron-beam data, the relative fraction of pion- and kaon-beam data was taken to be that expected for the strange and non-strange quark fraction in the photon. This corresponds to 40% kaon-beam and 60% pion-beam data.

The differential cross-sections for the production of charged particles as measured by the WA69 collaboration are shown in Fig. 4. The hadron-beam data is shown divided by a VDM factor of 215 and only the relative normalisations (not the absolute) are kept for the two sets of data in this figure. Both sets of data fall rapidly over about 7 orders of magnitude in the cross-section in the range of p_T between 0 and 4 GeV. At low momentum, the data sets show similar behaviour. However, the photon-proton data fall less rapidly than the hadron-proton data. This indicates that the photon-beam data contain a component in addition to the VDM contribution, the relative importance of which increases with increasing p_T . A similar measurement of the charged particle distribution in photoproduction was made by the H1 collaboration [43]. The measurement was performed at much larger centre-of-mass energies than those at WA69: $\sqrt{s_{\gamma p}} \approx 200$ GeV rather than $\sqrt{s_{\gamma p}} \approx 16$ GeV. The H1 measurement is compared to data from $\bar{p}p$ collisions measured by the UA1 experiment at a similar centre-of-mass energy of $\sqrt{s_{\bar{p}p}} \approx 200$ GeV. The two sets of data are also shown in Fig. 4 with the UA1 data normalised to the H1 data at $p_T = 1.5$ GeV. Both γp and $\bar{p}p$ data fall over many orders of magnitude in the cross-section and extend up to higher values of p_T than the WA69 data due to the larger centre-of-mass energy. The increased centre-of-mass energy also produces harder p_T spectra. As with the WA69 data, the γp data fall less rapidly with increasing p_T than the hadron-hadron collision data. This is again indicative of the QCD expectation that direct and anomalous processes are present in photoproduction, but absent in hadron-hadron collisions.

Evidence for hard photon scattering, in quantitative agreement with QCD calculations [44], had been observed in fixed-target experiments [42, 45]. Observing hard scattering in photoproduction was one of the first investigations performed at HERA [46]. Measurements of the total transverse energy in the event and the production of charged particles, similar to that in Fig 4, were made. The data were compared with theoretical predictions of soft interactions only, as well as predictions which included hard interactions, as implemented in the Monte Carlo models PYTHIA and HERWIG. The predictions for soft interactions were concentrated at low transverse energy of both the event and the charged particles.

With increasing transverse energy the prediction fell rapidly below the data by many orders of magnitude. With inclusion of the hard scattering component, both PYTHIA and HERWIG described the event and particle distributions well at high transverse energy.

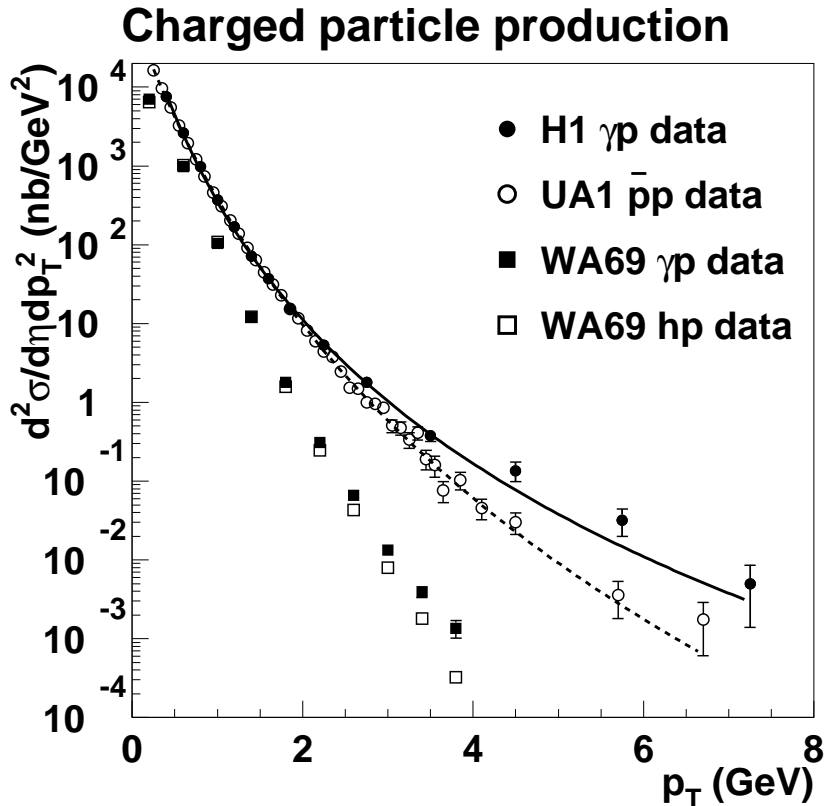


Figure 4: *Differential cross-section for the production of charged particles at a centre-of-mass energy $\sqrt{s_{\gamma p}} \approx 200$ GeV and $\sqrt{s_{p\bar{p}}} \approx 200$ GeV for the H1 and UA1 data, respectively. Curves of the functional form $A(1 + p_T/p_{T,0})^{-n}$ are fitted to the data. Also shown are data from WA69 at $\sqrt{s_{\gamma p}} \approx 16$ GeV and $\sqrt{s_{\text{hadronp}}} \approx 16$ GeV.*

The observation of hard-scattering led to the reconstruction of two back-to-back jets within events as expected from two-body scattering. The reconstruction of jets allows the kinematics and properties of the events to be investigated in more detail. A dijet sample was used to separate the contributions of direct and resolved photon processes [47].

In two-to-two parton scattering, the momenta of the incoming partons can be calculated from the momenta of the outgoing partons. Let x_p and x_γ be the fraction of momentum carried by the partons from the proton and photon, respectively. Conserving energy and momentum gives

$$x_p = \frac{\sum_{\text{partons}}(E + p_z)_{\text{partons}}}{2E_p}, \quad x_\gamma = \frac{\sum_{\text{partons}}(E - p_z)_{\text{partons}}}{2E_\gamma}$$

where E_γ is the initial photon momentum and the sum is over the two final state partons. For direct processes, $x_\gamma = 1$, whereas for resolved processes, $x_\gamma < 1$.

Obviously, partons cannot be measured, but hadronic jets provide a good approximation of their four-momenta. Experimentally, therefore, the quantity x_γ was reconstructed as

$$x_\gamma^{\text{meas}} = \frac{\sum_{\text{jets}}(E - p_z)_{\text{jets}}}{\sum_i(E - p_z)_i}$$

where $E_\gamma \approx yE_e \approx y_{\text{JB}}E_e$ and the sum in the denominator runs over all energy deposits in the calorimeter. The first measurement of this quantity is shown in Fig. 5 compared with expectations from the HERWIG Monte Carlo programme. The data exhibit a two-peak structure at high and low values of x_γ^{meas} . The Monte Carlo prediction gives a reasonable representation of the data when direct and resolved photon processes are added together. The direct and resolved components in the Monte Carlo have very different shapes. The resolved component describes the low x_γ^{meas} region reasonably well but cannot describe the data at high x_γ^{meas} . This data at high x_γ^{meas} can only be described with the inclusion of the component from direct processes. Hence these data constitute the first observation of direct processes in photoproduction.

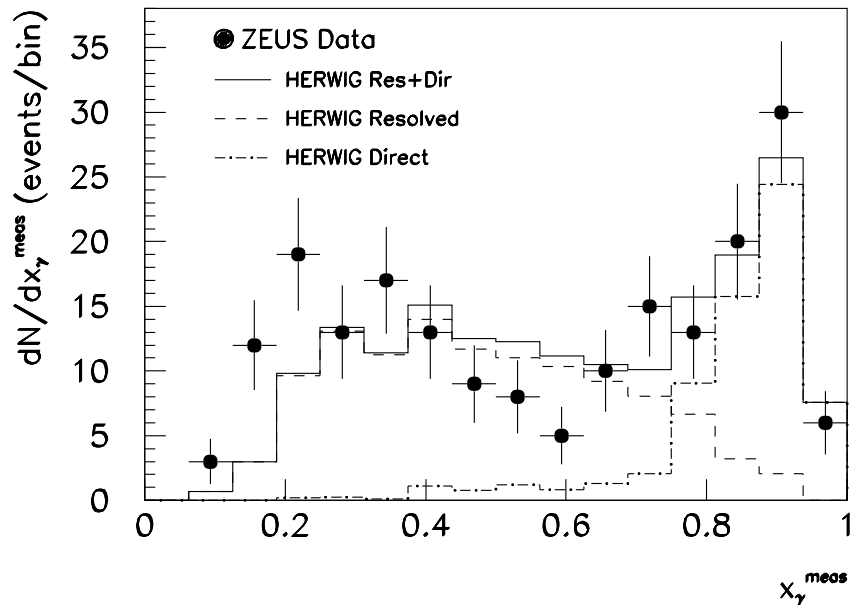


Figure 5: Measurement of x_γ^{meas} for events with two or more jets. The Monte Carlo prediction is shown fitted to the data. Taken from publication [47].

Resolved photon processes, like hadron-hadron collisions, have a more complicated structure than direct or deep inelastic scattering processes. As resolved photon processes are the effective collision of two composite objects, they are subject to extra unknowns from the structure of the photon (discussed in Sections 3.2 and 3.3), from the presence of the remnant of the photon and proton (left after the interacting partons have scattered), and from remnant-remnant interactions (or more generically the underlying event discussed in Section 2.3).

Although the point-like coupling of the photon to $q\bar{q}$ pairs is included in the parametrisations of the photon structure function, Monte Carlo simulations model the resolved photon as a hadron, with collinear incoming partons. This results in a photon remnant with low transverse momentum with respect to the beam-axis. Next-to-leading-order contributions of fluctuations of the photon into a $q\bar{q}$ pair with high virtuality may lead to a “photon remnant” which has sizeable transverse momentum with respect to the incident photon direction [48].

The photon remnant and its properties were studied by the ZEUS collaboration [49]. The photon remnant was isolated in two-jet events by requiring a cluster of low energy in the direction of the incident photon (electron) beam. The cluster exhibited a collimated energy flow with a limited transverse energy with respect to the cluster axis, characteristic of a jet structure. Indeed the cluster was compared with the other hard jets (assumed to come from the two-to-two scatter) in the event. Although the origin of these two types of jets may be different within statistics and the kinematic range studied, they exhibit similar properties for the energy flow and the transverse and longitudinal energy with respect to the jet axis. The η, p_T and energy distributions for this jet are shown in Fig. 6. The measured transverse momentum relative to the photon axis is $p_T = 2.1 \pm 0.2$ GeV, and is larger than that seen in the default HERWIG distribution, which generates the transverse momentum only via parton showers. Both PYTHIA (which includes intrinsic transverse momentum in the photon by default) and HERWIG with 1 GeV of such momentum added, give a better description of the data.

Early cross-section measurements [50, 51] showed discrepancies with predictions from Monte Carlo models, which were reduced with the inclusion of the possibility of secondary scatters. This underlying event (UE) or multiparton interaction (MPI) results from the collision of two composite objects and is a feature of hadron-hadron collisions (see Section 2.3). Examples of measured data compared with Monte Carlo predictions are shown in Fig. 7. The first measurement of a cross-section as a function of x_γ^{obs} is shown to be described by predictions which incorporate models for secondary scatters. The variable x_γ^{obs} [52] may be calculated to any order in QCD and for any final state, using energy deposits in a calorimeter, final state hadrons in a Monte Carlo simulation or partons in a QCD calculation. The quantity is defined as:

$$x_\gamma^{\text{obs}} = \frac{E_T^{\text{jet1}} e^{-\eta^{\text{jet1}}} + E_T^{\text{jet2}} e^{-\eta^{\text{jet2}}}}{2yE_e}.$$

The additional cross-section from the Monte Carlo MPI prediction is concentrated at low x_γ^{obs} and at high $\bar{\eta}$. However, in the MC models shown, it is not sufficient to describe the data in Fig. 7b.

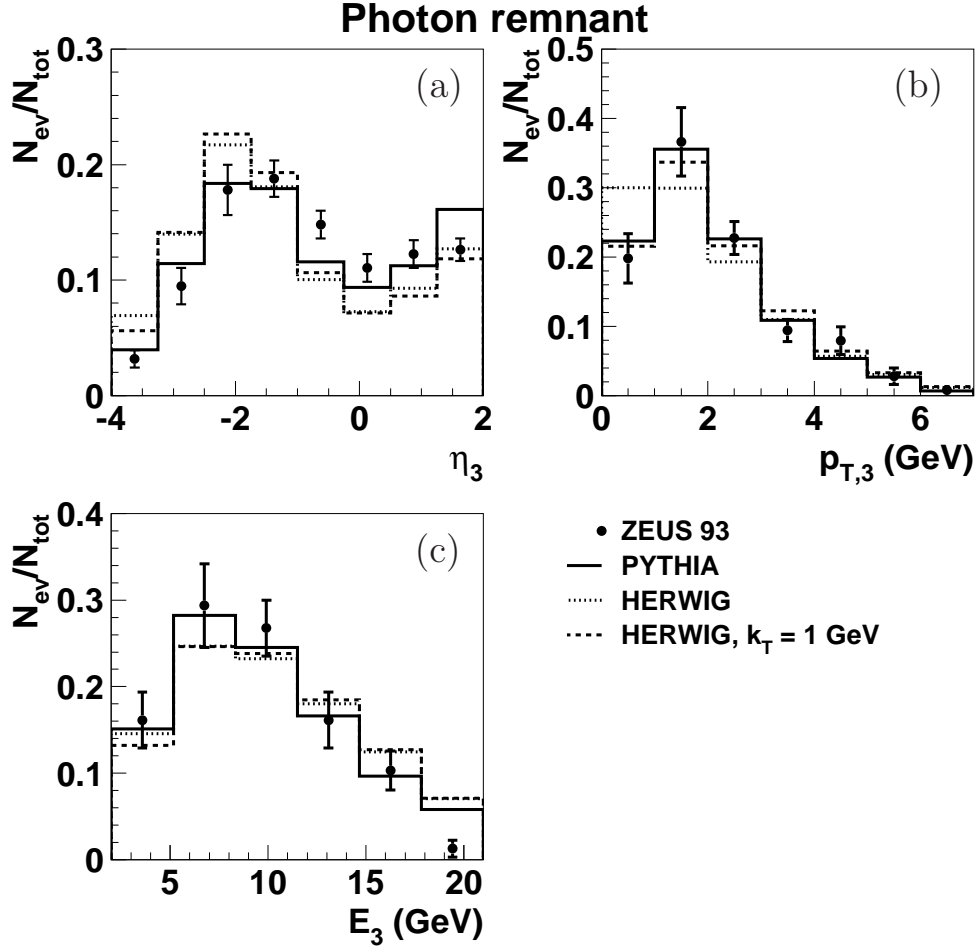


Figure 6: *Properties of the photon remnant [49]. (a) shows the the rapidity for the third jet (ordered in transverse energy) in events reconstructed using the K_\perp cluster algorithm. For (b) transverse momentum and (c) energy, the jet is required to have pseudorapidity $\eta < -1$, i.e. to be close to the photon direction. The default HERWIG distribution has no intrinsic K_\perp in the photon or proton, whereas PYTHIA has 1 GeV (Gaussian width) by default, as does the second HERWIG model (dashed lines).*

At the low transverse energies measured here, the corresponding x_γ value is low and hence the data are sensitive to the gluon distribution in the photon. However, to access

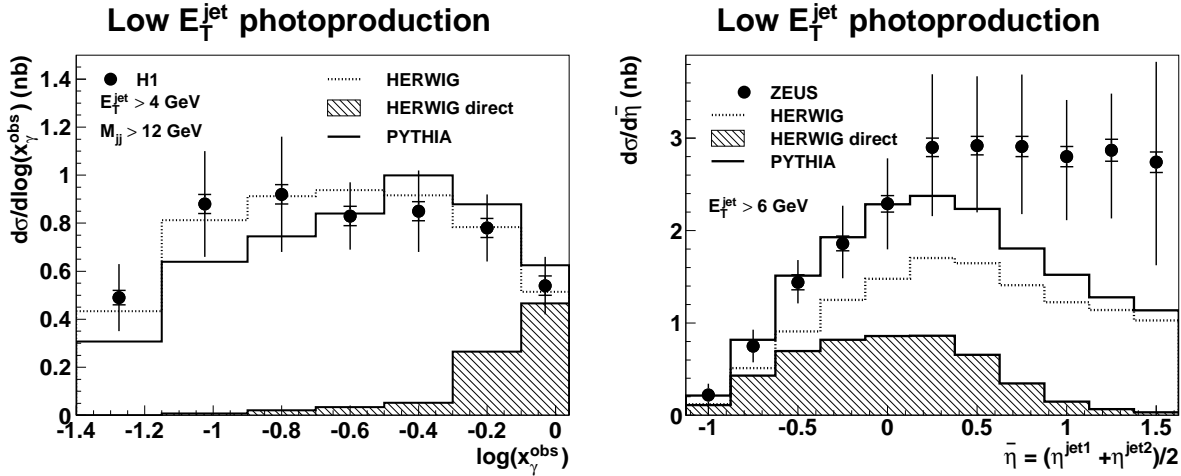


Figure 7: *H1* measurement of $d\sigma/dx_\gamma^{\text{obs}}$ at low E_T , and a *ZEUS* measurement of $d\sigma/d\bar{\eta}$ compared to various Monte Carlo models.

information on the photon structure, the nature of these secondary scatters has to be understood. Although their models generally improve the description of the data, there is as yet no definitive evidence for their occurrence in photoproduction. Investigations of these phenomena are discussed further in Section 4.7. A solution to extracting information on the photon structure without being affected by the underlying event is to make measurements at higher transverse energy where the effect is minimised.

3.2 Photon structure

The structure of the photon has traditionally been extracted from deep inelastic $e\gamma$ scattering at e^+e^- colliders (see [53] for a review). In this reaction, a virtual photon, emitted from the incoming electron or positron, probes the structure of the target photon. The range in scale of the interaction, Q^2 , depends on the centre-of-mass energy, \sqrt{s} of the collider, starting at a few GeV^2 and rising up to about 2000 GeV^2 for later LEP data taking. The corresponding range in momentum fraction of the parton, x_γ , is $0.001 < x_\gamma < 1$. The kinematic plane for LEP ($\sqrt{s} = 200 \text{ GeV}$) in x and Q^2 is shown in Fig. 8.

As discussed previously, photoproduction data from HERA are sensitive to the structure of the photon. Although the processes at the two colliders are different, the kinematic regions significantly overlap. The HERA data also extend to higher scales and, for low scales, to higher x as shown in Fig. 8. Note that, in the case of HERA, where the virtuality of the exchanged photon is small, the scale of the interaction is given by the p_T of the produced jets. Also shown in Fig. 8 is the kinematic region from a future e^+e^- linear collider. A similar detector coverage to those at LEP is assumed, hence the same

minimum x_γ , but higher Q^2 . The kinematic reach to high scales of the linear collider is significantly above that of LEP with HERA midway between. This demonstrates for the next 10 years the significance of HERA data in understanding the structure of the photon at high scales and its potential impact for studies at the linear collider.

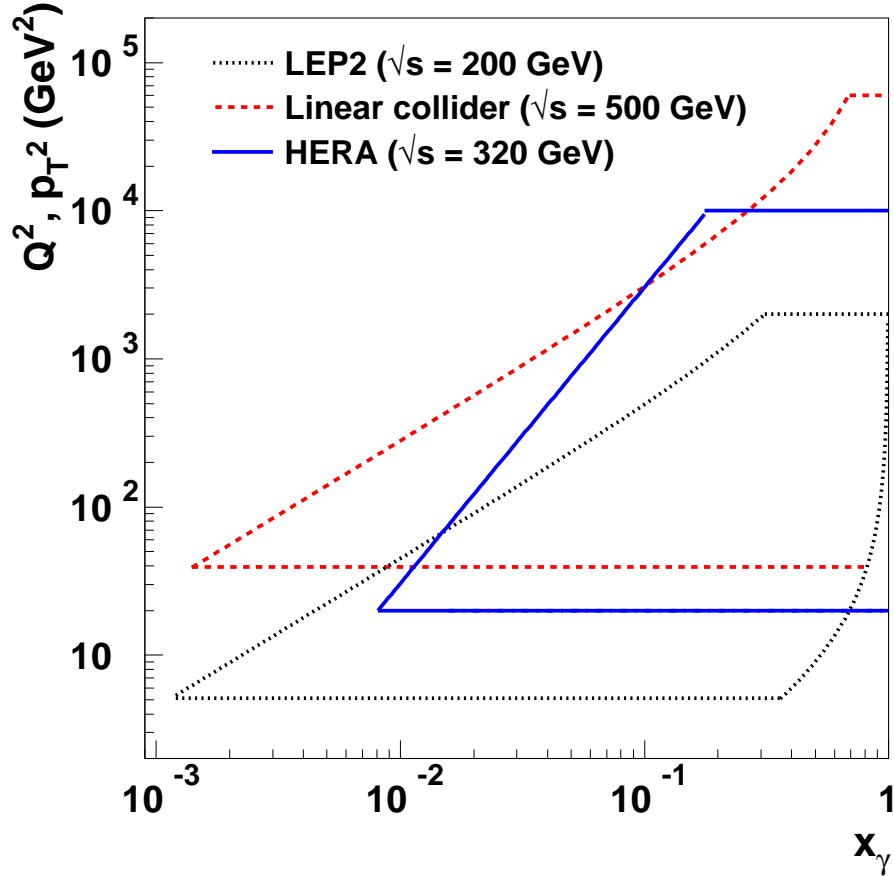


Figure 8: *The kinematic plane in Q^2 and x , showing the region of sensitivity of previous, current and possible future e^+e^- and γp experiments.*

The current status of measurements of F_2^γ from e^+e^- collisions is shown in Fig. 9 [53]. The data in Fig. 9a are generally flat as a function of x and the data from different experiments and colliders are broadly consistent with each other. At sufficiently low x , the gluon density is expected to dominate resulting in a rapid rise of the structure function with decreasing x . Unfortunately due to the precision of the measurements and coverage of the detector to investigate lower values of x this has not been demonstrated by these measurements, although they are consistent with the hypothesis as shown by the data at very lowest Q^2 and x . The data in Fig. 9b are shown to rise logarithmically as a function of Q^2 as expected from QCD [41]. This so-called asymptotic solution is shown to describe the rise in Q^2 . Such comparisons have lead to a rather competitive measurement of the

strong coupling constant α_s [54]. However, due to the accuracy of the data, the structure of the photon is not well constrained and has a significant uncertainty when extrapolated to the energies at a future linear collider.

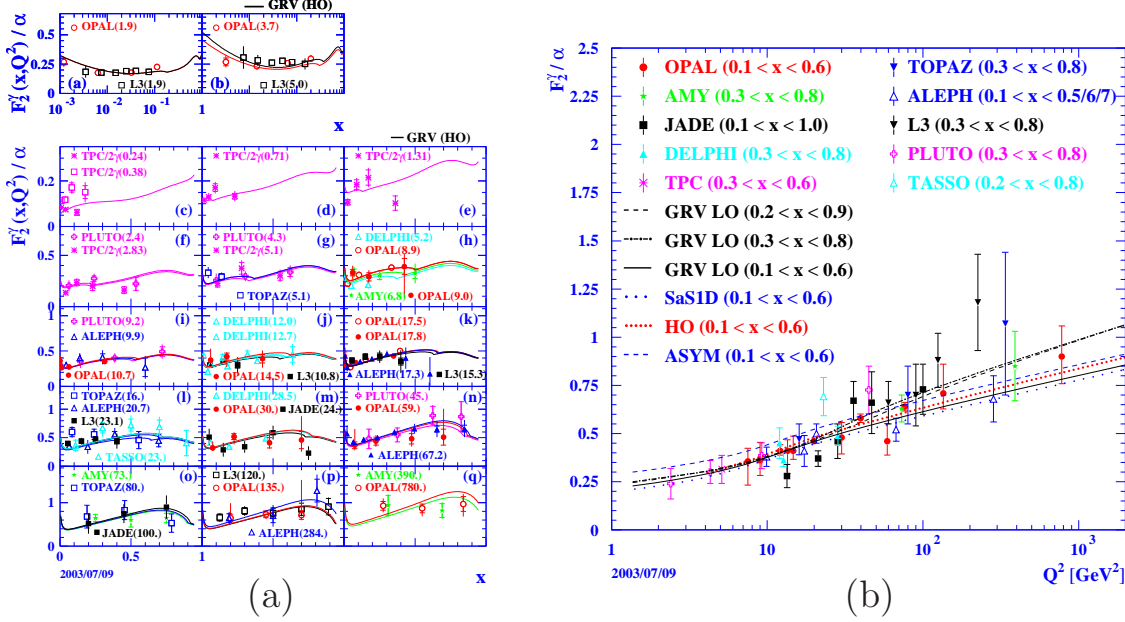


Figure 9: Measurements of the photon structure function, F_2^γ , as a function of (a) x for fixed values of Q^2 and (b) Q^2 for fixed values of x . Data from many experiments are shown compared with theoretical parametrisations derived from fits to a subset of the data. Taken from [53].

Measurements of photoproduction processes also provide valuable information on the structure of the photon because the gluon density of the photon is probed directly (see Fig. 10) rather than just the quark density as in the case of deep inelastic $e\gamma$ scattering. In fits to the photon structure function, F_2^γ , the gluon density is constrained via its contribution to the scaling violations.

In photoproduction F_2^γ is not measurable, since it is defined in terms of deep inelastic lepton-photon scattering. Sensitivity to the photon parton density functions (PDFs) is present in several measurable cross-sections, however. Thus, precision measurements in high-energy photoproduction can provide a test of QCD factorisation for the photon structure and constraints on the photon PDFs.

3.2.1 Jet photoproduction and photon structure

Jet cross-sections are sensitive to the structure of the photon and can be used to distinguish between parametrisations, although they are not as easily interpretable as F_2^γ since they

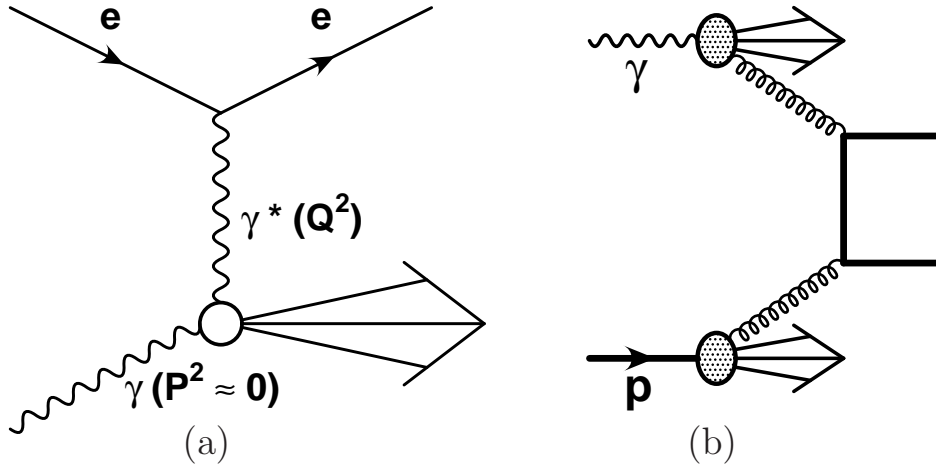


Figure 10: Feynman diagrams of (a) deep inelastic $e\gamma$ scattering in e^+e^- collisions and (b) gluon-gluon scattering in photoproduction.

are a convolution of the photon and proton parton densities and the short-distance matrix elements (see Eq.1). Alternatively the jet cross-sections could be fit along with F_2^γ in a fully consistent theoretical approach as has recently been performed for the proton, as discussed in Section 4.1.

A further complication in understanding jet cross-sections is the effect of the underlying event. This affects jet cross-sections most strongly at low transverse energies as discussed in Section 3.1. As the size and indeed nature of this effect is relatively unknown, constraining it and then being able to distinguish between different parametrisations of the photon structure is difficult. Therefore measurements are made in which sensitivity to the underlying event is drastically reduced; this is achieved by requiring jets of large transverse energy. This however has its disadvantages: the maximum possible range in scale, E_T^{jet} , and x is not explored; and the elimination of data at low E_T^{jet} and low x reduces sensitivity to the gluon density in the photon which is expected to dominate at low x . A solution to this problem would be to make measurements highly sensitive to the underlying event but weakly dependent on the photon structure. Using these constraints obtained for the underlying event, measurements at low E_T^{jet} which are sensitive to the photon structure could then be reinvestigated. However, this has not yet been performed so the best information currently attainable from HERA data is the comparison of NLO calculations with jet cross-sections at high transverse energies, above about 14 GeV as shown in Fig. 11 [55, 56].

The quantity x_γ^{obs} is shown in Fig. 11, measured for different regions of transverse energy of the leading jet. The data are compared with an NLO calculation using the three currently available parametrisations of the photon PDFs. It can be seen that within the large theoretical uncertainties at lower $E_T^{\text{jet}1}$ and both theoretical and experimental uncertainties at higher $E_T^{\text{jet}1}$ data and theory agree. However they exhibit a different shape

HERA dijet photoproduction

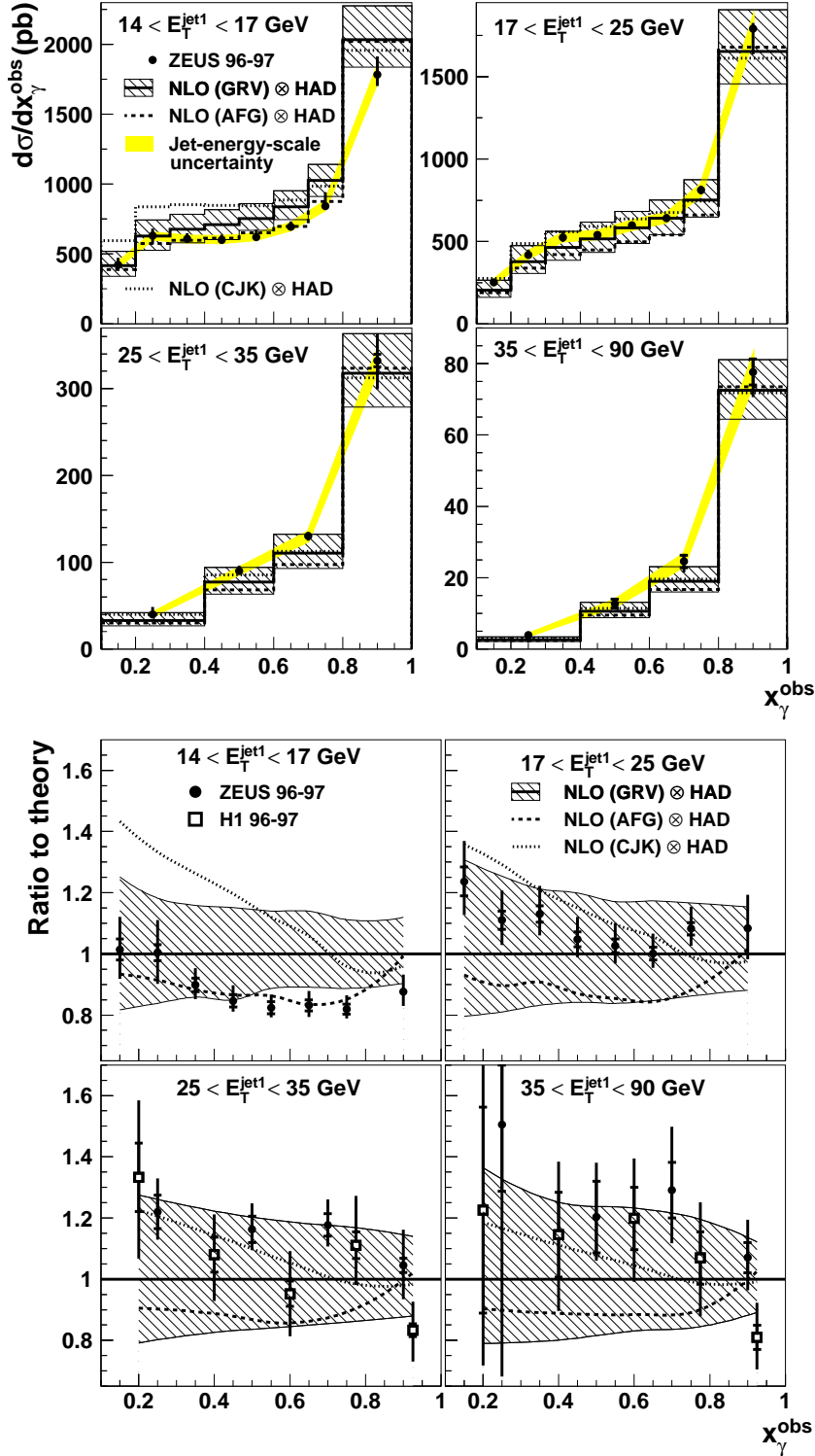


Figure 11: H1 and ZEUS measurements of $d\sigma/dx_\gamma^{\text{obs}}$ at high E_T^{jet} . The data [55,56] are compared to the NLO QCD program of Frixione and Ridolfi [30].

as a function of E_T^{jet1} ; the central theory prediction lies above the data at low E_T^{jet1} and below the data at high E_T^{jet1} . This results in preferring one photon PDF in one region of phase space and another PDF in a different region of phase space. The parametrisations AFG [57] and GRV [12] were fitted to similar data sets and used similar assumptions in their fit and hence give similar results. The result from CJK [58] is the newest² photon PDF using all data on F_2^γ and has a more careful treatment of heavy quarks. This parametrisation has a gluon density that rises faster to low x ; this is reflected in the larger cross-section at low x_γ^{obs} for low E_T^{jet} . As all three photon PDFs give a good description of the F_2^γ data, this demonstrates how poorly the data constrain the gluon density in the photon and how well the HERA data could constrain it. The average scale of the interaction measured here is also significantly larger than at LEP. The average E_T^2 for the highest transverse-energy region is about 2000 GeV². Measurements in bins of transverse energy extend up to about 5000 GeV². This and future HERA data could prove crucial in constraining the PDF at high scales and improve knowledge of the structure of the photon for physics at a linear collider.

The different trend with transverse energy in the data compared to that in the theory can be understood in terms of the effect of additional QCD radiation in the event. It should be noted that Monte Carlo predictions, which include multiple parton branching in the leading-logarithmic approximation, reproduce the transverse-energy dependence [55]. This can be explored by studying the requirement on the minimum transverse energy of the second jet. This is always 11 GeV, which means that in these distributions the difference between the cuts on the two jets varies from 3 GeV to 24 GeV. The difference in the transverse energies of the two jets is due to QCD radiation. The effect of the cut on the second jet was studied by fixing the cut on the first jet to be 25 GeV and varying that on the second jet from 11 GeV to 25 GeV. The (total) cross-section was then measured as a function of this cut [55]. The predictions of the shape of this distribution from $\mathcal{O}(\alpha_s^2)$ QCD are therefore the lowest non-trivial order predictions. The QCD predictions fall less rapidly at low $E_T^{\text{jet2,cut}}$ and more rapidly at high $E_T^{\text{jet2,cut}}$ than the data. This has been investigated further by considering the cross-section for regions of high and low x_γ^{obs} . For $x_\gamma^{\text{obs}} > 0.8$, the data and NLO QCD converge for low $E_T^{\text{jet2,cut}}$, both being reasonably insensitive to the cut and similar in shape. For the region $x_\gamma^{\text{obs}} < 0.8$, the predictions lie below the data at low $E_T^{\text{jet2,cut}}$, but within the theoretical uncertainties. By adjusting $E_T^{\text{jet2,cut}}$ separately in each E_T^{jet1} range, it would be possible to achieve agreement between the NLO prediction and the data. However, this seems to be a somewhat arbitrary procedure. This issue complicates the comparison with the photon PDFs and improved higher-order, or resummed, calculations would make the constraints more stringent.

² At the time of writing, two new parametrisations of the photon PDFs have become available [59] but have not yet been interfaced to the relevant QCD calculations.

3.2.2 Other final states as a probe of photon structure

Processes at HERA other than jet production can be measured which are sensitive to the structure of the photon. Of particular interest is the photoproduction of prompt photons which has been measured by both H1 and ZEUS collaborations [60, 61]. The process is dominated by the production of hard photons radiated by a quark from the proton. This is a well-understood process as the quark density in the proton is measured to high precision and the hard scatter is governed by QED; its measurement thereby provides a useful test of the assumed factorisation of the cross-section and quark density in the proton. The resolved processes, as with jet production, are a similar convolution of the proton and photon PDFs with the short-distance cross-section, but with fewer possible diagrams because of the requirement of a photon in the final state which is radiated by a quark. This advantage and also that of a cleaner experimental signature are outweighed by the small cross-section of this process. Current measurements are not of a high enough precision to distinguish between different parametrisations of the photon PDFs or constrain the quark density in the proton. The increased statistical sample expected at HERA II will prove invaluable.

Charged particle production also has a strong sensitivity to photon structure. Measuring charged particles [43, 62] is experimentally simpler than making measurements of jet cross-sections, but the price paid is an increased sensitivity to non-perturbative physics, in particular the fragmentation of quarks and gluons into hadrons. The sensitivity to the underlying event also remains a problem at low track momentum. An attempt has been made to estimate the gluon density in the photon at LO in QCD from such measurements [63]. A more sophisticated phenomenological technique and higher statistics at higher p_T could lead to interesting results in the future.

Photoproduction of lepton pairs via the Drell-Yan process has been discussed for some time as a process with the potential to provide information on photon structure [64]. However, the cross-section is rather small, and to date no measurement has been made. Within the full HERA I + II data sample, some few tens of events are expected per experiment in which both leptons are detected, and it seems likely that the background from Bethe-Heitler processes can be controlled, for example by requiring the presence of a photon remnant [65]. Thus after many years of waiting there is a real possibility that HERA could make the first measurement of this process. Such a measurement would at very least be a clear test factorisation. At best it would provide information on photon structure with systematics very different from jets; in particular, the absence of the hadronisation corrections associated with low E_T^{jet} jets may mean that this is the best method for studying low x_γ in photoproduction.

3.2.3 Photon structure and future experiments

Accurate constraints on the structure of the photon are vital for discovering new physics at a future linear collider. To be able to discover new physics at future colliders, the effects of conventional processes need to be understood. The discovery potential of both the Large Hadron Collider (LHC) and International Linear Collider (ILC) is enormous, but being able to see rarely-produced exotic events amongst, in particular, the copious events governed by QCD requires precise knowledge of the strong force. Current colliding-beam experiments can provide accurate measures of the ingredients of a QCD process: the structure of the incoming particles; the coupling strength of the strong force; the dynamics of the outgoing particles; and, more challengingly, “soft” physics not directly associated with the hard partonic scatter. In the absence of exact predictions from QCD, Monte Carlo generators are used to model the production of such processes and predict their rate at future colliders. The models often have many free parameters which can be constrained by tuning to measurements over a large phase space and, preferably, with different colliding objects.

Predictions for the production of jets of high transverse energy in $\gamma\gamma$ collisions at an e^+e^- linear collider are shown in Fig. 12 using the HERWIG Monte Carlo program. The background to new physics at high energy is large; about $(10^4 - 10^5)$ QCD events will be produced for a two-jet invariant mass above 100 GeV for a TESLA run of 500 fb^{-1} . Also shown are the ratios of the cross-sections for predictions using different PDFs or models of the underlying event to the default prediction. Differences between the four predictions from different PDFs are observed, although the SaS1D and SaS2D parametrisations are similar. However, particularly in the distribution of total transverse energy, E_T^{sum} , and missing transverse energy, E_T^{miss} , differences of over a factor of two exist between different PDFs. Since much of the data from LEP has been finalised, future constraints on the photon PDF, and hence reductions in the uncertainty of these backgrounds, can only come from HERA. Use of a different underlying event (see Section 2.3 for a discussion of the phenomenology): the JIMMY model for secondary hard scatters (default prediction); a soft underlying event; and no underlying event lead to much more significant differences. The cross-section in E_T^{sum} varies by up to almost an order of magnitude between models. Current understanding of such models from present data is discussed further in Section 4.7.

3.3 Where the photon structure comes from

Measurements of the cross-section of the angle between the jet-jet axis and the beam axis in the dijet centre-of-mass system, θ^* , have given insight into the nature of the sub-process and hence the “content” of the photon (and proton). The dependence of the dijet cross-

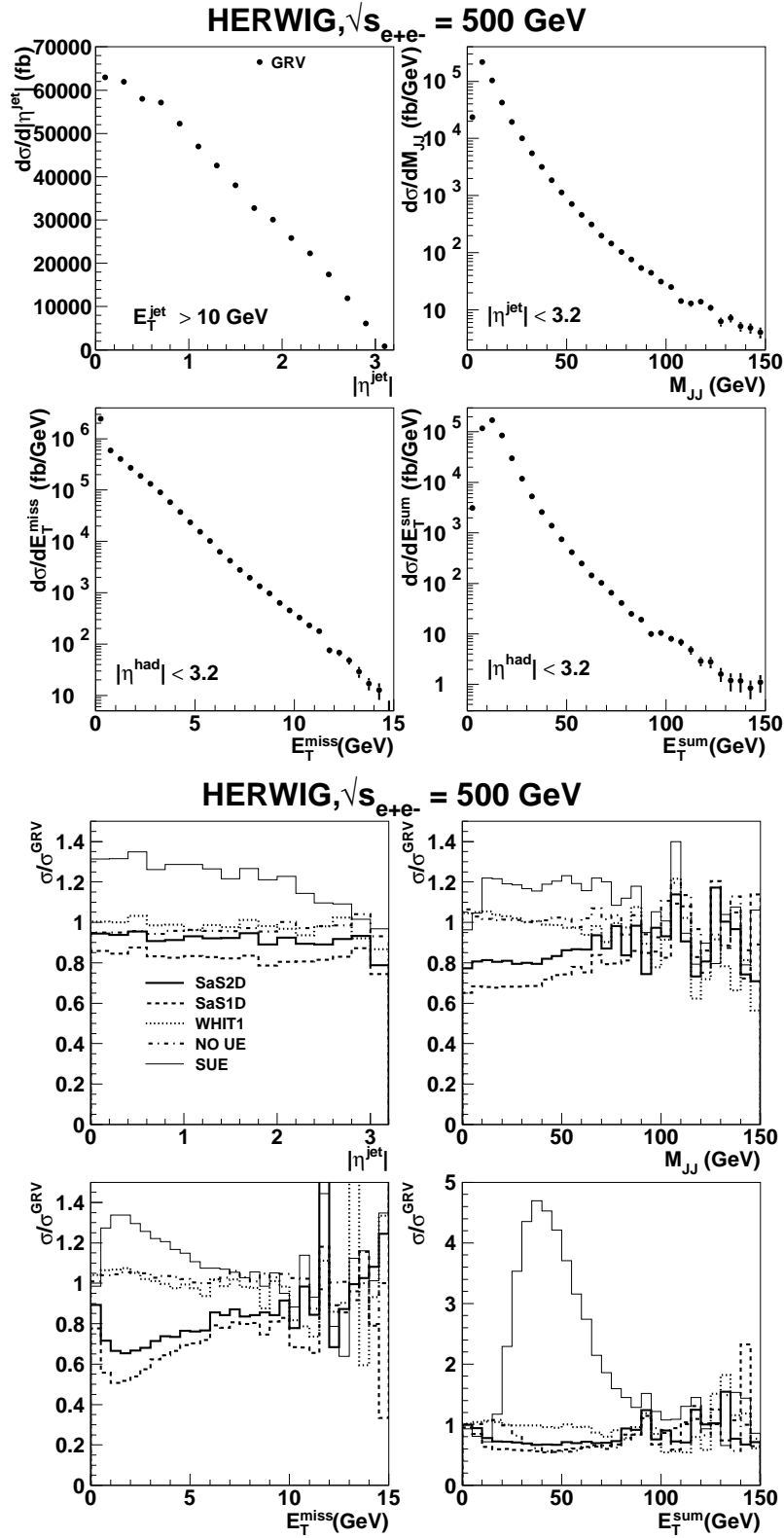


Figure 12: Predictions of cross-sections in $\gamma\gamma$ collisions at a future e^+e^- collider using the HERWIG Monte Carlo program (upper) and ratios to the default prediction using different parametrisations of the photon PDF or underlying event (lower).

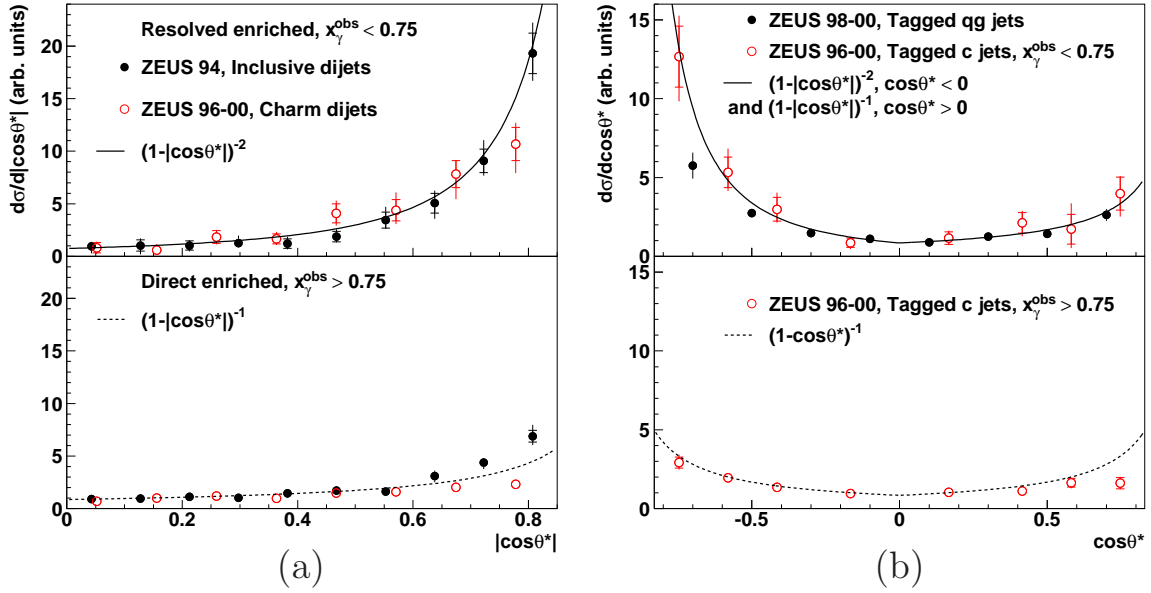


Figure 13: Angular distributions inclusively (solid points) and for charm (open points) for high and low x_γ^{obs} compared to simple analytic functions.

section on the cosine of the angle, $\cos\theta^*$, can be understood in terms of the propagator in the hard scatter. For direct photon processes where the dominant diagram is BGF, the angular dependence of the cross-section is approximately $\propto (1 - |\cos\theta^*|)^{-1}$ due to the spin-1/2 quark propagator. For resolved photon processes, which are dominated by processes with a spin-1 gluon propagator such as $qg \rightarrow qg$ and $gg \rightarrow gg$, the angular dependence is $\propto (1 - |\cos\theta^*|)^{-2}$.

The angular dependence of the cross-section was first studied inclusively in dijet photoproduction [66], where due to the indistinguishability of the two jets the modulus, $|\cos\theta^*|$, was measured. The measurement was performed at relatively low jet transverse energy, $E_T^{\text{jet}} > 6$ GeV, although an additional requirement on the mass of the dijet system, $M_{\text{jj}} > 23$ GeV, ensured that the effective energy was higher. The data were split into two regions, enhanced in direct photon ($x_\gamma^{\text{obs}} > 0.75$) and resolved photon ($x_\gamma^{\text{obs}} < 0.75$) events. The cross-sections were found to be well described by LO and NLO QCD calculations [66] and are shown in Fig. 13a compared with the simple analytic functions expected from the dominant propagator. The cross-section for the sample enriched in resolved photon events rises more rapidly than that for the sample enriched in direct photon events. The function $(1 - |\cos\theta^*|)^{-2}$ describes the low x_γ^{obs} data well. For high x_γ^{obs} , the data are reasonably well described by the function $(1 - |\cos\theta^*|)^{-1}$. The somewhat steeper rise of the data could be due to contamination of resolved photon events. The data clearly demonstrate the dominance of gluon and quark propagators in resolved and direct photon events, respectively. These trends were also seen at higher transverse energies and masses [55].

A measurement of dijet production in the presence of charm [67] demonstrated a significant cross-section at low x_γ^{obs} . Within the framework of Monte Carlo predictions, this was explained as arising from a large resolved-photon component dominated by charm in the photon's structure function. This interpretation was investigated further by measuring dijet angular distributions in events containing a charm quark reconstructed by tagging a D^* meson [68]. The dijet angular distributions were measured in a similar energy range ($E_T^{\text{jet}} > 5$ GeV and $M_{\text{jj}} > 18$ GeV) to that for inclusive dijet production and the data were again split into samples enriched in direct and resolved photon events by applying the same cut on x_γ^{obs} . The data are shown in Fig. 13a compared with the inclusive data and analytic functions. The charm data exhibits similar behaviour to that of the inclusive data and is well described by the two functions. The differences at high $|\cos\theta^*|$ between the data and the function can be explained by a small bias due to angular cuts on the D^* meson which are well reproduced by QCD calculations [68]. In fact for high x_γ^{obs} , the charm data agrees better with the function than does the inclusive data. The charm data in this region constitutes a purer sample of BGF processes, since QCD Compton events are heavily suppressed by the fact that the charm content of the proton is much smaller than the gluon content. Calculations performed at NLO in QCD describe the data in this region well. The data at low x_γ^{obs} indicate that the dominant process has a gluon propagator. The data at low x_γ^{obs} are not well described by an NLO calculation which does not have a charm component in the photon PDF. This suggests that the photon has significant component in which the photon splits into a $c\bar{c}$ pair.

By tagging one jet as arising from a charm quark, the sign of the angle can be measured. The tagged D^* meson is associated with one of the jets and the scattering angle of this jet defined with respect to the proton direction. The data are shown in Fig. 13b in the two regions of x_γ^{obs} . The angular distribution, enriched in direct photon processes ($x_\gamma^{\text{obs}} > 0.75$) exhibits a symmetric distribution with a shallow rise to high values of $\cos\theta^*$. This is indicative of the exchange of a quark in the hard sub-process with the charm produced via the boson-gluon fusion process. At low x_γ^{obs} , where the sample is enriched in resolved photon processes, the data are asymmetric, exhibiting a rapid rise to negative $\cos\theta^*$. This demonstrates that the charm comes from the photon and exchanges a gluon in the hard process. The shallow rise to positive $\cos\theta^*$ is consistent with the exchange of the charm quark itself.

Also shown compared to the charm jets at low x_γ^{obs} are dijets tagged as a quark and a gluon [69]. No flavour requirement is made for this quark which is defined with respect to the proton direction. This measurement has been performed at higher transverse energy and mass to reduce the effect of the underlying event. The jets are tagged by considering the different jet substructure for quark and gluon jets. As gluons radiate more than quarks, gluon-initiated jets are expected to be broader than those initiated by quarks.

Therefore a sample of events enriched in one quark and one gluon jet is achieved by requiring one broad and one narrow jet (see Section 4.5). The purity is 52% with the largest contamination from $q\bar{q}$ events. It should be noted that for the tagged qg events, there is no cut on x_γ^{obs} ; such a cut would improve the purity of the sample but also reduce statistics. The data show similar behaviour to the charm data and are reasonably well described by the function, although the large background results in a shallower rise at high negative $\cos\theta^*$. The consistency of the two sets of data confirms that the charm is coming from the photon.

3.4 Virtual photon structure

The evolution of the jet cross-section with the photon virtuality, Q^2 , can provide information [70–73] on the structure of the photon. As discussed in Section 2.5, the region above Q^2 of about 1 GeV^2 is (somewhat arbitrarily) defined as the domain of deep inelastic scattering. If no other hard scales are present, the photon acts as a pointlike probe. However, since the jets also provide a hard scale, there is a complex situation between the limit $(E_T^{\text{jet}})^2 \gg \Lambda_{\text{QCD}}^2 > Q^2$ (definitely photoproduction) and $Q^2 \gg (E_T^{\text{jet}})^2, Q^2 \gg \Lambda_{\text{QCD}}^2$ (definitely deep inelastic scattering). In particular, for the configuration $(E_T^{\text{jet}})^2 \gg Q^2 \gg \Lambda_{\text{QCD}}^2$, the virtuality of the photon regulates the collinear singularity in the photon structure and in principle the process is perturbatively calculable. In practice, large logarithms in the ratio of the scales given by E_T^{jet} and Q may be present and a resummation may be required to restore convergence of the perturbative series. It seems reasonable to suppose that such a resummation could take the form of a completely perturbative virtual photon structure. Amongst other things, this could offer a rather accurate determination of α_s , one of the original goals of real photon structure measurements. Unfortunately, despite some advances in this direction [74], no complete NLO calculation is currently available and the data are compared either to LO ansätze [75] or to conventional NLO calculations for deep inelastic scattering or photoproduction.

The H1 collaboration have measured triple differential cross-sections as a function Q^2 , E_T^{jet} and x_γ^{obs} shown in Fig. 14. A similar measurement by the ZEUS collaboration [71] was also presented as the ratio of the dijet cross-sections for low and high x_γ^{obs} as a function of Q^2 . This ratio was also measured in the photoproduction region *i.e.* down to $Q^2 \sim 0$. The fraction of the low x_γ^{obs} cross-section decreases with increasing Q^2 for all values of E_T^{jet} . However, the fall becomes less rapid as E_T^{jet} increases. These trends are generally reproduced by leading-logarithmic parton-shower Monte Carlo models (not shown) which introduce a virtual photon structure both transversely and longitudinally [76] polarised, suppressed with increasing Q^2 . NLO photoproduction calculations are consistent with the low Q^2 data [71]. However, the cross-section is not well-reproduced by deep inelastic

scattering NLO calculations for $Q^2 > 1 - 2 \text{ GeV}^2$. These calculations, which assume no explicit photon structure, have large uncertainties at low Q^2 and generally underestimate the data. Such effects may well be a sign of the large logarithms mentioned above. A NLO calculation, JETVIP [74], incorporating processes with a virtual photon is also shown in Fig. 14. This improves the description of the data significantly. However, the calculation is sensitive to a technical parameter in the calculation and so is not reliable. The best description [77] of the data is achieved by a NLO calculation for three-jet production, which has a significant cross-section at low x_γ^{obs} . This demonstrates the sensitivity of this cross-section to higher-order effects and the need for a full calculation including a virtual photon.

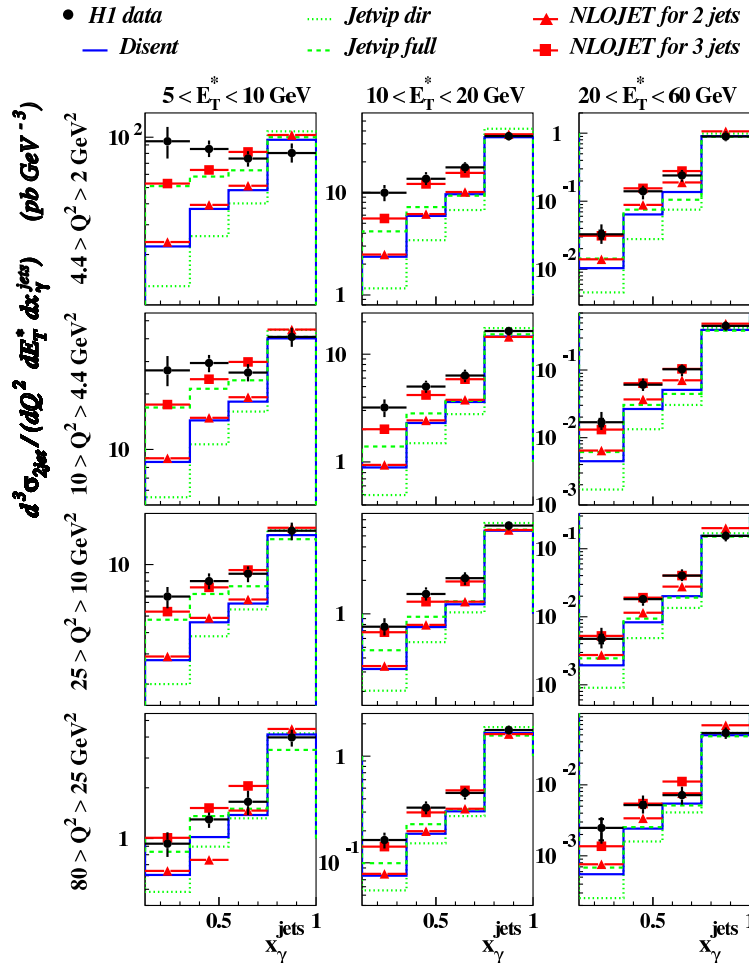


Figure 14: Triple differential cross section [70] compared to NLO calculations containing only direct photon processes, DISENT (full line) and JETVIP (dotted line), the sum of direct and resolved photon processes, JETVIP (dashed line) and for NLOJET for two- (triangles) and three-jet (squares) production, NLOJET. Taken from [77].

The ratio of the cross-sections for low and high x_γ^{obs} has also been studied [78, 79] for a more exclusive process where the event contains at least one charm quark, by tagging a D^* meson. The result for charm is then compared to the previous inclusive (*i.e.* all quark flavours) result in Fig. 15. The result is, however, complicated by the D^* meson which adds an extra kinematic constraint on one of the jets not present in the inclusive sample. This can only be corrected for using a Monte Carlo model; after this correction, the conclusions still remain the same. A difference is evident in the presence of charm; the ratio is flat as a function of Q^2 and in the photoproduction region lies well below the inclusive data. This can be understood in terms of the effect of the extra scale, the charm mass, which in addition to Q and E_T leads to a suppression of the photon structure.

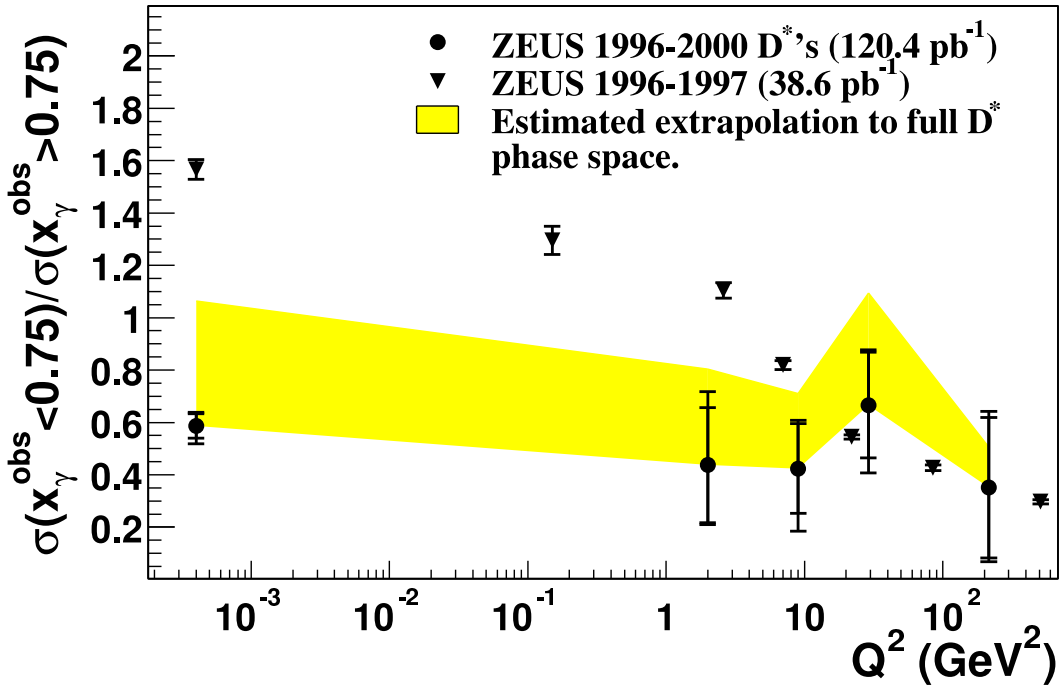


Figure 15: Dependence of the ratio of low- to high- x_γ^{obs} cross-sections on the virtuality of the incoming photon for inclusive (triangles) and charm (dots) dijet production (taken from [79]).

4 Photoproduction and QCD

Given the double identity of the photon as a fundamental gauge boson and a hadron-like object, studies of photoproduction reactions provide a number of unique opportunities for exploring QCD. Combining data from photon-proton collisions with deep inelastic scattering (DIS), photon-photon and proton-(anti)proton collisions can be a particularly fruitful exercise. In this chapter we explore the major areas in QCD where photoproduction data have had such an impact.

4.1 Proton structure

The parton densities in the proton constitute one of the best windows onto the physics of the strong interaction. They encapsulate the behaviour of quarks and gluons over a huge range of distance scales and densities, and their scale dependence provides one of the most precise measurements of the strong coupling, α_s . In addition, parton densities are a crucial input to all cross-section calculations at proton colliders. Finally, measurements of a range of different cross-sections at hadron colliders, all of which make use of the same parton densities, provide one of the most stringent tests of QCD, and in particular of factorisation.

As with photon structure (see Section 3.2), the principle measurements used to extract information of the proton's parton density function (PDF) are measurements of the structure functions in DIS, in particular the structure function F_2 . These data are fitted by several groups [80–85] using the conventional DGLAP evolution equations. Put simply, this approach makes no prediction as to the x dependence of the PDFs (apart from information indirectly derived from the conservation of momentum) but for Q^2 sufficiently above Λ_{QCD}^2 the Q^2 dependence (*i.e.* the scaling violation) is accurately predicted. Fits are currently carried out to NLO accuracy. However, the full calculation of the DGLAP evolution to NNLO has recently been performed [86]. This shows that the perturbative series converges well and that in most cases the NLO approach is rather a good approximation.

Measurements of F_2 are only directly sensitive to the quark densities. The gluon density is obtained from the fits since gluon radiation from quarks, as well as gluon splitting to quarks, drives the scaling violations. Nevertheless, measurements which are more directly sensitive to the gluon density are important, partly to test the QCD picture but also because they potentially have a sensitivity to higher x than do extractions based on scaling violations. Since high- x gluons are responsible for a big fraction of the highest energy collisions in the world (currently at the Tevatron and soon at the LHC), the high- x gluon density is a very important object to pin down.

Prompt photons and high transverse energy (E_T^{jet}) jets are two processes which have been used in fits to help constrain the gluon. However, theoretical uncertainties (in the case of prompt photons) and experimental uncertainties (in the case of jets) have limited the impact of these data. In addition, high- E_T^{jet} jet cross-sections at the Tevatron are sensitive to new physics, and much of this sensitivity is lost if the data is simply used to fit the gluon density [87].

High E_T^{jet} jet photoproduction is also directly sensitive to the gluon density in the proton. For direct photon events, this is via the boson-gluon fusion diagram, Fig. 3a. Resolved events are also sensitive (Fig. 3b) but the situation here is complicated by the photon PDFs, which are less well known than those of the proton. At high transverse energies (which also means high x) the uncertainties due to hadronisation and underlying events are also rather small.

Figure 16 shows the parton kinematics for several experiments. The region over which jet measurements in photoproduction at HERA constrain the gluon density is shown, as well as the regions where Tevatron and HERA DIS measurements provide constraints. The HERA DIS data, as well as fixed target data, extend to higher x and Q^2 than shown, but give little constraint on the gluon in that region. The region over which the LHC is sensitive to the gluon density is also shown. However over much of this region, actual measurement of the gluon at the LHC will be extremely difficult since the main sensitivity is at low E_T^{jet} , where other uncertainties due to hadronisation and the underlying event are important.

The ZEUS collaboration has published [82] the first QCD fits which incorporate jet photoproduction data [55] (as well as DIS jet data [88]). The inclusion significantly reduces the uncertainties on the gluon density at intermediate and high x , as shown in Fig. 17. This is a graphic demonstration of the power of high energy photoproduction data, but is not the full story. The data set used in these results was taken in 1996-1997, and is statistically limited at high E_T^{jet} , the kinematic region corresponding to high x . This is only around a third of the HERA I data set; HERA II should increase this again by a factor of around 5.

As well as simply using more data, the constraint on the gluon density could also be improved by optimising the cross-section for sensitivity to the high x gluon by (for example) extending to the forward region. In such studies [89] it has also been observed that resolved photon cross-sections exhibit a large sensitivity to the gluon in the proton. For the existing cross-sections, including the low- x_γ^{obs} cross-sections in the fit reduces the statistical errors, but increases the systematic errors due to the uncertainties associated with the photon structure, so that there is no net benefit [82]. Currently no NLO fit for the photon structure with full uncertainties exists, and so even this statement is an estimate. Obviously, a combined NLO QCD fit to the proton and the photon PDFs would bring

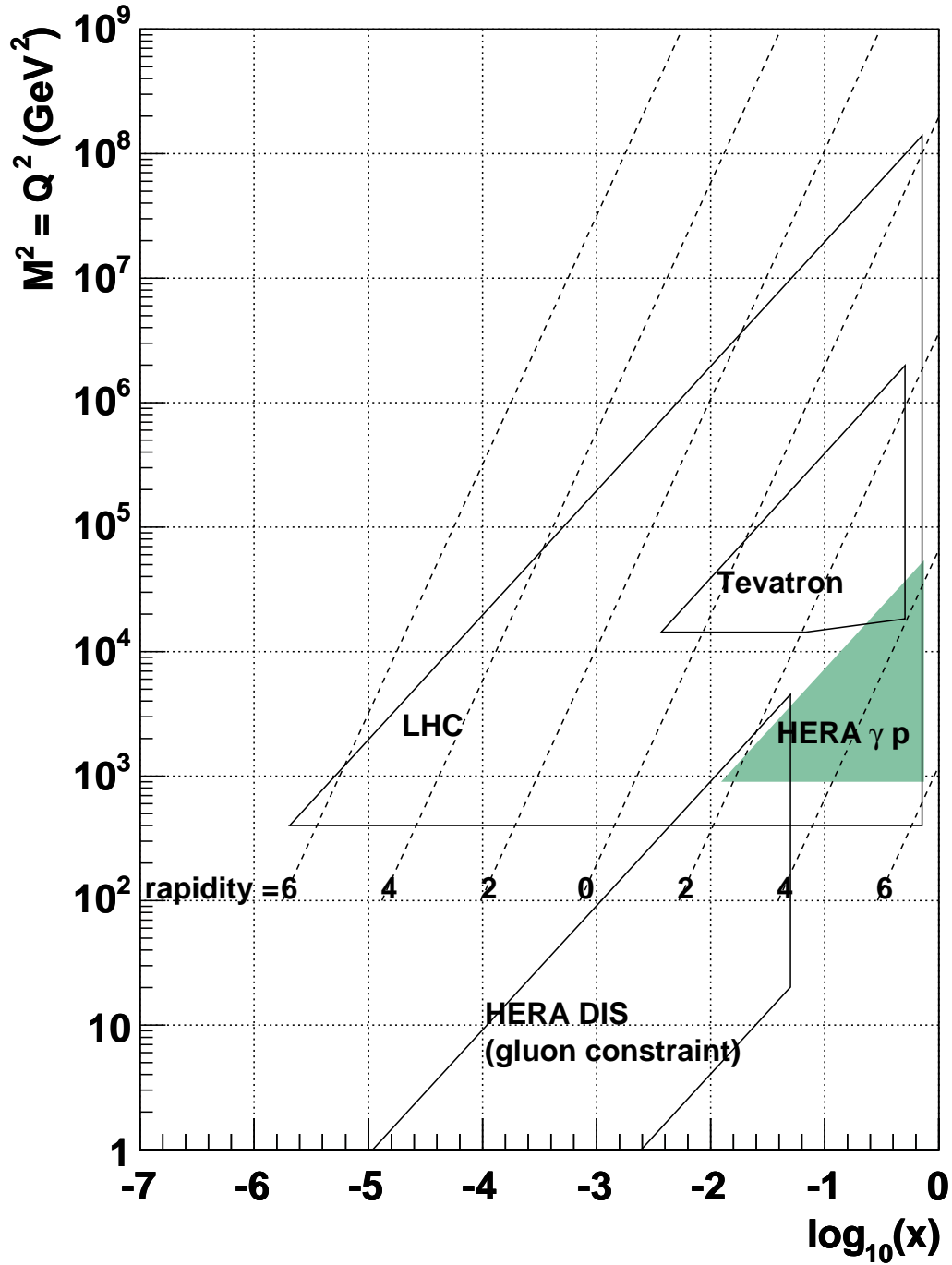


Figure 16: The parton kinematic plane. The approximate regions in which the gluon in the proton is constrained by various experiments are shown, as well as the whole region of sensitivity at the LHC. The variable $M^2 = Q^2$ is the dijet mass for LHC, Tevatron and photoproduction, and the negative four-momentum-transfer-squared for DIS. The dashed lines show the rapidity of the dijet system at the LHC. The assumptions are that precise jet measurements are possible down to $E_T = 60 \text{ GeV}$, $\eta = 2.0$ at Tevatron. The HERA jet region is taken from [55].

great benefits. Finally, it is also possible to determine α_s from such fits, as is discussed in Section 4.2.

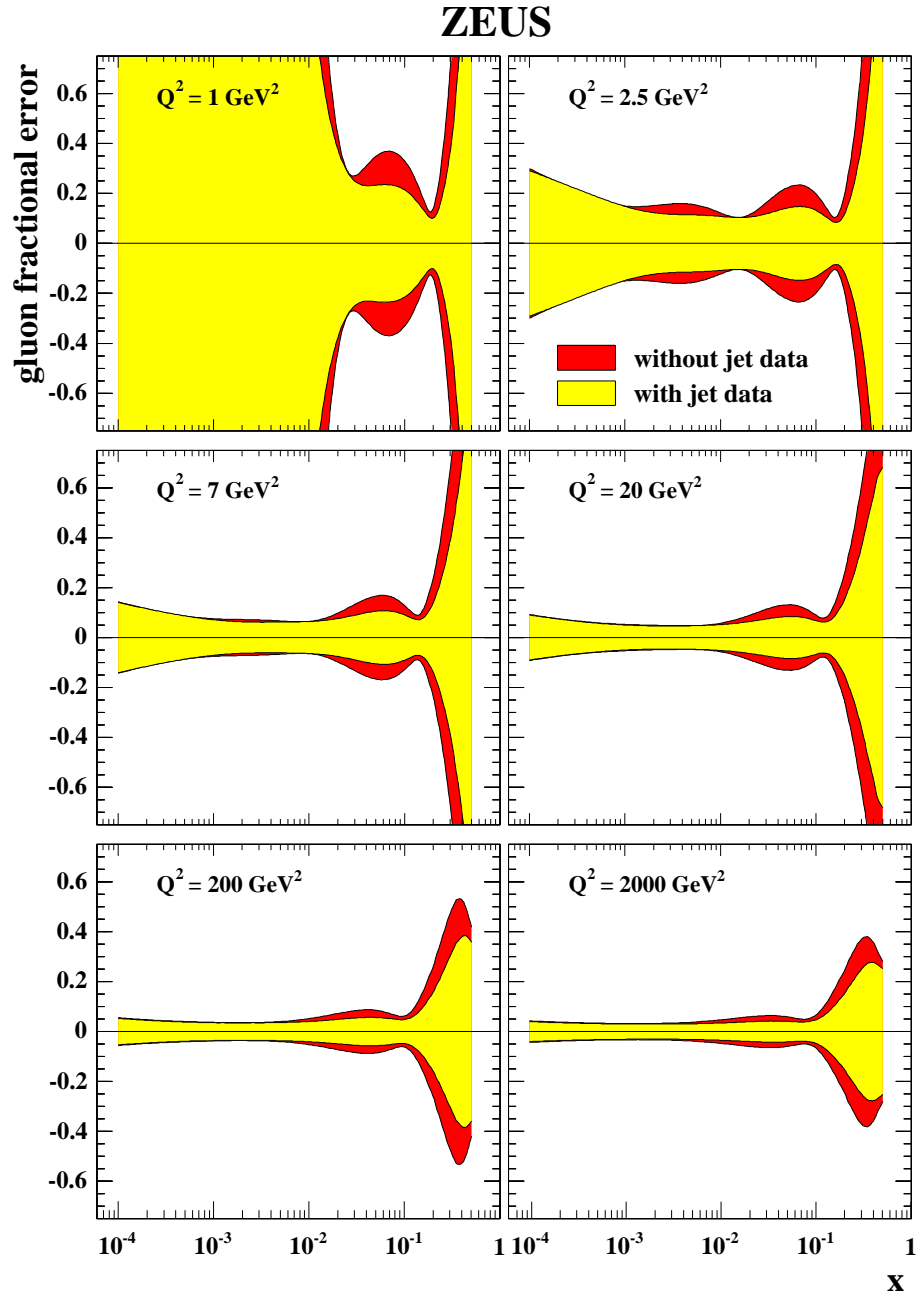


Figure 17: *The fractional uncertainty in the gluon PDF before (outer+inner shaded areas) and after (inner shaded area) the inclusion of DIS and photoproduction jet data in the QCD fit [82].*

It is to be hoped that these possibilities will be vigorously pursued by the fitting groups and experimental collaborations during HERA II. The whole topic of parton distributions

and their uncertainties is a very active area at present. Reviews and recent developments may be found elsewhere [90, 91].

4.2 Measurement of the strong coupling constant

According to QCD, jet cross-sections should exhibit a non-scaling behaviour due to both the evolution of the structure functions of the colliding beams and to the running of α_s . Scaling violations have been seen both in measurements of the inclusive deep inelastic scattering cross-section, F_2 and for jet cross-sections in $p\bar{p}$ collisions [92, 93]. In the absence of scaling violations, the ratio of jet invariant cross-section, $(E_T^{\text{jet}})^4 E^{\text{jet}} d^3\sigma/dp_x^{\text{jet}} dp_y^{\text{jet}} dp_z^{\text{jet}}$, at one γp centre-of-mass energy, $W_{\gamma p}$ to that at any other energy would be unity for all $x_T \equiv 2E_T^{\text{jet}}/W_{\gamma p}$. Measurements of inclusive jet photoproduction [94] are shown in Fig. 18a compared directly with data from $p\bar{p}$ collisions [93, 95]. The shape of the distributions for γp and $p\bar{p}$ data are compatible for $x_T < 0.2$. For larger values of x_T , the harder distribution in γp collisions arises from the increasing proportion of direct processes and the increasing proportion of the quark density in the resolved photon relative to that in the proton. These results are similar to the inclusive particle production discussed in Section 3.1 which led to the observation of the direct component. To test the scaling hypothesis, the ratio of the scaled jet invariant cross-sections as a function of x_T are shown in Fig. 18b for two chosen values of $W_{\gamma p}$ [96]. A clear deviation from unity, in agreement with NLO QCD predictions, is seen. This is the first observation of scaling violations in γp cross-sections.

The inclusive jet cross-section over a wide range of E_T^{jet} also allows a determination of α_s and its energy scale dependence. The high precision of the data, in particular the well-understood energy scale of the calorimeter, yielded a value of α_s with a total experimental uncertainty of less than 2%. The limitation of the analysis arises from the theory which has an uncertainty of 4%. This measurement of α_s and the many in deep inelastic scattering have also clearly demonstrated the energy scale dependence or “running” of α_s . The current collection [97] of all data is shown in Fig. 19a. The consistency of the data with the running hypothesis is clearly seen and the impact of the HERA data is significant.

The theoretical calculation used to fit the jet data also uses a parametrisation of the proton structure from global fits to deep inelastic scattering and other data. However, combining jet and inclusive F_2 data as described in the previous section, the full correlation of the gluon density and α_s can be accounted for and these both accurately extracted from HERA data alone [82]. The impact of the jet data can be seen in Fig. 19b, where the χ^2 profile is shown for the fit to inclusive deep inelastic scattering data with and without the jet measurements. The extracted value is $\alpha_s(M_Z) = 0.1183 \pm 0.0028(\text{exp.}) \pm 0.0008(\text{model})$.

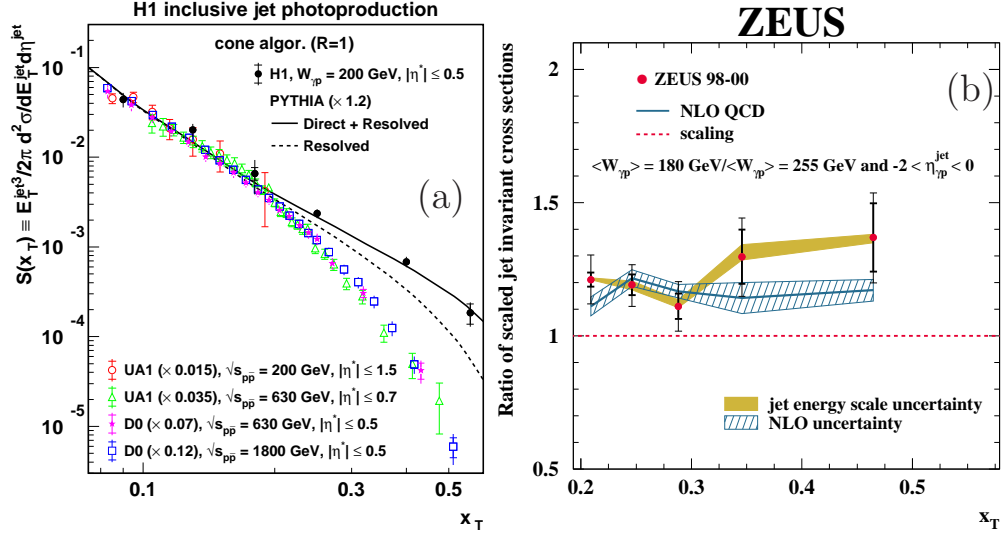


Figure 18: (a) Scaled jet cross-sections at one value of $W_{\gamma p}$ compared with results from $p\bar{p}$ collisions and PYTHIA. (b) Ratio of scaled jet cross-section at two different $W_{\gamma p}$ values compared with NLO QCD predictions.

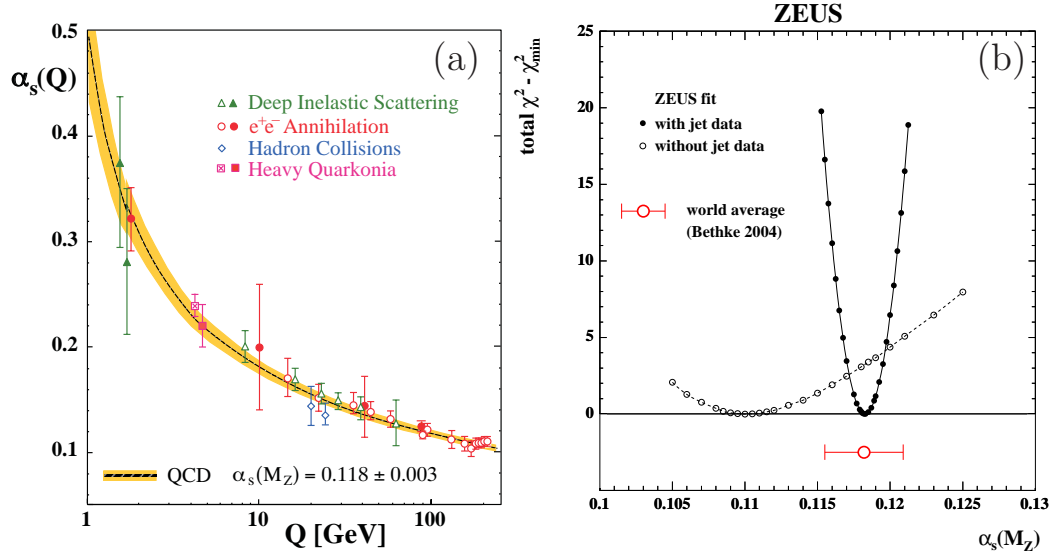


Figure 19: (a) The running of α_s from all experiments [97]. The HERA data in both photoproduction and deep inelastic scattering are shown as the open triangles. (b) The χ^2 profile for α_s before and after the inclusion of DIS and photoproduction jet cross-sections into the QCD fit [82].

4.3 Open heavy-quark production

Photoproduction of heavy quarks is again governed by QCD within the Standard Model. Figure 10b shows the production of heavy quarks in a resolved γp collision. In fact, a similar diagram would apply for resolved $\gamma\gamma$ collisions, or hadron-hadron process. Thus knowledge accumulated at HERA, LEP and the Tevatron will directly benefit future programmes such as the LHC and a future linear collider where heavy quarks will be produced by the same mechanism. Since heavy quarks feature in many signatures for new physics, understanding the QCD production mechanisms becomes even more important.

Theoretically, heavy quarks provide ideal tools for probing QCD due to their relatively large mass, $m_Q \gg \Lambda_{\text{QCD}}$, which entails a fast convergence of the perturbative expansion of the cross-section. The production of heavy quarks is also *directly* sensitive to the gluon density in the colliding hadron (see Fig. 10b). The gluon density is usually determined in the DGLAP-evolution fits to measurements of structure functions in inclusive deep-inelastic scattering, and more recently by including jets (Section 4.1). In the case of jets, the non-zero photon virtuality (in DIS) or the x_γ^{obs} cut (in photoproduction) reduces the uncertainties associated with photon structure. Requiring charm in the final state is another method of achieving the same effect, with a different set of associated benefits and problems.

Several measurements of charm photoproduction have been made at HERA, some of which were discussed in Section 3 in the context of the information they provide on the structure of the photon. Measurements of charm production in deep inelastic scattering provide information on the charm contribution to the proton structure function. This subject, although related, is outside the remit of this review and the interested reader is referred to the most recent relevant publications [98]. There are also several results on charm production from the HERA experiments which are preliminary and not yet published. Only the published results on charm and beauty production will be discussed here.

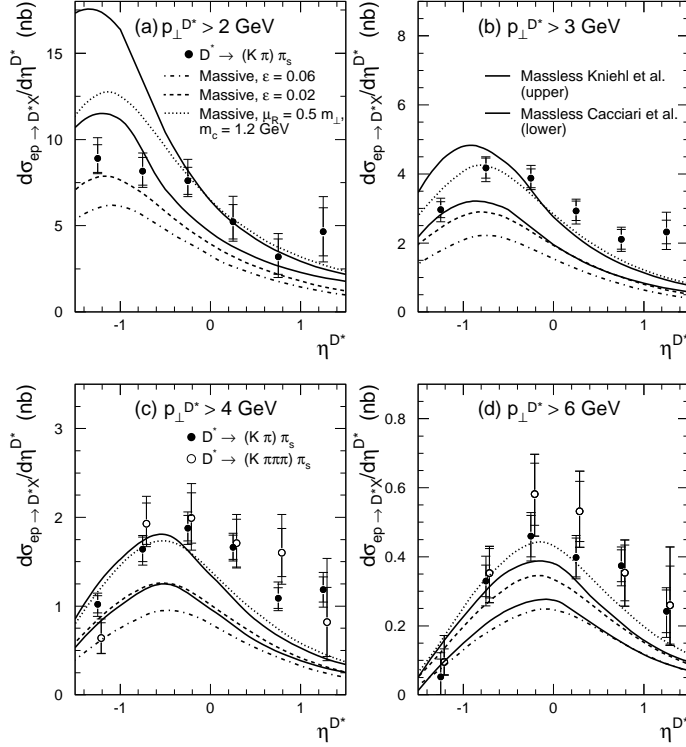
Much of the recent interest in heavy-quark production arose from discrepancies between data from the Tevatron experiments [99], CDF and D0, and NLO QCD predictions. The data, measured in many decay channels, was a factor of 2 – 3 above NLO QCD for all measured regions. This was in contrast to earlier UA1 results [100] at the $Spp\bar{S}$ collider and led to a mini-crisis in QCD. Many explanations were put forward as to reasons for this discrepancy: the input parameters to the QCD calculations such as the structure function of the proton and the beauty-quark mass; inaccurate values for the extrapolation of the data outside the measured region; and extensions beyond the Standard Model such as the presence of a light supersymmetric particle [101]. Results from HERA have contributed to the understanding of heavy-quark production in QCD as discussed below. Measurements from other colliders are also briefly discussed.

A measurement of inclusive D^* mesons currently provides the largest data sample for charm production at HERA. Experimentally, the tagging of D^* mesons via the decay chain $D^* \rightarrow D^0\pi_s \rightarrow K\pi\pi_s$ is very clean and although the branching ratio is small ($\approx 2\%$) high-precision physics with about 60 000 events is possible [102]. Published results on D^* photoproduction cross-sections use a smaller sample but already are of sufficient precision for an informative comparison with QCD calculations. Data can be compared to different types of calculations: the “massive” and “massless” scheme. In the fixed-order, or “massive”, scheme, u , d and s are the only active quarks in the proton and photon; charm and beauty are only produced in the hard scatter. This scheme is expected to work well in regions where the transverse momentum of the outgoing c quark is of the order of the quark mass. At higher transverse momenta, the “massless” scheme should be applicable in which charm and beauty are regarded as active flavours (massless partons) in the structure functions of the proton and photon and are fragmented into massive quarks only after the hard process. A calculation which matches the two schemes, called FONLL [103], is also available for inclusive D^* meson production at HERA but has not yet been compared to published data.

Data as a function of the pseudorapidity of the D^* meson are shown in Fig. 20 compared to two different types of NLO QCD calculations for charm production. Although roughly compatible with the data, none of the calculations fully reproduce the trends of the data, with discrepancies concentrated at high values of η^{D^*} and medium $p_T^{D^*}$. This could hint at, for example, a low value of the charm-quark mass or inadequacies in the fragmentation model.

In making the predictions, the fragmentation of the charm quark into a D^* meson is performed using the Peterson function [104] fitted to e^+e^- data. The applicability of this is unclear at HERA particularly at high η^{D^*} , *i.e.* in the direction of the proton, where the proton remnant may affect the production of the D^* meson. Clearly more phenomenological work on fragmentation is needed before stronger conclusions can be drawn. Combining NLO calculations with sophisticated models of hadronisation available in Monte Carlo models, such as the MC@NLO programme [105] is one promising path to understanding charm production in more detail. Another is to check the assumptions which go into the calculations in more detail. For example, the universality of hadronisation may be tested by measuring the production fractions for different charmed hadrons, as has been done very recently in DIS [106] and photoproduction [107]. In general the results are in agreement and, in the case of the photoproduction data, of competitive precision with e^+e^- data. However, in photoproduction the fraction of charm quarks fragmenting to Λ_c^+ is around 3σ higher and the D^{*+} fraction lower by a similar amount than the corresponding fractions in e^+e^- . About half of the difference in the D^{*+} fraction is due to the Λ_c difference. Since there is no asymmetry between Λ_c^+ and Λ_c^- , this effect,

ZEUS 1996+97



Inclusive D^* photoproduction

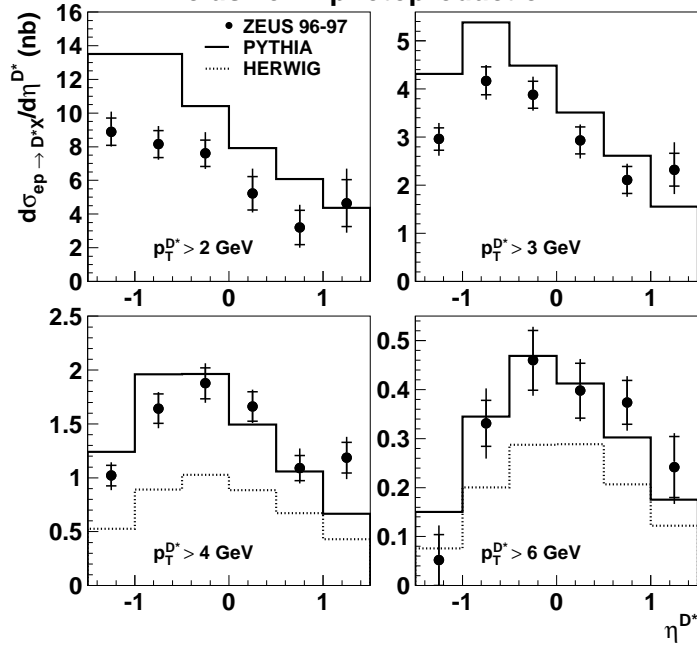


Figure 20: Cross-sections $d\sigma/d\eta^{D^*}$ for different regions of $p_T^{D^*}$ in charm photoproduction at HERA. The data are compared to calculations of NLO QCD in the massive and massless schemes. The data are also compared to predictions from PYTHIA and HERWIG Monte Carlo programs. Note the HERWIG prediction is not shown for the two lowest $p_T^{D^*}$ regions as there is an implicit minimum parton p_T cut in the calculation which would make the comparison invalid.

if real, is unlikely to be due simply to baryon number flow. However, one may speculate that it might be a hint of some non-trivial effects in fragmentation due to the incoming proton.

The first measurements [108] of beauty production at HERA were higher than the NLO prediction by a similar factor to those from the Tevatron. However, given the large uncertainties on the ZEUS result it was consistent with the theory. The precision of the data subsequently improved, and by measuring cross-sections in kinematic regions where the detector acceptance is good (rather than relying on models to extrapolate into unmeasured regions), the estimates of the systematic errors also became more reliable. The cross-section as a function of the pseudorapidity of the decayed muon for beauty events is shown in Fig. 21. Data from both H1 [109] and ZEUS [110] collaborations are shown compared with NLO QCD predictions performed in the massive scheme. The data are well-described by the theoretical calculation. Similar measurements have been made in deep inelastic scattering [109, 111]; here the data are above the NLO QCD predictions but consistent within the quoted uncertainties.

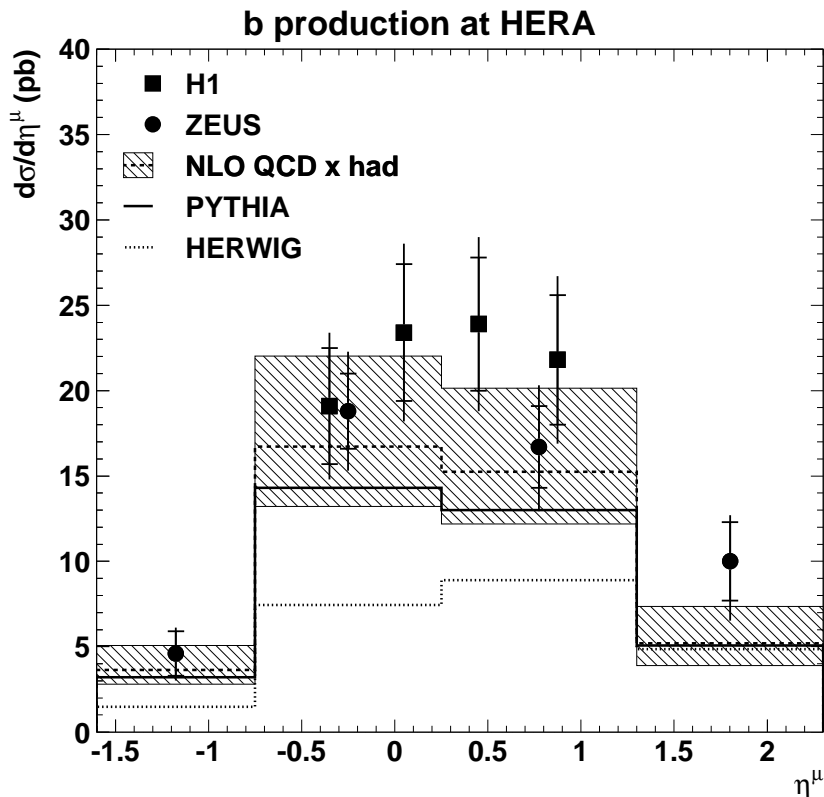


Figure 21: Cross-section $d\sigma/d\eta^\mu$ for beauty photoproduction at HERA. The data are compared to predictions of NLO QCD in the massive scheme and from PYTHIA and HERWIG Monte Carlo programs.

Recent theoretical improvements and their comparison with measured, rather than extrapolated, cross-sections have also led to an improved description of beauty production in $p\bar{p}$ collisions. Two new calculations have become available. The FONLL calculation discussed previously, matches the massive and massless schemes and should therefore be applicable for all energies. This prediction also has an improved fitting technique to e^+e^- data for the fragmentation function. The second, MC@NLO, matches a NLO calculation to parton showers and hadronisation in the HERWIG MC programme. These calculations are shown in Fig. 22 compared with recent CDF data [112]; both describe the data well. The rate of beauty production has also been measured in $\gamma\gamma$ collisions by the L3 collaboration [113] at LEP. The data are measured within the acceptance of the detector and then extrapolated by factors of $\sim 20 - 30$ to the full phase space for comparison with NLO QCD predictions. This measurement is experimentally challenging due to the poor separation power between beauty decays to leptons and background. The NLO QCD prediction, shown in Fig. 22, is a factor of three below the data although the difference is below three standard deviations. Were this result to persist with measurements from other LEP collaborations it would certainly be very puzzling as a large part of the cross-section comes from electromagnetic coupling of two photons to two beauty quarks.

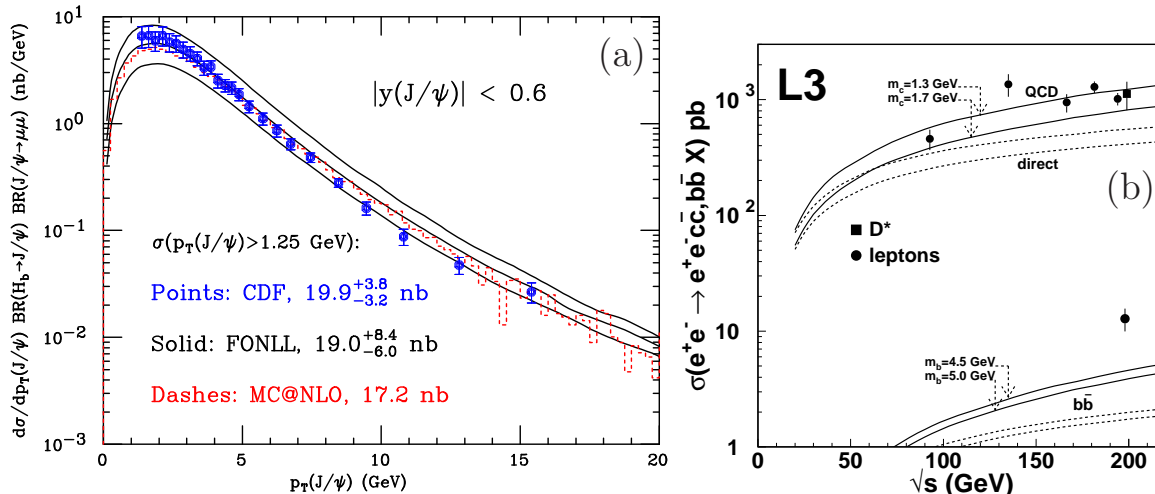


Figure 22: Cross-sections (a) $d\sigma/dp_T$ for J/ψ mesons from beauty decays at the Tevatron and (b) beauty production at LEP. The data are compared to the different NLO QCD calculations.

As well as NLO calculations, full final-state Monte Carlos can also give a reasonable description of most heavy flavour cross-sections which have been measured in photoproduction and other high-energy processes. Given the importance of heavy flavour production cross-sections, particularly beauty, in identifying interesting processes at LHC and a future linear collider, detailed validation of such models across all available measurements

is of considerable interest and importance, and is ongoing [90, 114, 115].

4.4 Charmonium production

The J/ψ meson was discovered over 30 years ago and thereby confirmed the existence of the charm quark. However, although the particle has been extensively measured, the nature of its production is poorly understood. Quasi-elastic production of the J/ψ and other vector mesons was briefly discussed in Section 2.1. The mechanism by which J/ψ mesons are “inelastically” produced is expected to be predictable in QCD. The inelastic domain arises from the presence of a large transfer of energy between the projectile and the target particle.

In the so-called colour-singlet model [116], $c\bar{c}$ pairs produced in a colour-singlet (CS) state are identified with physical ψ states. This model has been extended in the context of non-relativistic QCD [117] to account for the production of $c\bar{c}$ pairs which are not colourless. The charm quark pair can emit gluons (and hence change colour) until the pair is colourless. This model is referred to as the colour-octet (CO) model. Measurements by the CDF collaboration in $p\bar{p}$ collisions [118] indicate that the colour-singlet model greatly underestimates the production rate of ψ mesons, by factors of between 10 and 80. However, it has been claimed that calculations including colour-octet contributions can account for this difference. A test of this claim is the requirement that the colour-octet matrix elements extracted from ψ cross-section measurements in $p\bar{p}$ collisions can also account for photoproduction data.

The cross-sections $d\sigma/dp_T^2$ and $d\sigma/dz$ have been measured in photoproduction [119, 120], where z , the “inelasticity”, is the fraction of the incoming photon’s energy carried by the J/ψ meson. The distributions of these two variables are shown in Fig. 23 compared with theoretical calculations incorporating the models mentioned previously. In Fig. 23a, a prediction from the colour-singlet model alone (LO, CS) clearly does not describe the data being a factor of over 10 below at high p_T^2 . After the inclusion of NLO corrections [121], however, the theory agrees well with the data. This calculation is shown again in Fig. 23b for the inelasticity variable and again describes the data reasonably well. At low z , the NLO prediction is below the data although in this region more background from e.g. resolved photons is expected. Also shown are calculations which have both colour-singlet and colour-octet contribution, shown as (LO, CS+CO) [122]. They also describe the data well. However, other models incorporating colour-octet processes [123] give different results [119]. The amount of colour-octet in different calculations was extracted from the same $p\bar{p}$ data; thus it is evident these calculations suffer from large uncertainties from other sources, and hence a lack of predictive power.

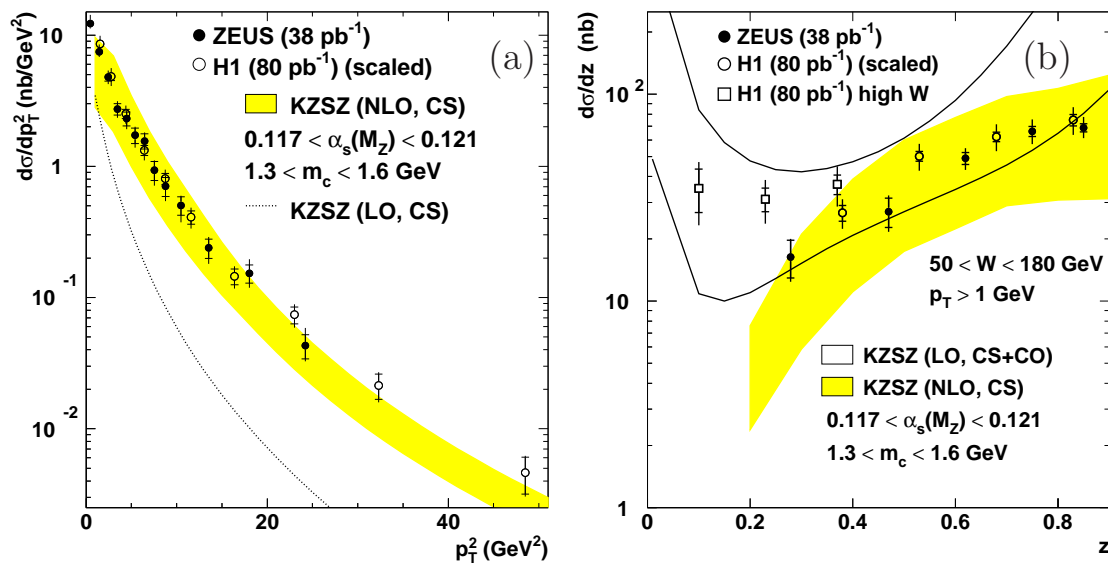


Figure 23: Cross-sections (a) $d\sigma/dp_T^2$ and (b) $d\sigma/dz$ for J/ψ photoproduction at HERA. Data from both H1 and ZEUS collaborations are compared with predictions at (a) LO and NLO in the framework of the colour-singlet model and (b) NLO in the framework of the colour-singlet model and LO with the addition of the colour-octet model.

In summary, there seems to be a real issue with the theory here. The very large NLO corrections to the CS calculations indicate, at least naively, poor convergence of the perturbative expansion. These corrections have not been calculated for the CS+CO model; the LO predictions for this model differ substantially from each other. Due to the large theoretical uncertainties affecting all predictions the presence of colour-octet processes in photoproduction cannot be excluded or definitely confirmed, and the matrix elements extracted from hadroproduction are consistent with photoproduction data within very large uncertainties. More precision comparisons with theory require a better theoretical understanding of the uncertainties, and/or the measurement of more accurately predicted variables, such as perhaps angular distributions.

4.5 Jet substructure and fragmentation functions

Measurement of jet substructure allows the possibility of distinguishing jets originating from quarks and gluons due to their different radiation amplitudes. This permits a stringent test of QCD, provides information on the properties of quark- and gluon-initiated jets and, by tagging the final state, reveals details of the initial state and hence proton and photon structure (see Section 3.3). At sufficiently high jet transverse energy, where the influence of hadronisation becomes negligible, the internal structure of a jet is calculable in pQCD. Such calculations predict that gluon-initiated jets are broader than

quark-initiated jets due to the larger colour charge of the gluon. The jet shape [124] and subjet multiplicity [125] have been used to study the internal structure of jets in photoproduction. The integrated jet shape, $\psi(r)$, using only those particles belonging to the jet, is defined as the fraction of the jet transverse energy that lies inside a cone in the $\eta - \phi$ plane of radius, r , concentric with the jet axis:

$$\psi(r) = \frac{E_T(r)}{E_T^{\text{jet}}}, \quad (2)$$

where $E_T(r)$ is the transverse energy within the given cone of radius r . The mean integrated jet shape, $\langle\psi(r)\rangle$, is defined as the averaged fraction of the jet transverse energy inside the cone r :

$$\langle\psi(r)\rangle = \frac{1}{N_{\text{jets}}} \sum_{\text{jets}} \frac{E_T(r)}{E_T^{\text{jet}}}, \quad (3)$$

where N_{jets} is the total number of jets in the sample.

The internal structure of a jet is expected to depend mainly on the type of primary parton from which it originated and to a lesser extent on the particular hard scattering process. This expectation is supported by comparisons such as that shown in Fig. 24. Here it is seen that in those processes which at LO give rise only to quark jets (e^+e^- annihilation, DIS), the jets are narrow, and very similar to each other. In photoproduction at these transverse energies, direct processes dominate. However, the presence of QCD Compton and resolved photon processes means that some gluon jets are present in the final state at LO, and the average jet shape is correspondingly broader. In $p\bar{p}$ events, where the gluon admixture is even stronger, the average jet shape is broader still.

The measured mean integrated jet shape for $E_T^{\text{jet}} > 17$ GeV in different regions of η^{jet} is shown in Fig. 25 [69]. The jets broaden as η^{jet} increases. Leading-logarithmic parton-shower predictions from PYTHIA for resolved plus direct processes and gluon- and quark-initiated jets are compared to the data. The description of the data is generally good, although the data are somewhat broader than the predictions. From the comparison with the predictions of gluon- and quark-initiated jets, it is seen that the measured jets are quark-like for $-1 < \eta^{\text{jet}} < 0$ and become increasingly gluon-like as η^{jet} increases. Jets become narrower as E_T^{jet} increases (not shown) consistent with the dominance of direct processes, and hence quark jets, at higher E_T^{jet} . These effects have also been seen in measurements of the subjet multiplicity [69].

The differences in gluon- and quark-initiated jets are used to select samples enriched in such jets to study their properties and the dynamics of the hard subprocesses in more detail. The two samples of jets were selected on a statistical basis and classified as follows:

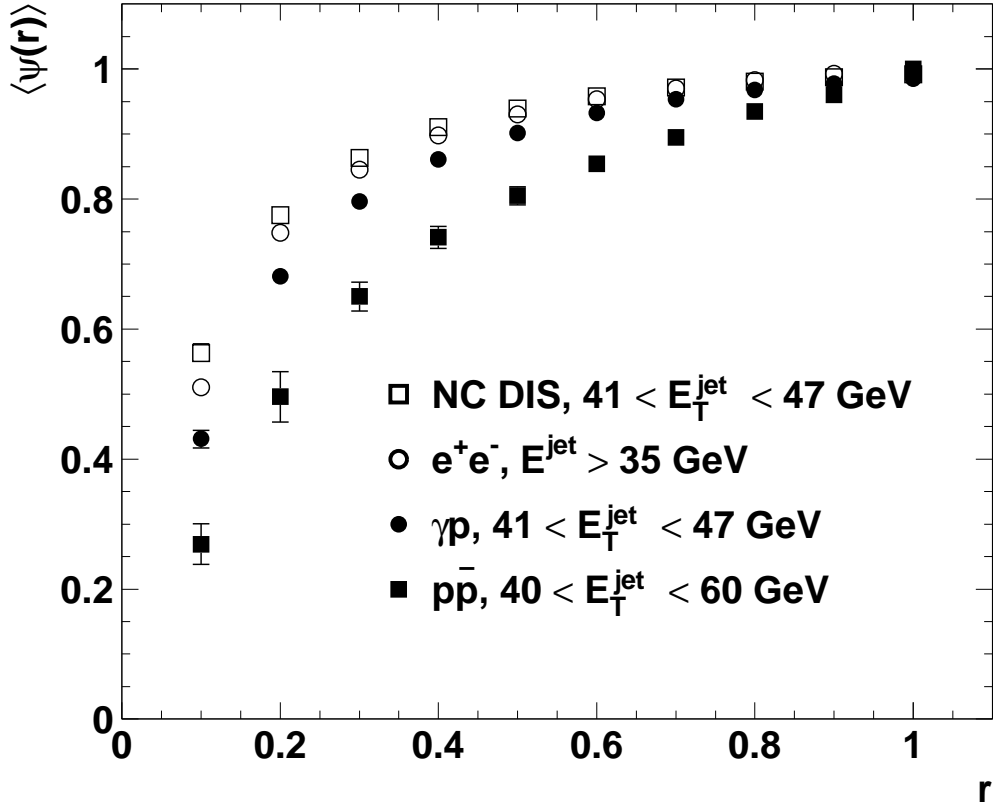


Figure 24: Measured jet shapes in e^+e^- [126], DIS [127], photoproduction [128] and $p\bar{p}$ [129].

- gluon-enriched sample (“broad jets”), defined as those jets with $\psi(r = 0.3) < 0.6$;
- quark-enriched sample (“narrow jets”), defined as those jets with $\psi(r = 0.3) > 0.8$.

Non-overlapping regions were chosen to suppress migration effects and the cuts values represent a compromise between purity and statistics. In dijet events, samples with two broad jets, two narrow jets and one broad and one narrow jet can also be selected. In Fig. 26, cross-sections for broad and narrow jets (Fig. 26a and 26b) and events with two broad or two narrow jets (Fig. 26c and 26d) are shown.

The measured cross-sections for broad and narrow jets exhibit a different behaviour: the η^{jet} distribution for broad jets increases up to the highest η^{jet} value measured whereas the distribution for narrow jets peaks at $\eta^{\text{jet}} \sim 0.7$; and the distribution in E_T^{jet} for narrow jets has a harder spectrum than for broad jets. The Monte Carlo prediction, normalised to the total cross-section, gives a good description of the narrow-jet sample but gives a poorer description of the broad-jet sample. The PYTHIA programme predicts that the broad-jet event sample consists of 15% gg , 50% gq and 35% $q\bar{q}$. The selection of narrow jets gives a reasonably pure sample of quark-initiated jets; the PYTHIA programme predicts

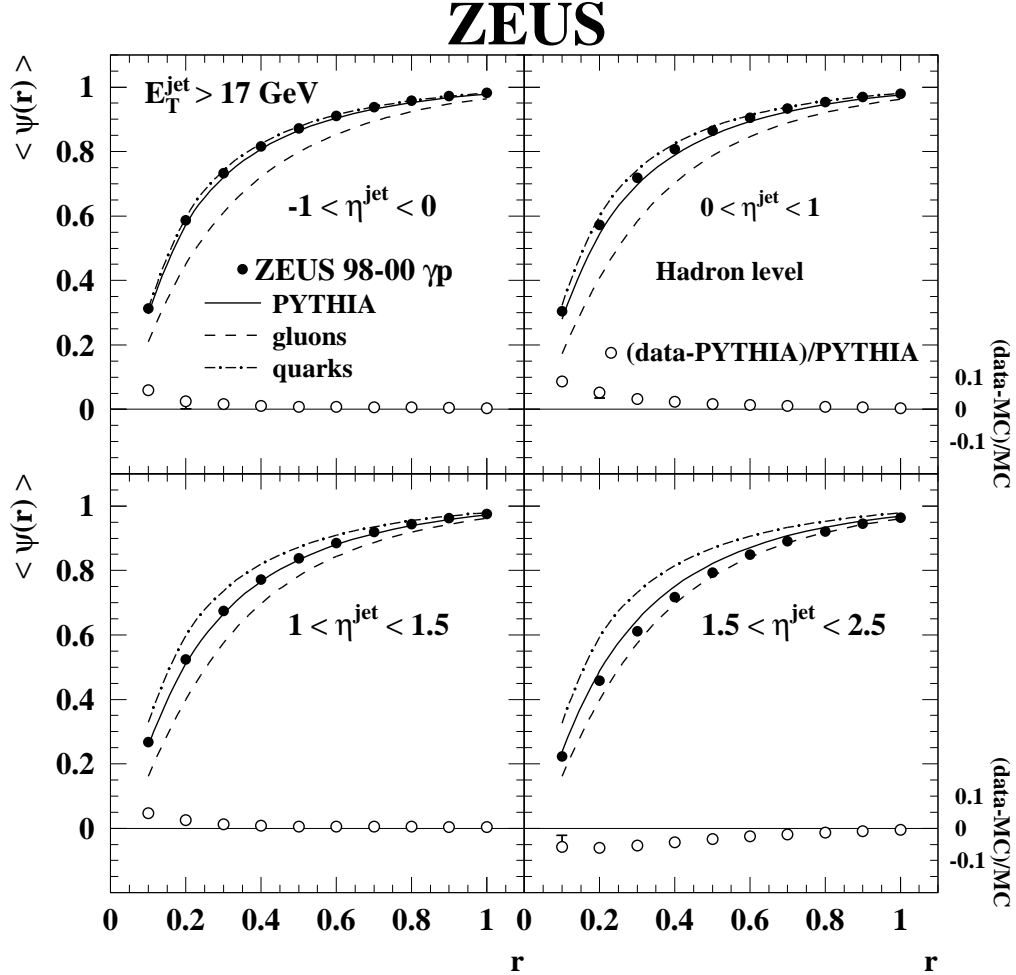


Figure 25: Measured mean integrated jet shape in different regions of η^{jet} . Predictions of the PYTHIA Monte Carlo program for quark (dot-dashed lines), gluon (dashed lines) and all (solid lines) jets are shown. The fractional difference of the data to the predictions of PYTHIA for all jets is also shown (open dots).

62% $q\bar{q}$, 34% qg and 4% gg . In Fig. 26a, predictions for quark-initiated jets describe the narrow-jet sample well, as expected due to its high quark purity. The prediction for gluon-initiated jets describes the broad-jet sample less well due to the higher impurity from quark-initiated jets. However, the result supports the expectation that the broad- and narrow-jet samples are dominated by gluon- and quark-initiated jets, respectively.

Dijet cross-sections in which either two broad or two narrow jets are tagged are shown in Fig. 26c and 26d. As these jets are indistinguishable, only the absolute value of $\cos\theta^*$ can be measured (in contrast to the case when one broad and one narrow jet are tagged, as in Fig. 13). The measured and predicted cross-sections were normalised at $|\cos\theta^*| = 0.1$. The cross-section for events with two broad jets exhibits a faster rise to high $\cos\theta^*$. The predictions from the PYTHIA Monte Carlo programme give an adequate description of the

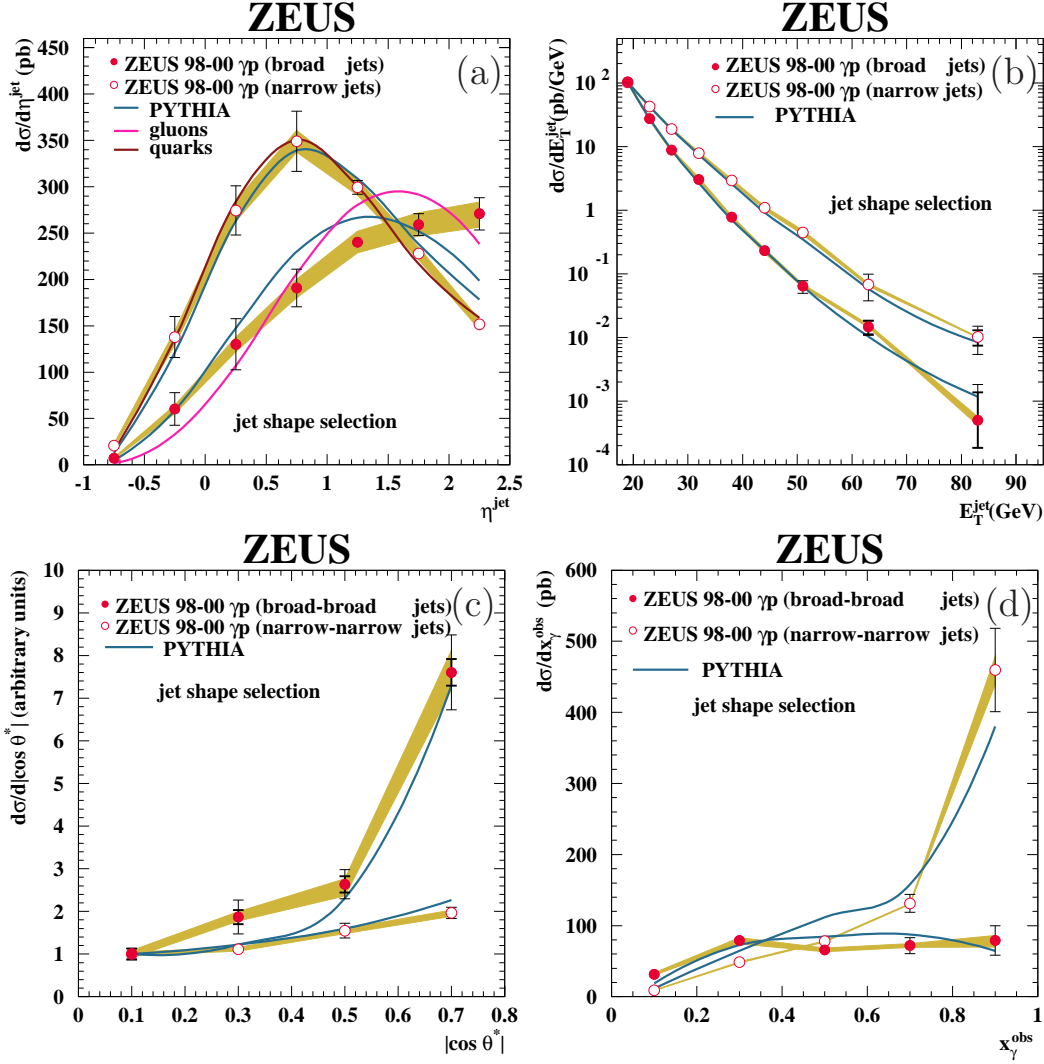


Figure 26: Cross-sections (a) $d\sigma/d\eta^{\text{jet}}$ and (b) $d\sigma/dE_T^{\text{jet}}$ for broad and narrow jets and (c) $d\sigma/d|\cos \theta^*|$ and (d) $d\sigma/dx_\gamma^{\text{obs}}$ for events with two broad jets or two narrow jets. The data are compared with PYTHIA MC predictions and in (a) for PYTHIA expectations for quark and gluon jets.

data. For events with two broad jets, PYTHIA predicts the parton final state to consist of 16% gg , 52% qg and 32% qq . As in the sample with only one broad jet, the impurity is relatively large. The sample with two narrow jets is a much purer sample of quark jets; PYTHIA predicts the parton final state to consist of 71% qq , 28% qg and 1% gg . The differences in the measured distributions can be understood in terms of the dominant two-body processes: the resolved subprocess $q_\gamma g_p \rightarrow qq$, mediated by gluon exchange for the broad-broad dijet sample and the direct subprocess $\gamma g \rightarrow q\bar{q}$, mediated by quark exchange for the narrow-narrow dijet sample. The dominance of resolved and direct processes for broad-broad and narrow-narrow dijet events, respectively is also confirmed by the cross-

section $d\sigma/dx_\gamma^{\text{obs}}$. The narrow-narrow dijet sample is strongly peaked at high x_γ^{obs} whereas the broad-broad dijet sample is roughly flat in x_γ^{obs} .

4.6 Multijet production and colour coherence

Jet photoproduction has so far mostly been discussed in terms of the LO diagrams (Fig. 3) where two jets are produced. In reality, a combination of QCD radiation and hadronisation will mean that there is a distribution of energy around the final state outside the two leading jets. This may be in the form of low energy particles from soft processes, or further high E_T^{jet} jets. The distribution of these jets, and to some extent even of softer particles, is predicted by QCD.

The three-jet photoproduction cross-section has been measured by the ZEUS collaboration [130]. The measurement was made for three-jet masses above 50 GeV and with a requirement that at least two jets satisfy $E_T^{\text{jet}} > 6$ GeV while the third has $E_T^{\text{jet}} > 5$ GeV. QCD calculations at $\mathcal{O}(\alpha\alpha_s^2)$ (which is LO for three jet production) are in good agreement with the data. In addition, since this cross-section is dominated by configurations in which the third jet has substantially lower E_T^{jet} than the two leading jets, leading-logarithmic parton-shower models are expected to describe the cross-sections rather well. They do indeed, as may be seen in Fig. 27. An interesting feature here is that coherent gluon radiation must be implemented in the Monte Carlo in order to reproduce the shape of the ψ_3 distribution (the angle, in the three-jet centre-of-mass system, between the plane containing the leading jet and the beam, and the plane containing the three jets). For coherent radiation, these planes tend to line up such that the region $\psi_3 \approx \pi/2$ is depopulated. If a large amount of incoherent radiation is allowed (see appendix), this effect is destroyed.

4.7 Energy flow, rapidity gaps and forward particles

As discussed in Section 2.1, total hadronic cross-sections in the limit of large s/t increase by some small (but positive!) power of s . In Regge theory this is an exchange of vacuum quantum numbers, known as the Pomeron. This is presumably an emergent behaviour of the QCD Lagrangian, but making a connection with the partonic language of perturbative QCD is a challenge which continues to throw up surprises in both data and theory³.

The high energy regime probed at HERA and the Tevatron means that the large s/t limit may be approached even when t is sufficiently large for perturbative techniques to be applied. It is also possible, even when the momentum exchange, t , with the proton

³ See [39] for a discussion and bibliography.

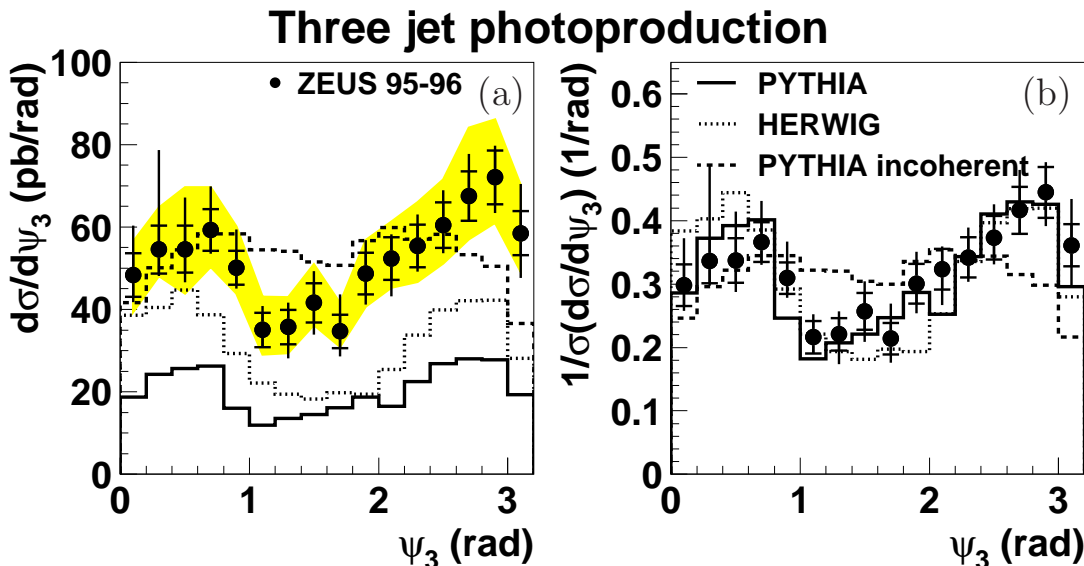


Figure 27: (a) The cross-section $d\sigma/d\psi_3$ and (b) the area-normalised distribution of ψ_3 . The correlated systematic uncertainty due to the jet energy-scale is shown as the shaded band in (a). The solid histogram shows the default PYTHIA prediction. In (a) and (b) the dotted and dashed histograms show the predictions of HERWIG and of PYTHIA with colour coherence switched off, respectively.

is small, for relatively high-mass final states to be produced, which opens up the phase space for short distance, high energy scale processes in the diffractively produced system. These two distinct cases both offer the possibility of describing some or all of “Pomeron” exchange in terms of perturbative quarks and gluons. Both have been measured in high energy photoproduction.

4.7.1 Hard colour singlet exchange

In configurations where the two leading jets are separated by a large rapidity interval, it is possible in high energy photoproduction to approach the regime where $t \approx p_T^2$ is of the order a few tens of GeV, but \hat{s} , the partonic centre-of-mass energy squared, is a few hundred GeV. Thus the scattering will be dominated by the exchange of vacuum quantum numbers, but yet the high t means that pQCD calculations should be applicable. The lowest order colour-singlet exchange in QCD is a pair of gluons. However, such a diagram is subject to large logarithmic corrections, which are resummed in the BFKL [131, 132] approach. This is a topic in QCD with a very extensive literature (see for example, references within [39]), but for our purposes here it is sufficient to say that there is a possible enhancement in the cross-section for colour-singlet exchange between jets separated by a large rapidity interval in hadronic collisions.

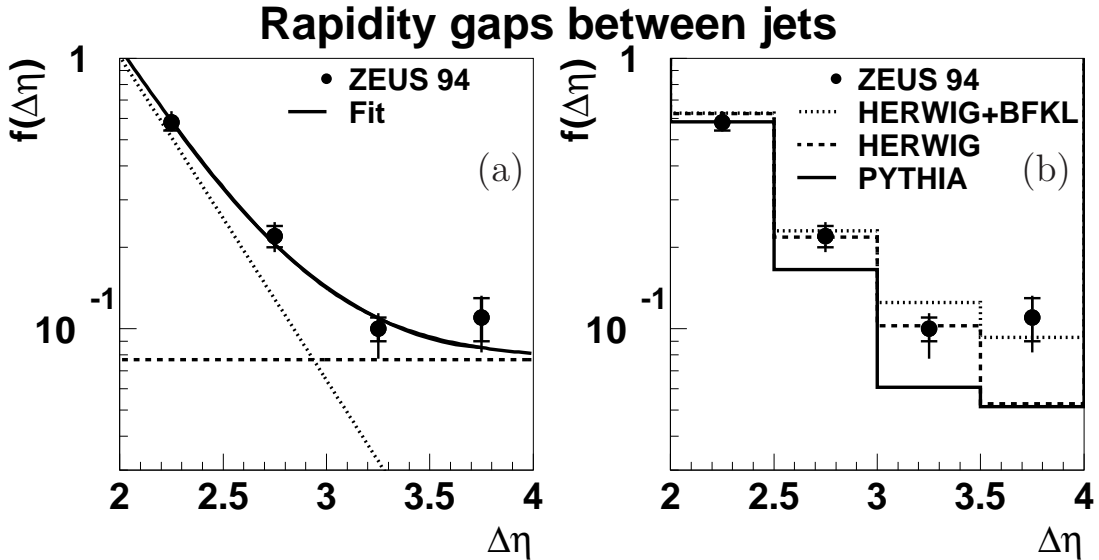


Figure 28: *ZEUS gap fraction measurement (solid points). In (a) the gap fraction is compared to a fit to the sum of an exponential (non-colour-singlet) and a flat (assumed colour singlet) contribution. In (b) the gap fraction is redisplayed and compared to PYTHIA and HERWIG non-diffraction MC, and to a HERWIG sample which includes a colour singlet exchange component from a BFKL-based calculation [135].*

If no colour is exchanged between the hadrons (in the case of photoproduction, the proton and a hadronic photon), colour coherence leads to a suppression of QCD radiation, and thus energy flow, between the jets. Hence the large rapidity interval is very likely to be a rapidity gap. This is the experimental signature searched for by the HERA collaborations. A key observable is the “gap fraction” measured as a function of the rapidity interval, $f(\Delta\eta)$. This is the ratio of the cross-section for dijet events with a rapidity gap between the jets (however the gap is defined) to the total number of dijet events.

In the first measurement [133], a gap was defined by the requirement that no particle with transverse energy > 300 MeV lay in the interval between the jets. In “normal” QCD events, the probability of zero radiation into the gap falls exponentially as the interval increases, and thus so does $f(\Delta\eta)$. This is seen in the first bins of Fig. 28a and 28b. However, for colour singlet exchange no such suppression is expected, and indeed the final bin is higher than one would expect given the fall in the first three. A simple fit to a flat fraction for colour singlet exchange combined with the exponential fall gives good description of the data. This was the first evidence for strongly interacting colour-singlet exchange in jet photoproduction. Such measurements have also been made at the Tevatron [134] and show similar evidence for such processes in $p\bar{p}$ events, albeit at a much lower rate.

The main problem with this measurement, apart from the limited statistics and rapidity reach available at the time, is that the method used to define a rapidity gap is not infrared safe. That is, a definition of activity in terms of particles is not amenable to calculation in perturbative QCD. A more robust definition can be made in terms of energy flow within the interval, and by using minijets rather than particles to calculate this energy flow [136–138]. Such a definition was used by the H1 collaboration in a subsequent measurement [139]. In this analysis, the K_{\perp} jet algorithm [140] was run over the final state in the inclusive mode. This produces a list of “jets”, some of which have very low transverse energy and consist of very few particles. However, since the algorithm is infrared safe, quantities based on these objects are, in principle at least, calculable. The highest E_T^{jet} pair define the rapidity interval, as usual. The cross-sections and gap fraction in the paper are defined in terms of E_T^{gap} , the transverse energy of all the jets within the rapidity interval between the jets. The requirement $E_T^{\text{gap}} < E_T^{\text{cut}}$ was applied, for values of E_T^{cut} ranging between 0.5 GeV and 2 GeV. For all values of E_T^{cut} studied, (Fig. 29) there is an excess of gap events at large rapidity intervals compared to the expected fall-off from normal QCD events.

The exponential fall of the gap fraction expected for non-colour-singlet processes is also seen in the non-colour singlet HERWIG and PYTHIA curves shown in Fig. 28b and in Fig. 29. The data are also compared to HERWIG predictions [141] implementing a leading-logarithmic BFKL-based calculation of hard colour-singlet exchange between two partons as computed by Mueller and Tang [135]. In the limit $\Delta\eta \gg 1$ the cross-section for quark–quark scattering may be approximated as

$$\frac{d\sigma(qq \rightarrow qq)}{d\hat{t}} \approx (C_F\alpha_s)^4 \frac{2\pi^3}{\hat{t}^2} \frac{\exp(2\omega_0 y)}{(7\alpha_s C_A \zeta(3)y)^3} \quad (4)$$

where

$$\omega_0 = C_A(4 \ln 2/\pi)\alpha_s, \quad (5)$$

and

$$y = \Delta\eta = \ln \left(\frac{\hat{s}}{-\hat{t}} \right) \quad (6)$$

Here, $1 + \omega_0$ is the perturbative Pomeron intercept, $C_F = \frac{4}{3}$ is the usual colour factor for quark–quark scattering, C_A is the number of colours, $-t \approx (E_T^{\text{jet}})^2$, and ζ is the Riemann ζ -function. In the leading-logarithm approximation, the values of α_s in Eqs.4 and 5 are free parameters. In the H1 analysis [139], where the exact rather than asymptotic form of Eq.4 was used [136], these were both set to 0.18. This corresponds to a choice of Pomeron intercept of $1 + \omega_0 = 1.48$, which was used for the asymptotic HERWIG curves shown here. For both ZEUS (Fig. 28) and H1 (Fig. 29), good agreement with the data is obtained for this model.

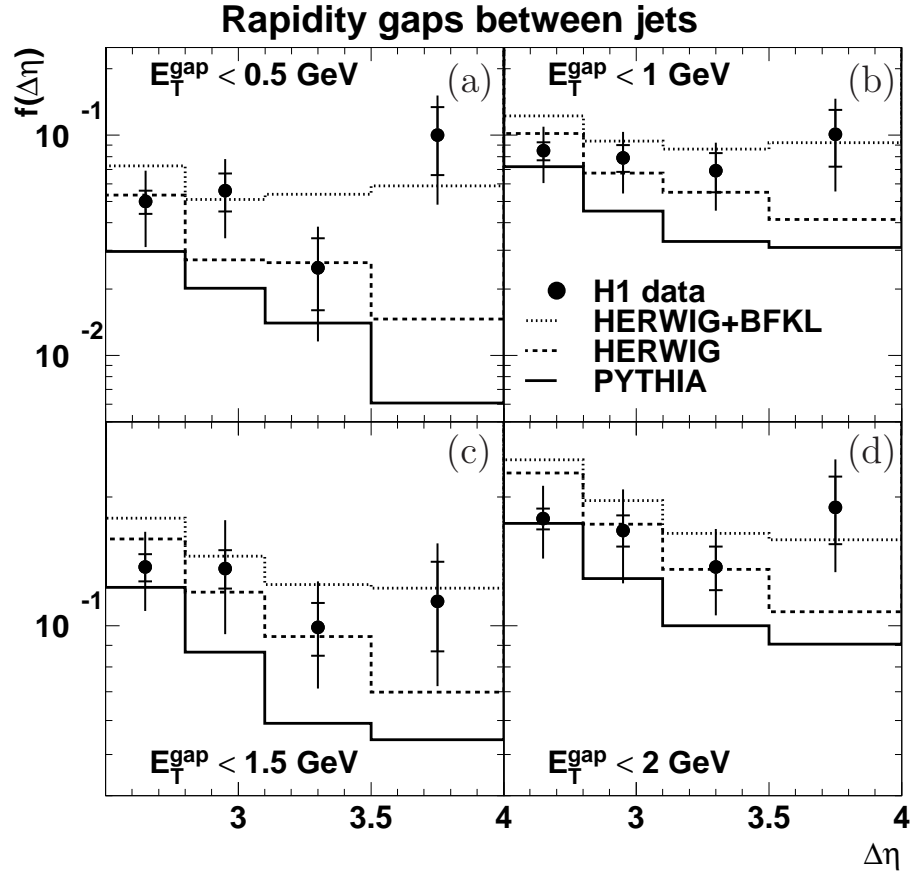


Figure 29: *H1 gap fraction measurement (solid points) differential in $\Delta\eta$. Gap events are defined for four values of E_T^{gap} , shown in (a-d). The gap fractions are compared to the prediction of HERWIG (dashed line) and PYTHIA (solid line). The dotted line shows HERWIG + BFKL colour singlet exchange (see text).*

For this kind of measurement in a real experiment with finite rapidity and non-zero E_T^{gap} , the large logarithms in rapidity, or x , which are summed in the BFKL approach are not necessarily the only, or even the most important, terms which should be included. There are also terms with logarithms in $E_T^{\text{gap}}/E_T^{\text{jet}}$ to be considered. Such logarithms have been resummed for various jet definitions [137, 142–144], and there is progress towards an approach which sums all important logarithms of both types [145].

Two other photoproduction processes which give access to hard colour singlet exchange are the high- $|t|$ diffractive photoproduction of vector mesons, and of photons.

The main advantage that diffractive photoproduction of vector mesons at high $|t|$ has over jet photoproduction is the experimental cleanliness of the measurement. At HERA, for example, the final state consists of; the decay products of the vector meson, an electron scattered through a very small angle (which may escape down the beam pipe), and a

low-mass hadronic system in the forward (proton) direction. The Q^2 is constrained to be low by the low scattering-angle of the electron, and thus t may be determined from the vector meson decay products. Theoretically, the unknown fragmentation and hadronisation effects involved in the formation of jets are absent, but the transition probability of a photon to a vector meson is introduced.

Calculations of high- $|t|$ vector meson exchange based upon BFKL resummation have been performed [146–149]. In this approach, as with the calculations of rapidity gaps between jets, a ladder of gluons (“hard Pomeron”) couples to a single parton in the proton at one end. At the other end things are very different; the photon splits into a $q\bar{q}$ pair. The probability to form a vector meson is calculated from the overlap between the photon and vector meson wavefunctions caused by the coupling to the two gluons at the top of the ladder to the dipole formed by the $q\bar{q}$ pair. The cross-section is predicted to fall as $1/|t|^N$, and to rise strongly with the photon-proton centre of mass energy, $W_{\gamma p}$. The calculations are able to describe the measured magnitude of the cross-sections for ρ , ϕ and J/ψ production [150–152]. They also describe the dependence on $W_{\gamma p}$ for J/ψ production for $|t| > 5$ GeV [152].

The transition of a quasi-real photon (helicity -1 or +1) to a vector meson (helicity -1, 0 or +1) is characterised by three independent helicity flip amplitudes. These may be extracted from measurements of the angular distribution of the vector meson decay products [151]. In lowest order QCD, $N = 4$ for transversely polarized mesons, and $N = 3$ for longitudinally polarized mesons. For massless quarks this helicity amplitude is suppressed, since the photon only couples to $q\bar{q}$ pairs of even chirality.

However, there are approximations involved at this stage since for light quarks the formation of the $q\bar{q}$ dipole cannot be perturbatively calculated, and nor can the vector meson wave function. With some flexibility introduced to allow for such effects, the calculations can also describe the $|t|$ dependence of the data [153], as well as the helicity structure of J/ψ production (where the charm mass adds reliability to the perturbative approximations). They still fail to describe the helicity structure of ρ and ϕ production. Nevertheless, the agreement with the cross-section measurements is further evidence that some understanding of diffraction has been obtained within QCD.

High- t photon production shares the advantages of vector meson production, with the added advantage that the hard subprocess is completely calculable in pQCD - there is no need for a Vector Meson form factor. The disadvantage is that the cross-section is smaller. However, given the enhancements expected from the large s/t logarithms, the process was predicted to be observable at HERA [154], and has indeed been observed [155], providing further compelling evidence, from photoproduction, for the understanding of diffraction within QCD.

Understanding hard colour singlet exchange is not only of great theoretical importance for our understanding of high energy QCD, but is of importance for critical measurements at hadron colliders. In particular, both forward (*i.e.* high rapidity) jet rates and a suppression of QCD radiation between jets will play a key part in measurements of WW scattering (see for example [156] and references therein). This is an important search channel for the Standard Model Higgs, and is also the process where perturbative unitarity is violated within the LHC energy range in the absence of a light Higgs.

Photoproduction has not has its final say on this topic. Preliminary jet and J/ψ data with higher statistics have already been presented [157]. In addition, there is a possibility of extending the rapidity reach of the jet measurement by using the “forward plug calorimeter” [141, 158] which was installed during part of HERA I data taking at ZEUS.

4.7.2 Forward rapidity gaps and forward particles

The other class of rapidity gap events observed in photoproduction is that in which the gap is not within the jet system, but is between the jets and the forward (proton) direction. In fact, in these cases the proton remains intact, or dissociates into a low-mass baryonic state. Thus, an alternative signature for these processes is a tag of a fast forward going proton or neutron. In these events, the moment transferred across the gap is small, and so the coupling between the exchanged colour singlet and the proton is not perturbatively calculable. However, in a subset of events there can be a large momentum scale involved in the scattering between the photon and the exchanged colour singlet, and thus partonic language may be useful for discussing some aspects of the event. In particular, one can assume factorisation, and discuss conditional parton distributions in the proton, *e.g.* diffractive parton distributions. Often a further assumption is made in which the exchange is treated as a particle with a momentum distribution and its own parton densities (Regge factorisation for diffraction, or the one pion exchange model for forward neutron production). While these models are known [159], or expected, to fail in detail, they remain a useful approximation over a wide range of phase space.

The distribution of the momentum fraction x_L for forward protons and neutrons is shown in Fig. 30. In the case of protons, a clear peak due to diffractive processes is seen at $x_L \approx 1$. In general, those processes where the proton or low-mass dissociated system carries more than around 99% of the initial proton energy are dominated by diffraction (this may even be seen as a definition of diffraction). In the case of neutrons, no such diffractive peak is seen, though the distribution does peak at lower values, around $x_L = 0.7$, as expected from single pion exchange models.

Of particular interest is the use of photoproduction to study factorisation and the breaking of factorisation in diffractive processes. There is a factorisation theorem for diffraction

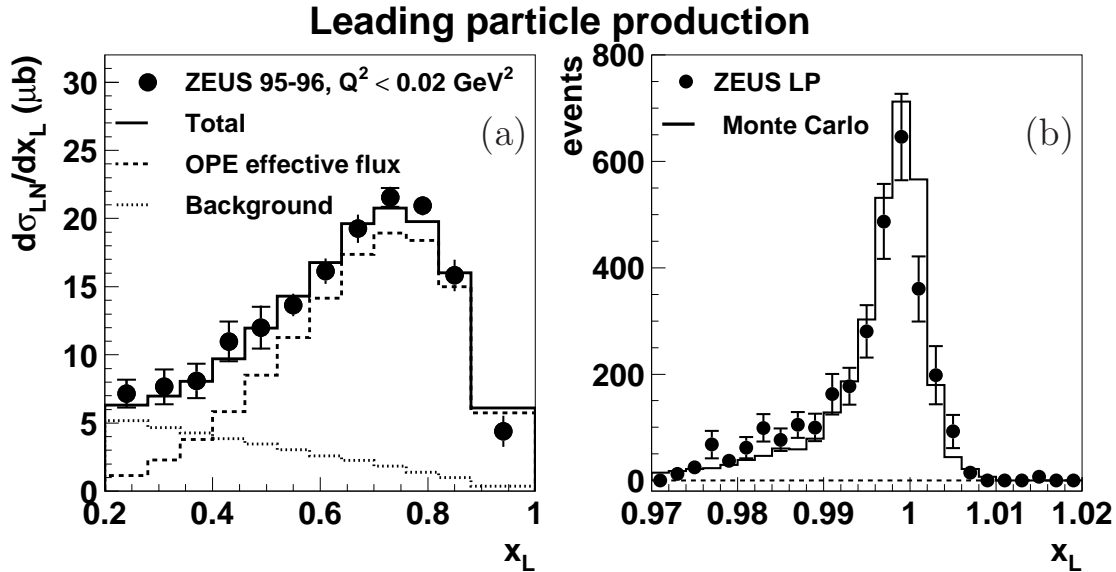


Figure 30: *The distribution x_L , of fraction of the incoming proton momentum carried by a tagged forward (a) neutron [160] and (b) proton [161]. Note the different horizontal scales!*

in DIS [162]; that is, one can define and use a set of diffractive parton densities for the proton and use them in different diffractive DIS processes as one would with the normal inclusive PDFs. However, this explicitly does not apply in hadron-hadron interactions because of the possibility of soft rescattering between the hadrons. At least naively then, one might expect direct photoproduction to exhibit factorisation, since there is only one incoming hadron, and resolved photoproduction to exhibit factorisation breaking, since it looks like a hadron-hadron collision. It is important to remember, however, that the terms resolved and direct photoproduction are short hand for kinematic extremes, the no unique separation between the two processes is possible (see Section 3). Specifically then, a lower fraction of diffractive processes might be expected at low x_γ^{obs} compared to high x_γ^{obs} .

Dijet photoproduction in association with a forward rapidity gap has been measured [163] and compared to LO Monte Carlo models as well as NLO QCD calculations [30,164], using diffractive PDFs extracted from DIS data. The LO Monte Carlos, which in this case do not include any remnant-remnant interactions, describe the shape of the data distributions well without any need for a rescattering correction. However, in the NLO calculations, agreement is only seen if a rescattering correction of around 0.5 is applied. Additionally, it seems that this must be applied over all x_γ^{obs} values. The predicted suppression [165] is around 0.34 for hadronic events. The validity or not of QCD factorisation here is, however, complicated by the uncertainty in the diffractive PDFs [166] and their application

in dijet production in deep inelastic scattering [167]. Fits to different data sets lead to significantly different diffractive parton densities which when used to calculate the diffractive dijet cross section in deep inelastic scattering differ by a factor of two. Only by further understanding of the inclusive diffractive data and the techniques used can this be resolved and the question of factorisation breaking in jet production in hadron-hadron collisions, photoproduction and deep inelastic scattering be addressed.

The leading neutron energy spectrum in photoproduction (as well as DIS) at HERA has been shown to be well described by single pion exchange [160,168]. Some of the most interesting aspects of these interactions concern what is variously described as rescattering, absorption, or the multiple interaction probability.

4.7.3 Survival and rescattering

In Section 2.3, underlying event models were discussed, with a particular emphasis on multiple hard scatters. However, soft scattering may also be eikonalised (*i.e.* repeated and exponentiated). For instance, multiple soft Pomeron exchange preserves unitarity in Regge based models which make no reference to partonic scattering. The natural “soft” counterpart of multiple parton scattering is soft rescattering, or absorption, which will affect the forward proton or neutron rate even if not enough momentum transfer is involved to throw particles into a detector and destroy a (pseudo)rapidity gap.

In hard multiple scattering models in hadron-hadron collisions, the presence of a hard scale is correlated to an increased probability of multiple interactions, since both are more likely in central collisions.

In inclusive photoproduction, where there is no hard scale, the photon is dominantly hadronic, and the forward neutron rate is expected to be reduced by soft rescattering. In DIS, two things are different. First there is a hard scale, and second, the photon is small, (that is, pointlike at the scale of the interaction). Obviously in DIS these are both due to the large photon virtuality. However, the statements are not equivalent. Because it is pointlike, the photon has no remnant to undergo rescattering. The forward neutron rate is correspondingly higher, even though if the photon were considered as a hadron, one might expect a hard scale to increase rescattering.

In charm photoproduction [169], there is again a hard scale, provided by the charm mass. Some contribution from the hadronic photon is expected to be present, but this is suppressed with respect to the inclusive case, at least for inclusive dijet charm events [67]. There is no evidence for rescattering in these events, with the measured neutron fraction of $9 \pm 1\%$ being in good agreement with the DIS rate, and inconsistent with the rate for inclusive photoproduction.

Finally one can consider dijet photoproduction. Here a hard scale is present, but one can select between hadronic and pointlike photons using the x_γ^{obs} variable. Measurements of dijet photoproduction as a function of x_γ^{obs} help clarify the situation. All jet cross-sections self-evidently involve a hard scale, but the x_γ^{obs} variable allows the “size” of the photon to be deconvoluted from this, in that larger, hadronic photons are more likely to give rise to events with low x_γ^{obs} . The H1 measurement [170] of the ratio of forward-neutron-tagged to inclusive dijet photoproduction in Fig. 31 confirms that, independent of the scale, there is a lower neutron rate in resolved photoproduction events, as expected from rescattering models in hadronic collisions.

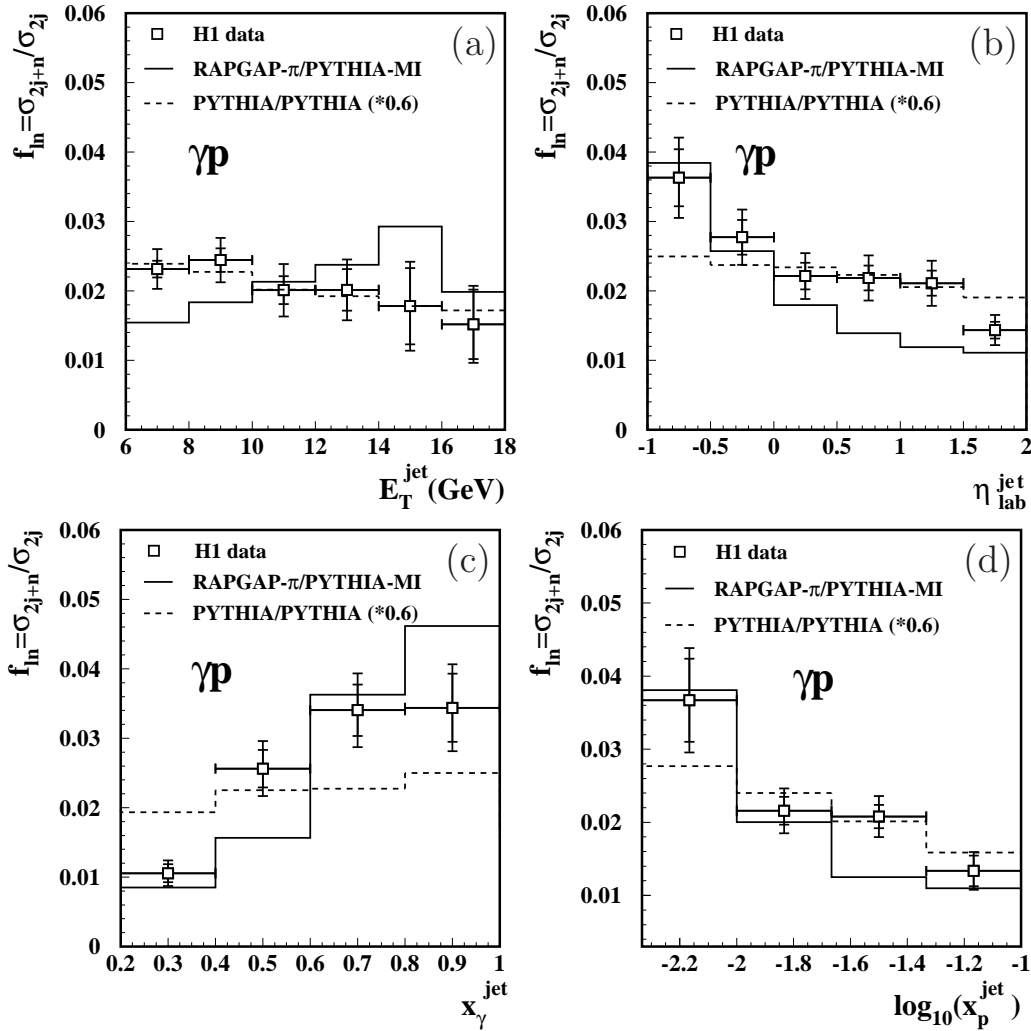


Figure 31: The ratio of the cross section for dijet photoproduction with a leading neutron to that for inclusive dijet photoproduction as a function of (a) E_T^{jet} , (b) η^{jet} , (c) x_γ^{jet} and (d) x_p^{jet} . The Monte Carlo predictions are shown for PYTHIA for inclusive production and either PYTHIA or RAPGAP with one-pion exchange for neutron production.

One major source of interest in the measurements of forward proton and neutron production, and the understanding of rescattering effects, is that exclusive diffractive production may be an important search channel for new physics at LHC [171]. The phenomenological predictions require a good understanding of diffractive processes, particularly diffractive PDFs and factorisation breaking. Comparison to high energy photoproduction data, as well as to $p\bar{p}$ data, is a critical factor in developing and demonstrating this understanding.

5 Photoproduction and the search for new physics

As discussed in Section 1, photon beams generally derive from electron or positron beams. Thus they carry some fraction the lepton energy, and so in general do not compete in terms of sheer centre-of-mass energy when it comes to searching for new physics. However, in some specialised cases photon-proton interactions do have an enhanced sensitivity to new physics which compensates for this energy disadvantage.

Of course, it is always possible that some new physics, or a model for new physics, will arise which is expected to show up uniquely in photoproduction due for instance to something unique in the photon-quark coupling. Therefore it is worthwhile, at the highest photoproduction energies, doing a general search for new signatures regardless of the existing theoretical prejudices. An example of such an analysis is the search for new heavy resonances (\mathcal{P}) in the channel $e^+p \rightarrow e^+\mathcal{P}X$ where the heavy resonance decays to two jets [172]. Since the search is made in the kinematic region $Q^2 < 1 \text{ GeV}^2$, this corresponds to the photoproduction of \mathcal{P} from almost-real photons. The upper limit for the production of such a resonance was measured to be about 1 pb for masses up to 155 GeV.

Taking an even more general approach, the H1 collaboration have made a general search for new phenomena in ep scattering at HERA [173] shown in Fig. 32. This involves a systematic comparison of a wide variety of signatures (leptons, jets, missing transverse energy) with SM expectations, and thus includes high energy photoproduction as well as DIS. Most event classes show good agreement with the SM, but there is an excess of events containing an isolated muon, missing transverse momentum and a jet. This corresponds to the observation, for transverse momentum of the hadronic system, $p_T > 40 \text{ GeV}$, of 3 events where the expected background is 0.54 ± 0.11 , which was already reported in a more specific analysis [174]. In this analysis there is also an excess in the channel with an isolated electron instead of muon (3 events for an expected background of 0.55 ± 0.12). A similar search has been carried out by ZEUS [174], where, disappointingly, no such excess is seen. The τ channel has also been studied by ZEUS [175], where one event is seen with an expected background of 0.07 ± 0.02 . The dominant contribution to SM backgrounds quoted above is the photoproduction of W bosons [176]. This cross-section peaks at lower missing p_T , however, where it is consistent with the observed number of events.

If the events are due to new physics, the initially favoured explanation would be single top quark production [177], arising from an anomalous $tu\gamma$ (flavour-changing neutral-current) coupling, $\kappa_{tu\gamma}$. However, the lack of an excess in the electron and muon channels from ZEUS sets a stringent limit on such a coupling [178]. Even H1 data, if the observed excess is taken to be a statistical fluctuation [179], sets a limit on $\kappa_{tu\gamma}$ which is more stringent than Tevatron or LEP limits in the case that the anomalous Z coupling is small (Fig. 33).

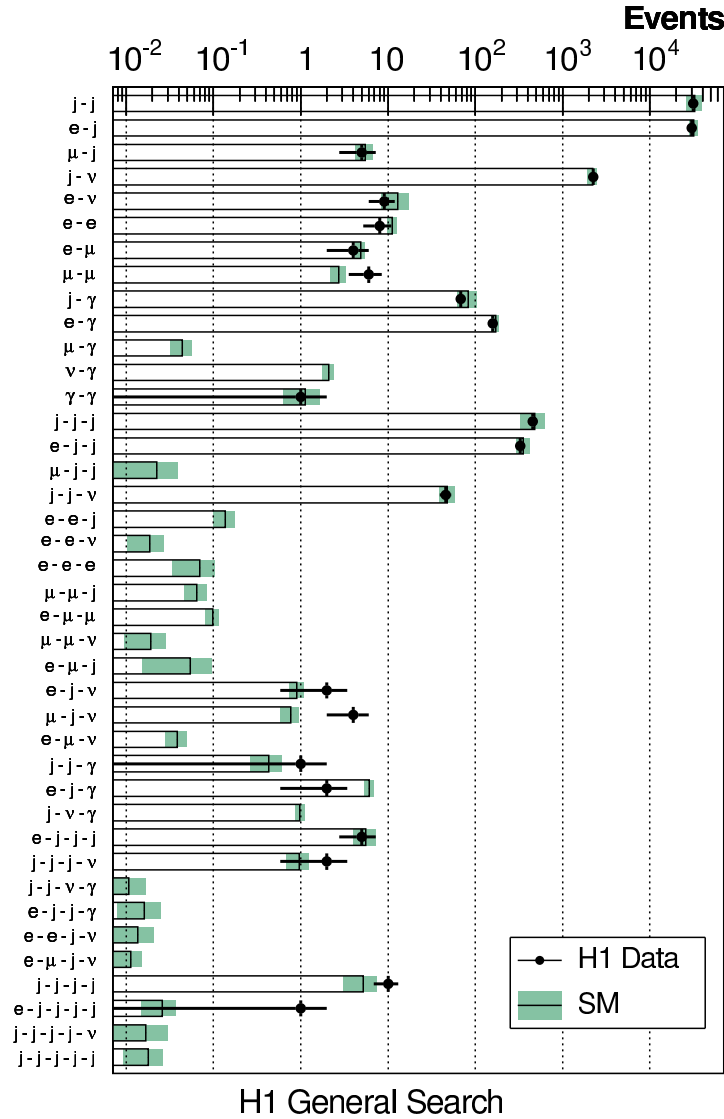


Figure 32: Data (integrated luminosity of 117 pb^{-1}) compared with the Standard Model expectation for all event classes with a Standard Model expectation of more than 0.01 events.

Supersymmetric-top production in R-parity-violating SUSY models [180] followed by either R-parity violating two-body decay or R-parity conserving cascade decays are another source of such signatures. Neither the SUSY or FCNC case involves photoproduction as the signal process. Nevertheless, if the excesses are confirmed in HERA-II data, and the observations of the two experiments are consistent, there is no doubt other new physics models will be proposed, and this represents perhaps the most exciting frontier in high energy photoproduction. At the time of writing, H1 have reported the observation of two further events, in the electron channel, with hadronic $p_T > 40 \text{ GeV}$ from HERA II data,

on an expected background of around 1 [181].

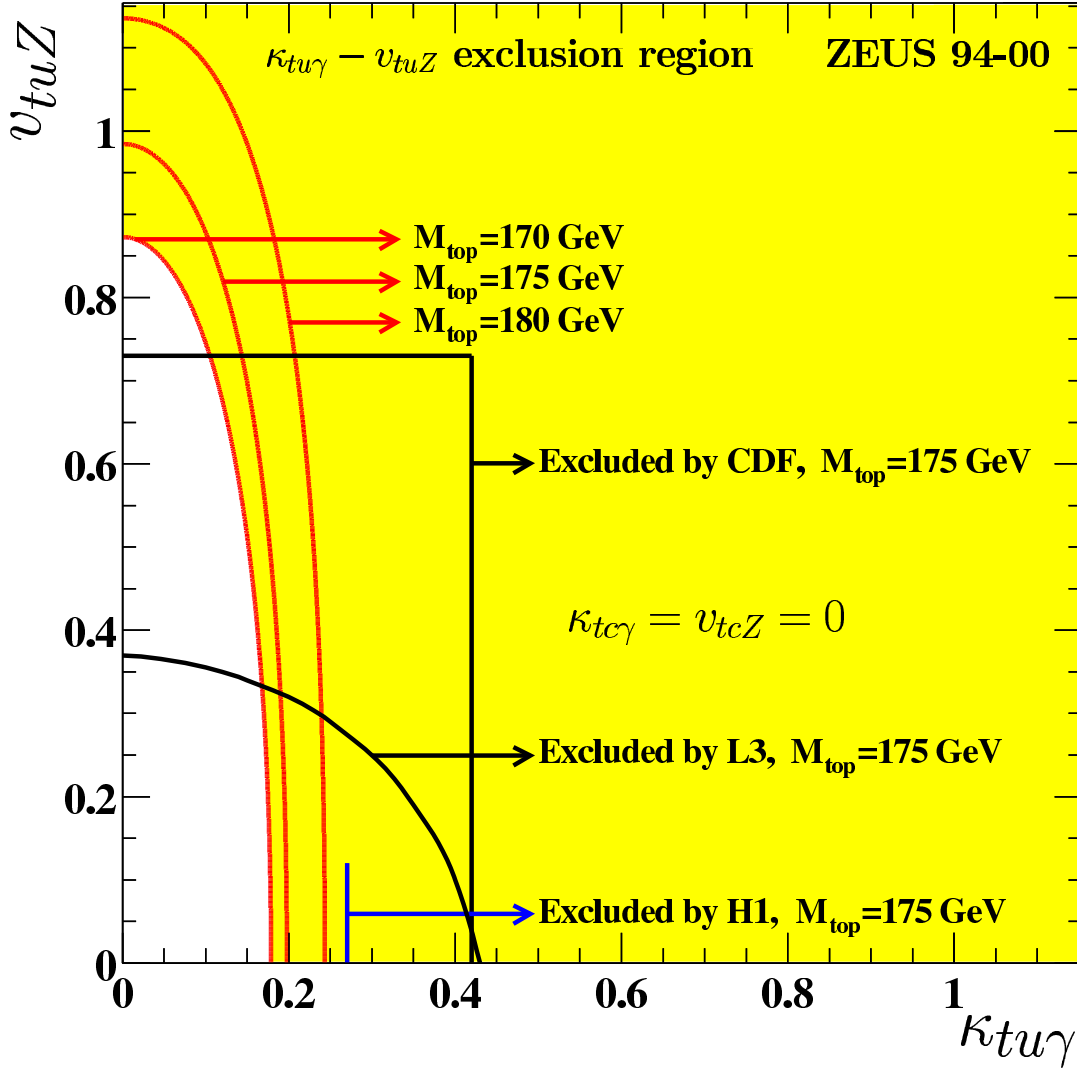


Figure 33: Exclusion regions at 95% CL in the $\kappa_{tu\gamma} - v_{tuZ}$ plane for three values of M_{top} (170, 175 and 180 GeV) assuming $\kappa_{tc\gamma} = v_{tcZ} = 0$. The CDF, L3 and H1 exclusion limits are also shown.

One sometimes exotic area we have not considered in this review is that of hadron spectroscopy. Recently, several low-energy photoproduction experiments reported evidence for 5-quark (pentaquark) states [182]. Possible candidates were also seen in DIS [183], proton-proton [184], proton-nucleus [185], neutrino-nucleus [186] and Kaon-nucleus [187] interactions, but several negative results have also been published [188] or presented. The only *high-energy* photoproduction observation of such a state [189] is less significant than

the observation in the same publication in DIS. The observation is contradicted in both photoproduction and DIS by other measurements [102] and to date remains unconfirmed. Deuteron photoproduction has been measured, and limits set on the photoproduction cross-section for other heavy stable charged particles [190]. This, and other studies of identified hadrons and resonances in DIS at HERA may indicate a potential for a major contribution in this area from high-energy photoproduction as well.

6 Summary: past, present and future

In the past few years, high energy photoproduction has lead to major advances in our understanding of the photon, the proton and QCD in general. Substantial progress has been made, with a great synergy between the HERA experiments and an active theory and phenomenology community.

In a review of resolved photoproduction in 1995 [191], Drees and Godbole concluded with a list of open issues in hard photon-proton scattering. It is interesting and fun to return to this and see how much progress has really been made since that year, as well to suggest what progress might be made in the next ten years. We quote from their paper:

- **1995:** *“No complete NLO treatment of di-jet production exists. Recall that one needs to measure the rapidities of both high- p_T partons/jets in a hard event in order to reconstruct the Bjorken- x variables.”*

2005: Several complete leading order programs are now available(Section 2.4). They have been used extensively in many of the results discussed herein (e.g. Sections 3.2.1, 3.3, 4.1, 4.2). Of course, physicists are never satisfied. To make best use of the data, it would be great if jet photoproduction processes could be made available within the Monte Carlo programs which include NLO terms, which are now becoming available for other processes [192].

- **1995:** *“The measured jet cross-sections should be extended both in rapidity and in p_T . The former increases the sensitivity to the interesting region of small x_γ , while the latter should allow to test theory cleanly, since a detailed understanding of the underlying event (see below) is less crucial at high p_T , and differences between parametrizations of photonic parton densities are small at large x_γ and large momentum scale.”*

2005: Both of these have been achieved experimentally. Going to high E_T^{jet} has indeed meant that model uncertainties can be reduced to the point that jet cross-section may be used with confidence to extract NLO parton densities for the proton (Section 4.1). This kind of approach is the best way to extract information on the photon structure as well. Unfortunately, the need to stay a reasonably high E_T^{jet} means it is unlikely that high energy photoproduction at HERA will ever produce strong constrains at x_γ below 0.05 or so.

- **1995:** *“It might be interesting to try to correlate properties of the photonic remnant jet with those of the high- p_T jets. In the usual “nonperturbative + anomalous” description of the hadronic photon, the nonperturbative component should always have a remnant jet with very small k_T ; this component is also characterized by soft parton densities. In this picture one therefore expects nontrivial correlations between x_γ and k_T .”*

2005: This is one where no data have been published since 1995 (Section 3.1). However, the anomalous and non-perturbative aspects of the photon structure are elucidated somewhat by studies of dijet and charm production from virtual photons (Section 3.3).

- **1995:** *“Studies of heavy flavour production hold great potential. We do not think it very interesting to try to derive total cross-sections from measurements covering only a limited region of phase space, which contains only a small fraction of all produced heavy quarks. It might be more fruitful to attempt to extract the resolved photon contribution, which is sensitive to the as yet poorly constrained gluon density in the photon. At high p_T , “excitation” contributions from the charm in the photon have to be taken into account. An important open problem is the fragmentation of rather soft (low- p_T) charm quarks, which contribute most to the total charm cross-section. Theoretical predictions are more reliable for b production, but it might be difficult to find a clean signal.”*

2005: On this issue, Drees and Godbole were particularly prescient. The field of heavy flavour photoproduction has exploded since 1995 (see Section 4.3), and one of the main reasons has been the fact that sophisticated programs were developed which could make QCD calculations of measured cross-sections in realistic kinematics regions, rather than being limited to total cross-sections. In addition, despite the lower cross-section, good measurements of beauty production have been made, and these have also benefitted from similar calculational advances. The result is a vastly improved confidence in our understanding of charm and beauty production in QCD.

- **1995:** *“The production of direct photons is by now quite well understood, although an NLO calculation of photon + jet production would certainly be welcome. Realistic background studies are also needed, but can presumably only be performed by members of HERA experiments.”*

2005: NLO calculations of γ +jet have indeed been made (Section 2.4) as have further measurements at HERA (Section 3.2.2). These have provided a convincing test of factorisation, as well as information on the effective transverse momentum of quarks in the proton [61].

- **1995:** *“In spite of the recent NLO calculation [121] of direct J/ψ production in the colour singlet model, much needs to be done here: The resolved photon contribution is only known to leading order in the colour singlet model. Nothing is known about the contribution from the colour octet component of the wave function of the J/ψ [117], which is accessible to resolved photons already in LO. In addition, there are contributions at high p_T coming from charm and gluon fragmentation.”*

2005: Inelastic J/ψ photoproduction has been measured, and calculated, with in-

creasing precision (Section 4.4). Certainly something is now known about colour-octet contributions, but more precision in the calculations, including NLO terms, is highly desirable. On the issue of high p_T production, fragmentation production may still have an effect in high p_T photoproduction data from HERA II, but no clear sign of it is seen in current data.

- **1995:** *“It is important to test our understanding of the hadronic photon in as many different channels as possible. The production of Drell–Yan lepton pairs, two photon final states, and associate $J/\psi + \gamma$ final states are all plagued by rather small cross-sections, but this should at least partly be compensated by the cleanliness of the final states.”*

2005: Thus far in most of these particular cases, we are still waiting for data (although inelastic photoproduction of $\psi' \rightarrow J/\psi + \gamma$ has been measured [119]). Towards the end of HERA II there should be enough luminosity to measure Drell-Yan lepton pairs (Section 3.2.2). Several other interesting final states, not obvious in 1995, have emerged. These include the whole class of rapidity gap events, both forward gaps and gaps between jets, which were measured in photoproduction very shortly after the 1995 review (Section 4.7). Along with high- $|t|$ J/ψ photoproduction and forward neutron production, these processes have led to great advances in the understanding of high energy, low- x QCD and related areas.

In addition to the above areas specific to photoproduction, several of the more generic areas highlighted by Drees and Godbole (minimum bias events, multiple parton interactions...) have seen major advances during the past decade.

As to the where the next photoproduction measurements will come from; HERA II still has much to say. Data taking is currently planned to stop in 2007, and data analysis is likely to be complete within a few years after that date. Following that, the future is less clear. At the LHC, the photoproduction of heavy quarks and vector mesons [193], including even $t\bar{t}$ pairs [194], in peripheral proton-proton or heavy ion collisions will have a significant cross-section and may provide valuable information on high-density, low- x QCD. Beyond that, the only high-energy photoproduction for the foreseeable future seems likely to be that from ultra-high-energy cosmic rays.

There is a necessary arbitrariness in choosing a particular process to review, and photoproduction in particular touches upon a wide variety of topics in high-energy physics. The inclusion of jet photoproduction in QCD fits for the proton structure represents something of a “coming of age” for the area, showing as it does that our understanding of these processes is comparable now to our knowledge of deep inelastic scattering. This clearly fits as well in a discussion of proton structure as in a review of photoproduction. Hopefully the reader is convinced by now that diffraction and low- x physics, heavy flavour physics

and searches for new physics are all areas on which high-energy photoproduction has an impact. Because we learn about these areas of physics, photoproduction data has value for physicists preparing for data analysis at the LHC. The nature and high energy reactions of the photon itself are of huge fundamental interest; they also have an impact on astrophysics and physics at the ILC. The study of the interactions of the photon remains one of the more fruitful areas within high-energy physics.

Appendix A: Monte Carlo models used in this review

Most of the Monte Carlo curves shown in the body of the text have been remade by the authors using the HZTOOL [195] package, released as part of CEDAR [115]. Further models and comparisons are available from the CEDAR/JetWeb pages.

For these MC distributions, unless otherwise stated explicitly, the proton PDF is CTEQ5 (LO) [13] and the photon PDF is GRV (LO) [12].

The standard HERWIG [24] curves use:

HERWIG 6.507, IPROC=15000 for direct photoproduction and 11500 for resolved, 12400 (hard colour singlet exchange). The underlying event is simulated using JIMMY [21], with PTJIM=3.0 GeV, and the JMRAD(73)=JMRAD(75)=2.13 GeV. For the colour singlet exchange, the changes OMEGA0=0.48 and ASFIXD=0.18 were made. For the photon remnant curve with intrinsic K_{\perp} (Fig. 6), PTRMS was set to 1 GeV.

The standard PYTHIA [196] curves use:

PYTHIA 6.206, MSTP(14) = 30 (mixture of resolved and direct QCD processes). To obtain the “incoherent” model of Fig. 27, the following parameters were changed from their defaults: PARP(67)=4.0, MSTP(62)=2, MSTP(63)=2, MSTP(67)=0, MSTJ(42)=1, MSTJ(46)=1, MSTJ(50)=0.

References

- [1] J.J. Sakurai, *Ann. Phys.* **11**, 1 (1960).
- [2] M. Gell-Mann and F. Zachariasen, *Phys. Rev.* **124**, 953 (1961).
- [3] E.D. Bloom et al., Preprint SLAC-PUB-0653, 1969;
T.A. Armstrong et al., *Phys. Rev.* **D 5**, 1640 (1972);
H.G. Hilpert et al., *Phys. Lett.* **B 27**, 474 (1968);
B.D. Dieterle et al., *Phys. Rev. Lett.* **23**, 1187 (1969);
M.L. Perl et al., *Phys. Rev. Lett.* **23**, 1191 (1969);
H. Meyer et al., *Phys. Lett.* **B 33**, 189 (1970);
S. Michalowski et al., *Phys. Rev. Lett.* **39**, 737 (1977);
J. Ballam et al., *Phys. Rev.* **D 5**, 545 (1972);
D.O. Caldwell et al., *Phys. Rev.* **D 7**, 1362 (1973);
G. Alexander et al., *Nucl. Phys.* **B 68**, 1 (1974);
H.H. Bingham et al., *Phys. Rev.* **D 8**, 1277 (1973);
D.O. Caldwell et al., *Phys. Rev.* **40**, 1222 (1978);
G.M. Vereshkov et al., *Phys. Atom. Nucl.* **66**, 565 (2003);
H1 Coll., S. Aid et al., *Z. Phys.* **C 69**, 27 (1995);
ZEUS Coll., S. Chekanov et al., *Nucl. Phys.* **B 627**, 3 (2002).
- [4] A. Donnachie and P.V. Landshoff, *Phys. Lett.* **B 296**, 227 (1992).
- [5] A. Donnachie and P.V. Landshoff, *Phys. Lett.* **B 595**, 393 (2004).
- [6] M.G. Ryskin, *Z. Phys.* **C 57**, 89 (1993);
S. Brodsky et al., *Phys. Rev.* **D 50**, 3134 (1994).
- [7] H1 Coll., I. Abt et al., *Nucl. Phys.* **B 407**, 515 (1993);
ZEUS Coll., M. Derrick et al., *Phys. Lett.* **B 316**, 412 (1993).
- [8] For early fixed-target data numbers and references, see:
S.I. Alekhin et al., *Total cross sections for reactions of high energy particles*, 1987.
CERN-HERA 87-01, Landolt Bornstein, New Series, Vol. 12b, ed. H. Schopper;
H1 Coll., S. Aid et al., *Nucl. Phys.* **B 463**, 3 (1996);
ZEUS Coll., M. Derrick et al., *Z. Phys.* **C 63**, 391 (1994);
ZEUS Coll., M. Derrick et al., *Z. Phys.* **C 69**, 39 (1995);
ZEUS Coll., M. Derrick et al., *Z. Phys.* **C 73**, 73 (1996);
ZEUS Coll., J. Breitweg et al., *Eur. Phys. J.* **C 2**, 247 (1998);
J. Busenitz et al., *Phys. Rev.* **D 40**, 1 (1989);
ZEUS Coll., M. Derrick et al., *Phys. Lett.* **B 377**, 259 (1996);
E401 Coll., M. Binkley et al., *Phys. Rev. Lett.* **48**, 73 (1982);
E516 Coll., B.H. Denby et al., *Phys. Rev. Lett.* **52**, 795 (1984);

- ZEUS Coll., S. Chekanov et al., Eur. Phys. J. **C 24**, 345 (2002);
H1 Coll., C. Adloff et al., Phys. Lett. **B 541**, 251 (2002);
ZEUS Coll., J. Breitweg et al., Phys. Lett. **B 437**, 432 (1998);
H1 Coll., C. Adloff et al., Phys. Lett. **B 483**, 23 (2000).
- [9] A. Levy, *DIFFRACTION 2004. Proceedings of the International Workshop on Diffraction in High-Energy Physics*, Vol. 146, p. 92. Nucl. Phys. Proc. Suppl. (2005). Also in preprint hep-ex/0501008;
A.B. Meyer. Private communication.
- [10] I.P. Ivanov, N.N. Nikolaev and A.A. Savin, Preprint hep-ph/0501034, 2005.
- [11] M. Klasen, Rev. Mod. Phys. **74**, 1221 (2002).
- [12] M. Glück, E. Reya and A. Vogt, Phys. Rev. **D 45**, 3986 (1992).
- [13] CTEQ Coll., H.L. Lai et al., Eur. Phys. J. **C 12**, 375 (2000).
- [14] M. Drees, F. Halzen and K. Hikasa., Phys. Rev. **D 39**, 1310 (1989);
M. Drees and F. Halzen, Phys. Rev. Lett. **61**, 275 (1988).
- [15] R. Gandhi et al., Phys. Rev. **D 42**, 263 (1990).
- [16] R. Gandhi and I. Sarcevic, Phys. Rev. **D 44**, 10 (1991).
- [17] M. Samorski and W. Stamm, Astrophys. J. **268**, L17 (1983);
B.L. Dingus et al., Phys. Rev. Lett. **61**, 1906 (1988).
- [18] J.R. Forshaw, and J.K. Storrow, Phys. Lett. **B 268**, 116 (1991). Erratum-ibid. **B 276**, 565 (1992).
- [19] C.M. Hoffman et al., Rev. Mod. Phys. **71**, 897 (1999).
- [20] J.R. Forshaw and J.K. Storrow, Phys. Rev. **D 46**, 4955 (1992).
- [21] J.M. Butterworth, J.R. Forshaw and M.H. Seymour, Z. Phys. **C 72**, 637 (1996).
- [22] T. Sjöstrand and M. van Zijl, Phys. Rev. **D 36**, 2019 (1987).
- [23] T. Sjöstrand and P.Z. Skands, Eur. Phys. J. **C 39**, 129 (2005).
- [24] G. Corcella et al., JHEP **01**, 010 (2001);
G. Corcella et al., Preprint hep-ph/0210213, 2002.
- [25] T. Sjöstrand, L. Lönnblad, S. Mrenna and P. Skands, Preprint hep-ph/0308153, 2003.
- [26] R. Engel, Z. Phys. **C 66**, 203 (1995).
- [27] H. Jung, Comp. Phys. Comm. **86**, 147 (1995).
- [28] H. Jung, Comp. Phys. Comm. **143**, 100 (2002).

- [29] P. Aurenche et al., Eur. Phys. J. **C 17**, 413 (2000).
- [30] S. Frixione and G. Ridolfi, Nucl. Phys. **B 507**, 315 (1997);
S. Frixione, Z. Kunszt and A. Signer, Nucl. Phys. **B 467**, 399 (1996);
S. Frixione, Nucl. Phys. **B 507**, 295 (1997).
- [31] M. Klasen and G. Kramer, Z. Phys. **C 76**, 67 (1997).
- [32] B.W. Harris and J.F. Owens, Phys. Rev. **D 56**, 4007 (1997).
- [33] L.E. Gordon and J.K. Storrow, Phys. Lett. **B 291**, 320 (1992).
- [34] M. Fontannaz, J.P. Guillet and G. Heinrich, Eur. Phys. J. **C 26**, 209 (2002).
- [35] J. Binnewies, B.A. Kniehl and G. Kramer, Phys. Rev. **D 52**, 4947 (1995).
- [36] M. Krawczyk and A. Zembrzuski, Phys. Rev. **D 64**, 114017 (2001).
- [37] M. Fontannaz, J.P. Guillet and G. Heinrich, Eur. Phys. J. **C 21**, 303 (2001).
- [38] L.E. Gordon and J.K. Storrow, Z. Phys. **C 63**, 581 (1994).
- [39] J.R. Forshaw and D.A. Ross, *Quantum Chromodynamics and the Pomeron*,
Cambridge Lecture Notes in Physics, Vol. 9. Cambridge University Press, 1997.
- [40] J.R. Forshaw, G. Kerley and G. Shaw, Phys. Rev. **D 60**, 074012 (1999).
- [41] E. Witten, Nucl. Phys. **B 120**, 189 (1977).
- [42] OMEGA Photon Coll., R.J. Apsimon et al., Z. Phys. **C 43**, 63 (1989).
- [43] H1 Coll., I. Abt et al., Phys. Lett. **B 328**, 176 (1994).
- [44] P. Aurenche et al., Phys. Lett. **B 135**, 164 (1984).
- [45] NA14 Coll., R. Barate et al., Phys. Lett. **B 168**, 163 (1986);
NA14 Coll., R. Barate et al., Phys. Lett. **B 174**, 458 (1986);
NA14 Coll., E. Auge et al., Phys. Lett. **B 182**, 409 (1986);
EMC Coll., J.J. Aubert et al., Phys. Lett. **B 100**, 433 (1981);
EMC Coll., M. Arneodo et al., Z. Phys. **C 36**, 527 (1987).
- [46] H1 Coll., T. Ahmed et al., Phys. Lett. **B 297**, 205 (1992);
ZEUS Coll., M. Derrick et al., Phys. Lett. **B 297**, 404 (1992).
- [47] ZEUS Coll., M. Derrick et al., Phys. Lett. **B 322**, 287 (1994).
- [48] M. Drees, *23rd International symposium on multiparticle dynamics (1993):
proceedings*, M.M. Block and A.R. White (eds.), p. 110. World Scientific, River
Edge, N.J. (1993);
G. A. Schuler and T. Sjöstrand, *Two-photon physics: from Daphne to LEP 200
and beyond: proceedings*, F. Kapusta and J.J. Parisi (eds.), p. 163. World
Scientific, River Edge, N.J. (1994);
J. Chýla, Phys. Lett. **B 320**, 186 (1994).

- [49] ZEUS Coll., M. Derrick et al., Phys. Lett. **B 354**, 163 (1995).
- [50] H1 Coll., C. Adloff et al., Phys. Lett. **B 483**, 36 (2000).
- [51] ZEUS Coll., J. Breitweg et al., Eur. Phys. J. **C 1**, 109 (1998).
- [52] ZEUS Coll., M. Derrick et al., Phys. Lett. **B 348**, 665 (1995).
- [53] R. Nisius, Phys. Rep. **332**, 165 (2000)
(see also: <http://www.mppmu.mpg.de/~nisius/welcomeaux/struc.html>).
- [54] S. Albino, M. Klasen and S. Söldner-Rembold, Phys. Rev. Lett. **89**, 122004 (2002).
- [55] ZEUS Coll., S. Chekanov et al., Eur. Phys. J. **C 23**, 615 (2002).
- [56] H1 Coll., C. Adloff et al., Eur. Phys. J. **C 25**, 13 (2002).
- [57] P. Aurenche, J.P. Guillet and M. Fontannaz, Z. Phys. **C 64**, 621 (1994).
- [58] F. Cornet, P. Jankowski, and M. Krawczyk, Phys. Rev. **D 70**, 093004 (2004);
F. Cornet et al., Phys. Rev. **D 68**, 014010 (2003).
- [59] P. Aurenche, M. Fontannaz and J.Ph. Guillet, Preprint hep-ph/0503259, 2005;
W. Slominski, H. Abramowicz and A. Levy, Preprint hep-ph/0504003, 2005.
- [60] ZEUS Coll., J. Breitweg et al., Phys. Lett. **B 472**, 175 (2000).
- [61] ZEUS Coll., S. Chekanov et al., Phys. Lett. **B 511**, 19 (2001);
H1 Coll., A. Aktas et al., Eur. Phys. J. **C 38**, 437 (2005).
- [62] ZEUS Coll., M. Derrick et al., Z. Phys. **C 67**, 227 (1995).
- [63] H1 Coll., C. Adloff et al., Eur. Phys. J. **C 10**, 363 (1999).
- [64] L.M. Jones et al., Phys. Rev. **D 20**, 2749 (1979). Erratum-ibid. **D 22**, 2922 (1980);
I. Kang and C.H. Llewellyn Smith, Nucl. Phys. **B 166**, 413 (1980);
A.C. Irving and D.B. Newland, Z. Phys. **C 6**, 27 (1980);
A. Vourdas, J. Phys. **G 6**, 789 (1980).
- [65] P.J. Bussey, B. Levchenko and A. Shumilin, *Prompt photon, Drell-Yan and Bethe-Heitler processes in hard photoproduction*, 1996. Proceedings of the workshop Future Physics at HERA Editors G. Ingelman, A. De Roeck, R. Klanner, DESY 1996, p.574 [hep-ph/9609273].
- [66] ZEUS Coll., M. Derrick et al., Phys. Lett. **B 384**, 401 (1995).
- [67] ZEUS Coll., J. Breitweg et al., Eur. Phys. J. **C 6**, 67 (1999).
- [68] ZEUS Coll., S. Chekanov et al., Phys. Lett. **B 565**, 87 (2003).
- [69] ZEUS Coll., S. Chekanov et al., Nucl. Phys. **B 700**, 3 (2004).

- [70] H1 Coll., A. Aktas et al., Eur. Phys. J. **C 37**, 141 (2004).
- [71] ZEUS Coll., S. Chekanov et al., Eur. Phys. J. **C 35**, 487 (2004).
- [72] H1 Coll., C. Adloff et al., Eur. Phys. J. **C 13**, 397 (2000).
- [73] ZEUS Coll., J. Breitweg et al., Phys. Lett. **B 479**, 37 (2000).
- [74] B. Pötter, Comp. Phys. Comm. **133**, 105 (2000).
- [75] G.A. Schuler and T. Sjöstrand, Phys. Lett. **B 376**, 193 (1996).
- [76] J. Chyla, Phys. Lett. **B 488**, 289 (2000).
- [77] J. Chyla et al., Eur. Phys. J. **C 40**, 469 (2005).
- [78] B.J. West, *Charm and the Virtual Photon at HERA and a Global Tracking Trigger for ZEUS*. Ph.D. Thesis, University College London, 2001.
- [79] M.S. Lightwood, *Dijet production and multiscale QCD at HERA*. Ph.D. Thesis, University College London, 2004.
- [80] S. Kretzer et al., Phys. Rev. **D 69**, 114005 (2004).
- [81] A.D. Martin et al., Eur. Phys. J. **C 39**, 155 (2005).
- [82] ZEUS Coll., S. Chekanov et al., Eur. Phys. J. **C 42**, 1 (2005).
- [83] H1 Coll., C. Adloff et al., Eur. Phys. J. **C 30**, 1 (2003).
- [84] S. Alekhin, Phys. Rev. **D 68**, 014002 (2003).
- [85] M. Glück, E. Reya and A. Vogt, Eur. Phys. J. **C 5**, 461 (1998).
- [86] A. Vogt, S. Moch and J.A.M. Vermaseren, Nucl. Phys. **B 691**, 129 (2004);
S. Moch, J.A.M. Vermaseren and A. Vogt, Nucl. Phys. **B 688**, 101 (2004);
S. Moch, J.A.M. Vermaseren and A. Vogt, Phys. Lett. **B 606**, 123 (2005);
J.A.M. Vermaseren, A. Vogt and S. Moch, Preprint hep-ph/0504242, 2005.
- [87] D. Stump et al., JHEP **10**, 046 (2003).
- [88] ZEUS Coll., S. Chekanov et al., Phys. Lett. **B 547**, 164 (2002).
- [89] C. Targett-Adams. Personal Communication. To appear in University College London PhD Thesis, 2005;
J.M. Butterworth and T. Carli, *QCD uncertainties at the LHC and the implications of HERA*, 2004. Published in Strbske Pleso 2004, Deep inelastic scattering 22-37, hep-ph/0408061.
- [90] A. DeRoeck and H. Jung (Editors). Proceedings of the CERN-DESY workshop on the implications of HERA for LHC physics, available on <http://www.desy.de/~heralhc/>.

- [91] R. Devenish and A. Cooper-Sarkar, *Deep inelastic scattering*. Oxford University Press, 2004.
- [92] CDF Coll., F. Abe et al., Phys. Rev. Lett. **70**, 1376 (1993).
- [93] D0 Coll., B. Abbot et al., Phys. Rev. Lett. **86**, 2523 (2001).
- [94] H1 Coll., C. Adloff et al., Eur. Phys. J. **C 29**, 497 (2003).
- [95] D0 Coll., B. Abbot et al., Phys. Rev. Lett. **82**, 2451 (1999);
UA1 Coll., G. Arnison et al., Phys. Lett. **B 172**, 461 (1986);
UA1 Coll., C. Albajar et al., Nucl. Phys. **B 309**, 405 (1988).
- [96] ZEUS Coll., S. Chekanov et al., Phys. Lett. **B 560**, 7 (2003).
- [97] S. Bethke, *Loops and Legs in Quantum Field Theory. Proceedings of the 7th DESY Workshop on Elementary Particle Theory*, Vol. 135, p. 345.
Nucl. Phys. Proc. Suppl. (2004). Also in preprint hep-ex/0407021.
- [98] ZEUS Coll., S. Chekanov et al., Phys. Rev. **D 69**, 012004 (2004);
H1 Coll., A. Aktas et al., Eur. Phys. J. **C 40**, 349 (2005).
- [99] CDF Coll., F. Abe et al., Phys. Rev. Lett. **71**, 500 (1993);
CDF Coll., F. Abe et al., Phys. Rev. Lett. **71**, 2396 (1993);
CDF Coll., F. Abe et al., Phys. Rev. **D 53**, 1051 (1996);
CDF Coll., F. Abe et al., Phys. Rev. **D 55**, 2546 (1996);
D0 Coll., B. Abbot et al., Phys. Lett. **B 487**, 264 (2000).
- [100] UA1 Coll., C. Albajar et al., Phys. Lett. **B 256**, 121 (1991). Erratum-ibid.
B 262, 497 (1991).
- [101] E.L. Berger et al., Phys. Rev. Lett. **86**, 4231 (2001).
- [102] ZEUS Coll., S. Chekanov et al., Eur. Phys. J. **C 38**, 29 (2004).
- [103] M. Cacciari, M. Greco and P. Nason, JHEP **05**, 007 (1998).
- [104] C. Peterson et al., Phys. Rev. **D 27**, 105 (1983).
- [105] S. Frixione and B.R. Webber, JHEP **0206**, 029 (2002);
S. Frixione, P. Nason and B. R. Webber, JHEP **0308**, 007 (2003).
- [106] H1 Coll., A. Aktas et al., Eur. Phys. J. **C 38**, 447 (2005).
- [107] ZEUS Coll., S. Chekanov et al., Preprint hep-ex/0508019, 2005.
- [108] H1 Coll., C. Adloff et al., Phys. Lett. **B 467**, 156 (1999);
ZEUS Coll., J. Breitweg et al., Eur. Phys. J. **C 18**, 625 (2001).
- [109] H1 Coll., A. Aktas et al., Eur. Phys. J. **C 41**, 453 (2005).
- [110] ZEUS Coll., S. Chekanov et al., Phys. Rev. **D 70**, 012008 (2003).

- [111] ZEUS Coll., S. Chekanov et al., Phys. Lett. **B 599**, 173 (2004).
- [112] CDF Coll., D. Acosta et al., Phys. Rev. **D 71**, 032001 (2005).
- [113] L3 Coll., M. Acciarri et al., Phys. Lett. **B 503**, 10 (2001).
- [114] O. Gutsche, *Measurement of Beauty Quark Cross Sections in Photoproduction with the ZEUS detector*. Hamburg University PhD Thesis, DESY-THESIS-2005-010, March, 2005, available on <http://www-zeus.desy.de/physics/hfla/public/Theses/theses.html>.
- [115] J.M. Butterworth et al., *The CEDAR project*. In Computing in High-Energy Physics (CHEP'04), Interlaken, Switzerland, 27th September - 1st October, 2004, available on <http://www.cedar.ac.uk>;
J.M. Butterworth and S. Butterworth, Comput. Phys. Commun. **153**, 164 (2003).
- [116] E.L. Berger and D.L. Jones, Phys. Rev. **D 23**, 1521 (1981).
- [117] G.T. Bodwin, E. Braaten and G.P. Lepage, Phys. Rev. **D 51**, 1125 (1995);
P.L. Cho and A.K. Leibovich, Phys. Rev. **D 53**, 150 (1996);
M. Cacciari and M. Krämer, Phys. Rev. Lett. **76**, 4128 (1996);
P. Ko, J. Lee and H.S. Song, Phys. Rev. **D 54**, 4312 (1996).
- [118] CDF Coll., F. Abe et al., Phys. Rev. Lett. **79**, 572 (1997).
- [119] ZEUS Coll., S. Chekanov, et al., Eur. Phys. J. **C 27**, 173 (2003).
- [120] H1 Coll., C. Adloff et al., Eur. Phys. J. **C 25**, 25 (2002).
- [121] M. Krämer et al., Phys. Lett. **B 348**, 657 (1995);
M. Krämer, Nucl. Phys. **B 459**, 3 (1996).
- [122] M. Krämer, Prog. Part. Nucl. Phys. **47**, 141 (2001).
- [123] M. Beneke, G. A. Schuler, and S. Wolf, Phys. Rev. **D 62**, 034004 (2000);
B.A. Kniehl and G. Kramer, Eur. Phys. J. **C 6**, 493 (1999).
- [124] S.D. Ellis, Z. Kunszt and D.E. Soper, Phys. Rev. Lett. **69**, 3615 (1992).
- [125] S. Catani et al., Nucl. Phys. **B 383**, 419 (1992);
M.H. Seymour, Nucl. Phys. **B 421**, 545 (1994);
M.H. Seymour, Phys. Lett. **B 378**, 279 (1996);
J.R. Forshaw and M.H. Seymour, JHEP **9909**, 009 (1999).
- [126] OPAL Coll., R. Akers et al., Z. Phys. **C 63**, 197 (1994).
- [127] ZEUS Coll., J. Breitweg et al., Eur. Phys. J. **C 8**, 367 (1999).
- [128] ZEUS Coll., J. Breitweg et al., Eur. Phys. J. **C 2**, 61 (1998).
- [129] CDF Coll., F. Abe et al., Phys. Rev. Lett. **70**, 713 (1993);
D0 Coll., S. Abachi et al., Phys. Lett. **B 357**, 500 (1995).

- [130] ZEUS Coll., J. Breitweg et al., Phys. Lett. **B 443**, 394 (1998).
- [131] E.A. Kuraev, L.N. Lipatov and V.S. Fadin, Sov. Phys. JETP **45**, 199 (1977).
- [132] Ya.Ya. Balitskii and L.N. Lipatov, Sov. J. Nucl. Phys. **28**, 822 (1978).
- [133] ZEUS Coll., M. Derrick et al., Phys. Lett. **B 369**, 55 (1996).
- [134] D0 Coll., S. Abachi et al., Phys. Rev. Lett. **76**, 734 (1996);
D0 Coll., B. Abbott et al., Phys. Lett. **B 440**, 189 (1998);
CDF Coll., F. Abe et al., Phys. Rev. Lett. **74**, 855 (1995);
CDF Coll., F. Abe et al., Phys. Rev. Lett. **80**, 1156 (1998).
- [135] A.H. Mueller and W.K. Tang, Phys. Lett. **B 284**, 123 (1992).
- [136] B.E. Cox, J.R. Forshaw and L. Lönnblad, JHEP **10**, 023 (1999);
A. C. Wyatt, *Energy Flow and Rapidity Gaps between Jets in Photoproduction*,
2001. Manchester University PhD Thesis;
B.E. Cox, M.H. Seymour and A.C. Wyatt. Unpublished.
- [137] G. Oderda, Phys. Rev. **D 61**, 014004 (2000).
- [138] G. Oderda and G. Sterman, Preprint hep-ph/9910414, 1999.
- [139] H1 Coll., C. Adloff et al., Eur. Phys. J. **C 24**, 517 (2002).
- [140] S. Catani et al., Nucl. Phys. **B 406**, 187 (1993).
- [141] J.M. Butterworth, M.E. Hayes, M.H. Seymour and L.E. Sinclair, *Rapidity gaps between jets*, 1995. Proceedings of the workshop Future Physics at HERA Editors G. Ingelman, A. De Roeck, R. Klanner, DESY 1996, p.566 [hep-ph/9609227].
- [142] G. Oderda and G. Sterman, Phys. Rev. Lett. **81**, 3591 (1998).
- [143] C.F. Berger, T. Kucs and G. Sterman, Phys. Rev. **D 65**, 094031 (2002).
- [144] R.B. Appleby and M.H. Seymour, JHEP **12**, 063 (2002);
R.B. Appleby and M.H. Seymour, JHEP **09**, 056 (2003).
- [145] J.R. Forshaw, A. Kyrieleis and M.H. Seymour, JHEP **0506**, 034 (2005).
- [146] J.R. Forshaw and M.G. Ryskin, Z. Phys. **C 68**, 137 (1995).
- [147] J. Bartels et al., Phys. Lett. **B 375**, 301 (1996).
- [148] D.Yu. Ivanov et al., Phys. Lett. **B 478**, 101 (2000). Erratum-ibid.
Phys. Lett. **B 498**, 295 (2001).
- [149] R. Enberg et al., JHEP **09**, 008 (2003).
- [150] ZEUS Coll., J. Breitweg et al., Eur. Phys. J. **C 14**, 213 (2000).
- [151] ZEUS Coll., S. Chekanov, et al., Eur. Phys. J. **C 26**, 389 (2003).

- [152] H1 Coll., A. Aktas et al., Phys. Lett. **B 568**, 205 (2003).
- [153] G.G. Poludniowski et al., JHEP **12**, 002 (2003).
- [154] I.F. Ginzburg and D.Yu. Ivanov,, Phys. Rev. **D 54**, 5523 (1996);
 N.G. Evanson. and J.R. Forshaw, Phys. Rev. **D 60**, 034016 (1999);
 D.Yu. Ivanov and M. Wusthoff, Eur. Phys. J. **C 8**, 107 (1999);
 B.E. Cox and J.R. Forshaw, J. Phys. **G 26**, 702 (2000);
 P. Hoyer et al., Eur. Phys. J. **C 17**, 113 (2000).
- [155] M. Beckingham, *Diffraction Photoproduction of High p_T Photons at HERA*, 2004. Manchester University PhD Thesis;
 L. Favart for the H1 Coll., Eur. Phys. J. **C 33**, s509 (2004). H1prelim-03-012.
- [156] ATLAS Coll., *Technical proposal for a general-purpose $p p$ experiment at the Large Hadron Collider at CERN*. CERN-LHCC-94-43;
 ATLAS Coll., *Detector and Physics Performance Technical Design Report*. CERN-LHCC-99-15;
 CMS Coll., *Technical proposal for a general-purpose $p p$ experiment at the Large Hadron Collider at CERN*. CERN-LHCC-94-38.
- [157] ZEUS Coll., *Study of interjet energy flow at HERA*. Abstract 06-289, 32nd International Conference on High Energy Physics, Beijing, China (ICHEP2004), July 2004, available on
<http://www-zeus.desy.de/physics/phch/conf/ichep04/>;
 ZEUS Coll., *Measurement of proton-dissociative diffractive photoproduction of J/ψ mesons at HERA*. Abstract 549, International Europhysics Conference on High Energy Physics, Aachen, Germany (EPS2003), July 2003, available on
http://www-zeus.desy.de/physics/phch/conf/eps03_paper.html.
- [158] A. Bamberger et al., Nucl. Instrum. Meth. **A 450**, 235 (2000).
- [159] ZEUS Coll., S. Chekanov et al., Nucl. Phys. **B 713**, 3 (2005).
- [160] ZEUS Coll., S. Chekanov et al., Nucl. Phys. **B 637**, 3 (2002).
- [161] ZEUS Coll., J. Breitweg et al., Eur. Phys. J. **C 2**, 237 (1998).
- [162] J.C. Collins, Phys. Rev. **D 57**, 3051 (1998);
 J.C. Collins, J. Phys. **G 28**, 1069 (2002).
- [163] H1 Coll., *Comparison between diffractive dijet electroproduction and photoproduction*. Abstract 177, 32nd International Conference on High Energy Physics, Beijing, China (ICHEP2004), July 2004, available on
<http://www-h1.desy.de/h1/www/publications/conf/list.ICHEP2004.html>;
 ZEUS Coll., *Diffractive photoproduction of dijets at HERA*. Abstract 249, 32nd

International Conference on High Energy Physics, Beijing, China (ICHEP2004),
July 2004, available on
<http://www-zeus.desy.de/physics/phch/conf/ichep04/>.

- [164] M. Klasen and G. Kramer, Phys. Lett. **B 508**, 259 (2001).
- [165] A.B. Kaidalov et al., Phys. Lett. **B 567**, 61 (2003).
- [166] H. Abramowicz, M. Groys and A. Levy, Preprint hep-ph/0507090, 2005;
P. Laycock, P. Newman, F.-P. Schilling, 2005. Talk presented at DIS2005.
- [167] ZEUS Coll., *Dijet production in diffractive deep-inelastic scattering at HERA*.
Abstract 342, HEP2005 International Europhysics Conference on High Energy
Physics, Lisboa, Portugal (EPS2005), July 2005, 2005, available on
http://www-zeus.desy.de/physics/phch/conf/lp05_eps05.
- [168] H1 Coll., C. Adloff et al., Eur. Phys. J. **C 6**, 587 (1999).
- [169] ZEUS Coll., S. Chekanov et al., Phys. Lett. **B 590**, 143 (2004).
- [170] H1 Coll., A. Aktas et al., Eur. Phys. J. **C 41**, 273 (2005).
- [171] A. Schafer, O. Nachtmann and R. Schopf, Phys. Lett. **B 249**, 331 (1990);
A. Bialas and P.V. Landshoff, Phys. Lett. **B 256**, 540 (1991);
H.J. Lu and J. Milana, Phys. Rev. **D 51**, 6107 (1995);
J. Cudell and O.F. Hernandez, Nucl. Phys. **B 471**, 471 (1996);
V.A. Khoze et al., Phys. Lett. **B 401**, 330 (1997);
V.A. Khoze, A.D. Martin and M.G. Ryskin, Eur. Phys. J. **C 14**, 525 (2000);
V.A. Khoze, A.D. Martin and M.G. Ryskin, Eur. Phys. J. **C 23**, 311 (2002);
A. De Roeck et al., Eur. Phys. J. **C 25**, 391 (2002);
B.E. Cox et al., Phys. Rev. **D 68**, 075004 (2003);
M. Boonekamp, R. Peschanski and C. Royon, Phys. Lett. **B 598**, 243 (2004);
B.E. Cox et al., Preprint hep-ph/0505240, 2005;
M. Boonekamp et al., Preprint hep-ph/0504199, 2005.
- [172] ZEUS Coll., S. Chekanov et al., Phys. Lett. **B 531**, 9 (2002).
- [173] H1 Coll., A. Aktas et al., Phys. Lett. **B 602**, 14 (2004).
- [174] H1 Coll., V. Andreev et al., Phys. Lett. **B 561**, 241 (2003).
- [175] ZEUS Coll., S. Chekanov et al., Phys. Lett. **B 583**, 41 (2004).
- [176] U. Baur and D. Zeppenfeld, Nucl. Phys. **B 325**, 253 (1989).
- [177] T. Han, R.D. Peccei and X. Zhang, Nucl. Phys. **B 454**, 527 (1995);
V.F. Obraztsov, S.R. Slabospitsky and O.P. Yushchenko, Phys. Lett.
B 426, 393 (1998);

- T. Han et al., Phys. Rev. **B 426**, 073008 (1998);
T. Han and J.L. Hewett, Phys. Rev. **D 60**, 074015 (1999);
H. Fritzsche and D. Holtmannspotter, Phys. Lett. **B 457**, 186 (1999).
- [178] ZEUS Coll., S. Chekanov, et al., Phys. Lett. **B 559**, 153 (2003).
- [179] H1 Coll., A. Aktas et al., Eur. Phys. J. **C 33**, 9 (2004).
- [180] T. Kon, and T. Kobayashi, Phys. Lett. **B 270**, 81 (1991);
J.M. Butterworth and H.K. Dreiner, Nucl. Phys. **B 397**, 3 (1993);
W. Porod, Phys. Rev. **D 59**, 095009 (1999).
- [181] H1 Coll., *Events with an isolated lepton and missing transverse momentum at HERA*. Abstract 637, HEP2005 International Europhysics Conference on High Energy Physics, Lisboa, Portugal (EPS2005), July 2005, available on <http://www-h1.desy.de/h1/www/publications/conf/list.EPS2005.html>.
- [182] LEPS Coll., T. Nakano et al., Phys. Rev. Lett. **91**, 012002 (2003);
SAPHIR Coll., J. Barth et al., Phys. Lett. **B 572**, 127 (2003);
CLAS Coll., S. Stepanyan et al., Phys. Rev. Lett. **91**, 252001 (2003);
CLAS Coll., V. Kubarovsky et al., Phys. Rev. Lett. **92**, 032001 (2004);
HERMES Coll., A. Airapetian et al., Phys. Lett. **B 585**, 213 (2004).
- [183] ZEUS Coll., S. Chekanov et al., Phys. Lett. **B 591**, 7 (2004).
- [184] COSY-TOF Coll., M. Abdel-Bary et al., Phys. Lett. **B 595**, 127 (2004);
NA49 Coll., C. Alt et al., Phys. Rev. Lett. **92**, 042003 (2004).
- [185] SVD Coll., A. Aleev et al., Preprint hep-ex/0401024, 2004.
- [186] A.E. Asratyan, A.G. Dolgolenko and M.A. Kubantsev, Phys. Atom. Nucl. **67**, 682 (2004).
- [187] DIANA Coll., V.V. Barmin et al., Phys. Atom. Nucl. **66**, 1715 (2003).
- [188] BES Coll., J.Z. Bai et al., Phys. Rev. **D 70**, 012004 (2004);
HyperCP Coll., M.J. Longo et al., Phys. Rev. **D 70**, 111101 (2004);
ZEUS Coll., S. Chekanov et al., Phys. Lett. **B 610**, 212 (2005);
HERA-B Coll., I. Abt et al., Phys. Rev. Lett. **93**, 212003 (2004);
HERMES Coll., A. Airapetian et al., Phys. Rev. **D 71**, 032004 (2005);
SPHINX Coll., Yu.M. Antipov et al., Eur. Phys. J. **A 21**, 455 (2004).
- [189] H1 Coll., A. Aktas et al., Phys. Lett. **B 588**, 17 (2004).
- [190] H1 Coll., A. Aktas et al., Eur. Phys. J. **C 36**, 413 (2004).
- [191] M. Drees and R.M. Godbole, J. Phys. G **G 21**, 1559 (1995).
- [192] M.A. Dobbs et al., Preprint hep-ph/0403045, 2004.

- [193] N. Baron and G. Baur, Phys. Rev. **C 48**, 1999 (1993);
M. Greiner et al., Phys. Rev. **C 51**, 911 (1995);
S.R. Klein, J. Nystrand and R. Vogt, Phys. Rev. **C 66**, 044906 (2002);
S.R. Klein and J. Nystrand, Phys. Rev. Lett. **92**, 142003 (2004).
- [194] S.R. Klein, J. Nystrand and R. Vogt, Eur. Phys. J. **C 21**, 563 (2001).
- [195] J. Bromley et al., *HZTOOL: A package for Monte Carlo-data comparison at HERA (version 1.0)*. Prepared for Workshop on Future Physics at HERA (Preceded by meetings 25-26 Sep 1995 and 7-9 Feb 1996 at DESY), Hamburg, Germany, 30-31 May 1996.
- [196] T. Sjöstrand et al., Comp. Phys. Comm. **135**, 238 (2001).